Nanospheres with Shielded Phosphorescent Dyes as Labels for Bioassays

Dissertation zur Erlangung des Doktorgrades der Naturwissenschaften
(Dr. rer. nat.)
an der Fakultät für Chemie und Pharmazie
der Universität Regensburg

vorgelegt von
Jens M. Kürner
Regensburg, im Januar 2002

Nanospheres with Shielded Phosphorescent Dyes as Labels for Bioassays

Dissertation zur Erlangung des Doktorgrades der Naturwissenschaften
(Dr. rer. nat.)
an der Fakultät für Chemie und Pharmazie
der Universität Regensburg

vorgelegt von
Jens M. Kürner
Regensburg, im Januar 2002

Nanospheres with Shielded Phosphorescent Dyes as Labels for Bioassays

Doctoral Thesis
by
Jens M. Kürner

Meinen Eltern gewidmet

This work was performed at the Institute of Analytical Chemistry, Chemo- and Biosensors of the University of Regensburg between April 1999 and January 2002 under the supervision of Prof. Otto S. Wolfbeis.

Date of colloquium: 26.02.2002

Board of examiners:
Chairperson: Prof. Claudia Steinem
First expert: Prof. Otto S. Wolfbeis
Second expert: Prof. Bernhard Dick
Third expert: Prof. Andreas Merz

Acknowledgments

Above all, I would like to thank Prof. Otto S. Wolfbeis for providing the fascinating subject, for the support during this thesis and for the great working conditions at our institute. He also gave me the opportunity and strong support to visit various conferences and workshops and to do two research stays abroad.

I gratefully acknowledge the extensive help, abundance of profound ideas and calm personality of the head of my working group, Prof. Ingo Klimant, who largely contributed to the completion of this thesis.

Furthermore, I received valuable chemical advice and all the copolymers used in this work from my colleague Dr. Christian Krause. I also think highly of his honesty and the discussions on matters other than chemistry with him.
I would like to thank Gisela Hierlmeier for the wonderful atmosphere in our laboratory.
Edeltraud Schmid is the most enthusiastic and diligent secretary I have ever met.
I appreciate the support of Athanasios Apostolidis, Sarina Arain, Jochen Gerlach, Dr. Christian Huber, Dr. Gregor Liebsch, Torsten Mayr, Claudia Schröder, Achim Stangelmayer and all other colleagues at our institute.

Wolfgang Bachleitner, Michael Büschel, Dietmar Heigl, Roland Reichenbach-Klinke and Andreas Roduch are the ones at the University of Regensburg whose friendship I would not want to miss.

The funding by CRAFT project SMT4-CT98-5510 of the European Union only made this thesis possible. I would like to thank the *Verein der Freunde der Universität Regensburg e.V.* and the DFG Graduate College *Sensory Photoreceptors in Natural and Artificial Systems* for financial assistance for travel expenses to conferences and funding of the research stays abroad.

Harald Preu (Institute of Physical and Theoretical Chemistry, University of Regensburg) performed experiments on the static and dynamic light scattering and laser Doppler velocimetry of the nanospheres. Dr. Jürgen Spinke and Dr. Ludger Jürgens, both from Roche (Mannheim, Germany), recorded all TEM pictures of the nanospheres. Dr. Gordon Graham from BTTG (Manchester, UK) recorded several SEM pictures of the nanospheres.

Jördis Böttcher is the one person who gives me the great motivation to look ahead in my life.

Finally, a very special thanks to my parents, Hans and Liselotte Kürner, for their emotional and financial support during my whole studies, which just made everything possible.

Table of Contents

1. Introduction ... 1

1.1. Detection of a binding event ... 1

1.1.1. Label-free detection of a binding event ... 2

1.1.2. Detection of a binding event using a label ... 2

1.1.2.1. Competitive assays ... 2

1.1.2.2. Sandwich assays ... 3

1.1.2.3. Immunosorbent or ELISA assays ... 4

1.2. Different types of labels ... 4

1.2.1. Radioactive labels ... 4

1.2.2. Enzymatic labels ... 5

1.2.3. Luminescent labels ... 5

1.2.4. Requirements for an ideal luminescent label ... 7

1.3. Ways to increase the sensitivity of a luminescence-based assay ... 7

1.3.1. Increasing the luminescence intensity ... 7

1.3.2. Elimination of background fluorescence ... 9

1.3.2.1. Use of long-wavelength luminophores ... 9

1.3.2.2. Use of long-lived luminophores ... 10

1.4. Aim of this thesis ... 14

2. Physico-chemical Background ... 15

2.1. Luminescence decay time ... 15

2.2. Quantum yield ... 18

2.3. Correction of amplitude and phase angle ... 19

2.4. Fluorescence quenching ... 20

2.4.1. Dynamic quenching ... 21

2.4.2. Static quenching ... 22

2.4.3. Comparison of dynamic and static quenching ... 24

2.5. Resonance energy transfer (RET) ... 24

2.6. Light scattering ... 27

2.6.1. Static light scattering ... 27

2.6.2. Dynamic light scattering (DLS) ... 28

2.7. Zeta potential and laser Doppler velocimetry (LDV) ... 29

2.8. Electron microscopy 31

2.8.1. Transmission electron microscopy (TEM) 32

2.8.2. Scanning electron microscopy (SEM) 33

3. Preparation and Characterization of Inert Phosphorescent Nanospheres 34

3.1. Introduction 34

3.2. Materials and methods 36

3.2.1. Chemicals and reagents 36

3.2.2. Instrumentation and measurements 38

3.2.2.1. Buffers and ionic strength 38

3.2.2.2. Absorbance measurements 38

3.2.2.3. Luminescence measurements 39

3.2.2.4. Fluorescence decay time measurements 40

3.2.2.5. Phosphorescence decay time measurements 40

3.2.2.6. pH measurements 42

3.2.2.7. Instruments for analyses of organic compounds 42

3.2.2.8. Electron microscopy 43

3.2.2.9. Light scattering 44

3.2.2.10. Laser Doppler velocimetry 44

3.2.2.11. Freeze drying 45

3.2.3. Preparation of ruthenium(II)-tris-4,7-diphenyl-1,10-phenanthroline bis-trimethylsilylpropanesulfonate [Ru(dpp)$_3$(TMS)$_2$] and ruthenium(II)-tris-4,7-diphenyl-1,10-phenanthroline dichloride [Ru(dpp)$_3$Cl$_2$] 45

3.2.4. Preparation of nanospheres 47

3.2.4.1. Preparation of polyacrylonitrile nanospheres 47

3.2.4.2. Preparation of poly-(acrylonitrile-co-polymer) nanospheres 48

3.2.5. Preparation of membranes 48

3.3. Results and discussion 49

3.3.1. Choice of polymer matrix 49

3.3.1.1. Choice of polyacrylonitrile copolymer 50

3.3.1.2. Matrix concentration 51

3.3.2. Choice of dye 52

3.3.2.1. Ligand 53

3.3.2.2. Counterion 53

3.3.2.3. Dye loading 54

3.3.3. Precipitation details 54

3.3.4. Buffer composition and storage conditions 57

3.3.5. Photophysical characterization of nanospheres (suspensions) 59

3.3.5.1. Excitation and emission spectra 59

3.3.5.2. Brightness 60

3.3.5.3. Luminescence frequency spectra 61

3.3.5.4. Dilution behavior 62

3.3.6. Physical characterization of nanospheres (suspensions) 63

3.3.6.1. Diameter and shape 64

3.3.6.2. Surface charge 66

3.3.6.3. Apparent decay time, quantum yield and cross-sensitivity to oxygen 67

3.3.6.4. Luminescence detection limit 68

3.3.7. Physical characterization of nanospheres (membranes) 69

3.4. Conclusion 71

4. Phosphorescent Nanospheres for Use in Advanced Time-Resolved Multiplexed Bioassays 72

4.1. Introduction 72

4.2. Materials and methods 77

4.2.1. Chemicals and reagents 77

4.2.2. Instrumentation and measurements 79

4.2.3. Preparation of dye solutions 79

4.2.4. Preparation of luminescent nanospheres 82

4.3. Results and discussion 83

4.3.1. Choice of dyes 83

4.3.1.1. Phosphorescent donor dye 83

4.3.1.2. Fluorescent acceptor dyes 84

4.3.2. Choice of encapsulation matrix 87

4.3.3. Photophysical characterization of nanospheres 88

4.3.3.1. Absorbance and emission spectra 89

4.3.3.2. Luminescence frequency spectra 97

4.3.4. Physical characterization of nanospheres 101

4.3.4.1. Diameter, shape and surface charge 101

4.3.4.2. Apparent decay time, quantum yield and cross-sensitivity to oxygen 101
4.4. Conclusion 104

5. Homogeneous Luminescence Decay Time-Based Assay Using Energy Transfer From Nanospheres 106
5.1. Introduction 106
5.2. Materials and methods 107
5.2.1. Chemicals and reagents 107
5.2.2. Instrumentation and measurements 109
5.2.3. Preparation of phosphorescent donor nanospheres 109
5.2.4. Coupling of biotin to carboxy-modified nanospheres 109
5.2.5. Preparation of polyelectrolyte acceptor solution 110
5.2.6. Implementation of polyelectrolyte binding study 111
5.2.7. Implementation of assay 111
5.3. Results and discussion 112
5.3.1. Choice of luminescent donor and acceptor dyes 113
5.3.2. RET calculations for the Ru(dpp)/bromophenol blue system 117
5.3.3. Choice of polymer matrix for donor encapsulation 119
5.3.4. Choice of polyelectrolyte matrix for acceptor encapsulation 120
5.3.5. Concept of polyelectrolyte binding study 120
5.3.6. Concept of assay 122
5.3.7. Prototype assay for avidin 123
5.4. Conclusion 126

6. Abbreviations, Acronyms and Symbols 128

7. References 131

8. Summary 145
8.1. Summary 145
8.2. Zusammenfassung 148

9. Curriculum Vitae 152

10. Publications and Patents 154

1. Introduction

Diagnostics as a whole represent a very large, well established and continually expanding market. Particularly in the current climate of ‘prevention rather than cure’ the need for detection at increasingly lower detection limits in more diverse applications is being added to a continuing requirement for low-cost monitoring and control in more traditional areas[1]. One of the biggest diagnostic markets worldwide is undoubtably that of clinical testing and within this field alone, labels play a key role.

In very general terms, as per IUPAC definition, a label[2] – or marker or tag – is a chemical compound that is distinguishable by the observer but not by the system and that is used to identify a tracer[3] which is a labelled member of a population used to measure certain properties of that population. In practice, biomolecules (such as proteins, nucleic acids, polysaccharides or lipids) labelled with a luminescent dye selectively bind to a particular antigen, carbohydrate, nucleic acid sequence or previously bound hapten, thus providing a means of detecting these biological targets[4].

1.1. Detection of a binding event

Any binding event, such as antibody-antigen binding, can be described by the binding constant of the respective equilibrium. In order to detect a binding event, two basic paths can be taken: (1) working without a label or (2) using labelled molecules. Figure 1.1. shows the complete path taken in this thesis, starting from the need to detect a binding event to the final application of nanospheres[5].

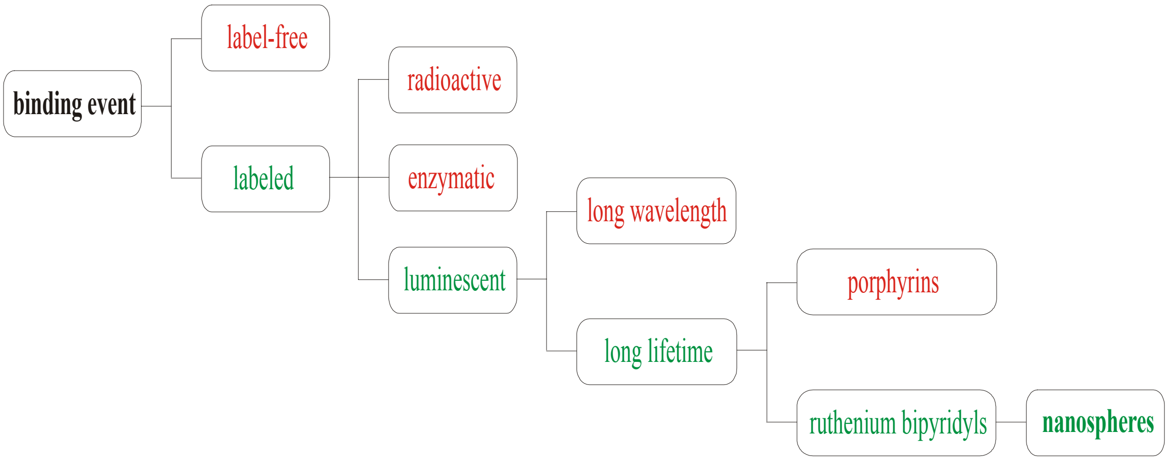

Figure 1.1. Flow chart to illustrate the (green) research path taken in this work.

1.1.1. Label-free detection of a binding event

A binding event can be detected label-free by observing the change in surface properties of a molecule upon interaction of that molecule with another species. Among the parameters that can be measured are (1) the refractive index n, (2) the layer thickness d and (3) the electric resistance R. The underlying measuring principles are interferometry, surface plasmon resonance (SPR) measurements, the use of a quartz microbalance, or capacitive resistance measurements.

The advantage of a label-free detection is the avoidance of the addition of reagents. Yet, due to unspecific binding, e.g. in serum, there is a limited sensitivity.

1.1.2. Detection of a binding event using a label

The second possibility to detect a binding event – the one taken in this work – is the use of a label. This has the tremendous advantage that unspecific binding is not detected. The three most common types of assays using labelled molecules to identify a binding event are (1) competitive assays, (2) sandwich or immunometric assays and (3) immunosorbent or ELISA assays.

1.1.2.1. Competitive assays

In a competitive assay (Figure 1.2.)[6] a single antibody to a small molecular weight antigen, typically less than 10,000 Dalton, is used. This antibody, at a very specific defined limited concentration, binds to the antigen in the sample and antigen labelled with a radionuclide (such as ^{125}I) or an enzyme (such as alkaline phosphatase). The amount of either bound or free labelled antigen added to the reaction is measured at the end of the immunoreaction and the percentage bound is inversely proportional to the amount of unlabelled antigen in either the standards or the samples. The separation at the end of the immunological binding reaction can be performed in various ways, but typical separation systems use a microtiter plate, paramagnetic beads or dextran-coated charcoal.

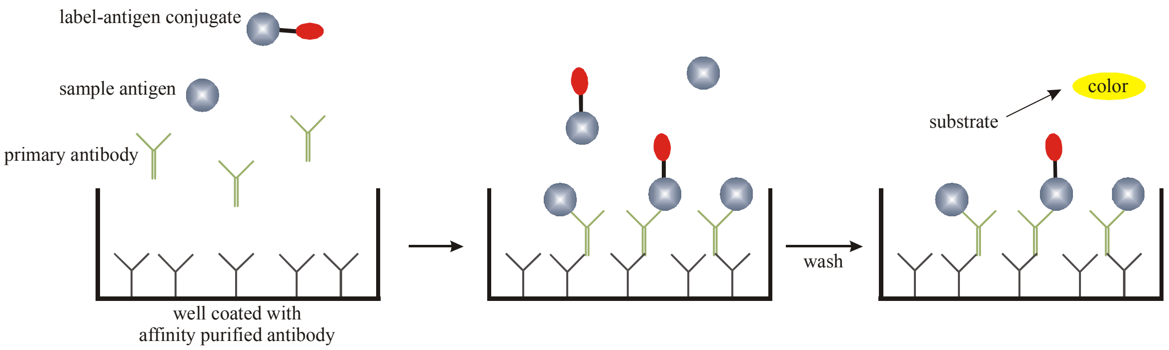
label-antigen conjugate
sample antigen
primary antibody
well coated with
affinity purified antibody
wash
substrate
color

Figure 1.2. Competitive assay.

1.1.2.2. Sandwich assays

In a sandwich assay (Figure 1.3.)[7], two or more antibodies to the antigen are used to sandwich the antigen. Typically one antibody is bound to the separation system, such as a microtiter plate, and one antibody is used to detect the antigen. The signal is inverserly proportional to the amount of antigen in the sample. It can be seen above that the antigen is 'sandwiched' between two antibodies, one attached to the solid phase, the other labelled with an enzyme. Typically the amount of solid phase antibody and enzyme-conjugated antibody are in a large excess over the amount of antigen in the sample. This forces the kinetics of binding of the antigen to the solid phase and the antibody conjugate to the antigen to be pseudo-first order, resulting in very rapid kinetics and high sensitivity. The result is an assay that produces a signal that is proportional to the amount of antigen in solution.

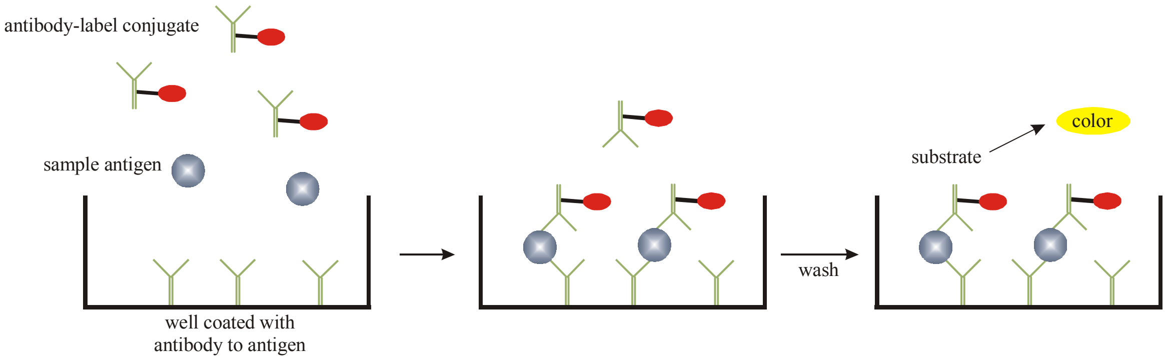
antibody-label conjugate
sample antigen
well coated with
antibody to antigen
wash
substrate
color

Figure 1.3. Sandwich assay.

1.1.2.3. Immunosorbent or ELISA assays

An immunosorbent assay or ELISA assay (Figure 1.4.)[8] is commonly used to detect the presence of antibodies to specific antigenic sites on viruses. This format uses a solid phase coated with either killed or neutralized virus, or synthetic peptide fragments from the viral overcoat. Samples, typically from donated blood, are then applied to the solid phase. Any antibodies to the virus, suggesting viral exposure, will bind to the viral antigen on the solid phase. After a wash step, a second antibody, labelled with an enzyme is added. This antibody binds to the sample antibody binding to the viral antigen. After a wash step the presence of enzyme is detected by addition of substrate.

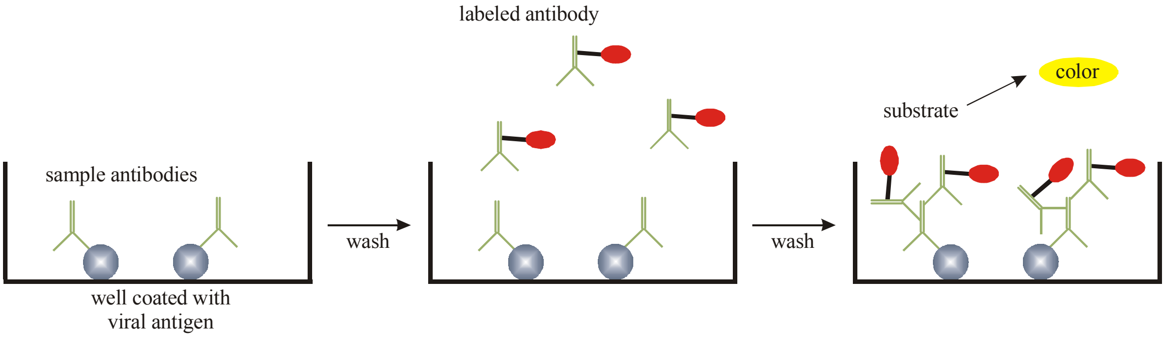

Figure 1.4. Immunosorbent or ELISA assay.

1.2. Different types of labels

In general, labels can be categorized into three main groups: (1) radioactive labels, (2) enzymatic labels and (3) luminescent labels. Their advantages and disadvantages will be explained in the following chapters.

1.2.1. Radioactive labels

Radioactive labels are the smallest available labels with the advantage of no steric hindrance. They allow a nearly background-free measurement, making these labels very sensitive so that even single particles can be detected. Unfortunately, they sometimes possess a limited working life due to their radioactive decomposition. More seriously, the handling and disposal of radioactive material requires a high degree of safety monitoring and leads to high costs.

1.2.2. Enzymatic labels

Enyzmes are the most widespread labels. The most familiar assay type using enzymatic labels is the ELISA assay, described in chapter 1.1.2.3. Examples of often used enzymatic labels include peroxidases and alkaline phosphatases (APs) because of their stability, turnover number and lack of interferences.

An enzymatic assay has a high sensitivity since the detectable reaction product is continuously generated enzymatically. The main disadvantages of enzymatic assays are the need to add reagents, the requirement of repeated washing steps and a time-consuming incubation which can lead to the denaturation of proteins. Finally, the use of large proteins may cause steric hindrance of binding events.

1.2.3. Luminescent labels

Luminescent – in particular fluorescent – labels have gained tremendous popularity during the last ten years. They possess a very high sensitivity since each binding event continuously generates a signal due to a ‘regeneration’ of the emitted photons. Furthermore, a host of luminescent dyes is commercially available at various wavelengths. Among the most common examples of luminescent labels (Table 1.1.) are (1) cyanine dyes, such as Cy3 and Cy5, (2) xanthene dyes (also called phthalein dyes), such as reactive fluorescein or rhodamine derivatives, and (3) intercalating dyes (classic nucleic acid stains), such as ethidium bromide and propidium iodide (both non-covalent labels).

When using luminescent labels in assays, the measurement of several parameters becomes feasible: (1) luminescence intensities, (2) lifetimes τ, (3) anisotropy or (4) emission spectra.

Table 1.1. Parent compounds of popular luminescent labels.

luminescent label	chemical structure
Cy3	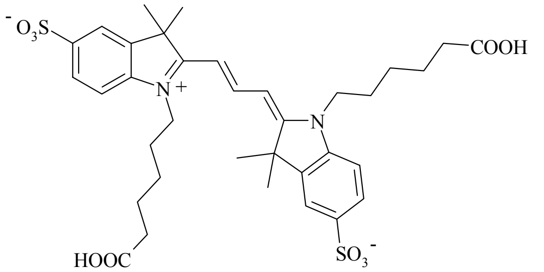
Cy5	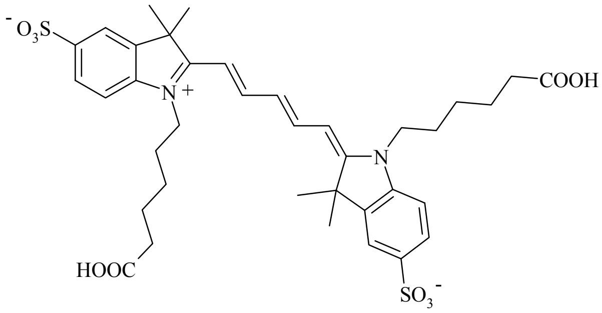
fluorescein	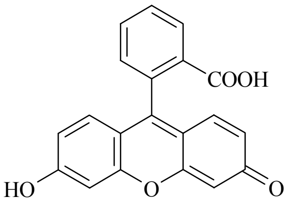
rhodamine	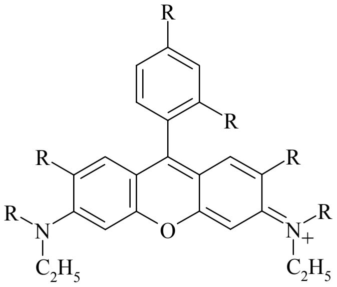
ethidium bromide	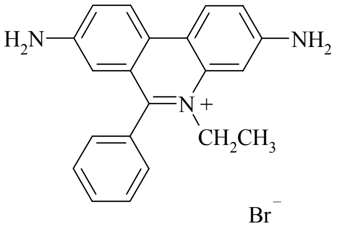
propidium iodide	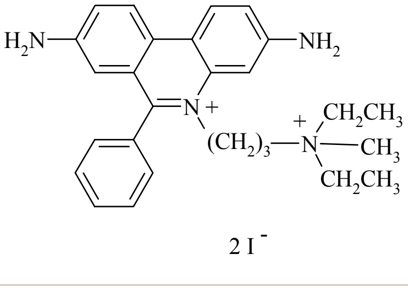

1.2.4. Requirements for an ideal luminescent label

An ideal luminescent label should possess the following properties[9]: (1) a large molar absorbance ε and (2) a large quantum yield Φ in order to obtain a high light intensity, (3) photostability, (4) water solubility, (5) commercial availability at low cost, (6) high reactivity in order to perform covalent coupling to proteins at ambient temperature and mild reaction conditions, (7) no interaction of any species present with the label that leads to changing spectrophysical properties, such as ε, τ or Φ, (8) a long-wavelength (not UV) absorbance maximum in order to eliminate shortwave background fluorescence and (9) possibly nontoxicity.

1.3. Ways to increase the sensitivity of a luminescence-based assay

The major feature of luminescent assays that still needs to be improved is sensitivity. Any luminescence signal is superimposed by background fluorescence. Therefore, the signal must be large enough in order to distinguish it from undesirable background (noise). Basically, two ways are possible to achieve this: (1) increasing the luminescence intensity or (2) elimination of background fluorescence.

1.3.1. Increasing the luminescence intensity

Tackling the problem of too low a luminescence signal by playing with the molar absorbance ε and the quantum yield Φ of a luminophore does not lead to satisfactory solutions since ε can at most be approximately 200,000 L mol^{-1} cm^{-1} and Φ is limited to 1. Yet, in order to obtain a higher luminescence intensity, the use of particles opens new perspectives and provides the system with a desired intensity amplification factor[10]. Within one single particle a large number of luminophores can be encapsulated, leading to brighter labels and furthermore providing a shielding effect against interfering species. Available particles (compare Table 1.2.) are made from polystyrene, silica gel, polymethacrylate, melamine resins or quantum dots[11-13].

Table 1.2. Common particle materials.

particle material	**chemical structure**
polystyrene	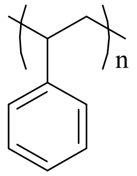
silica gel	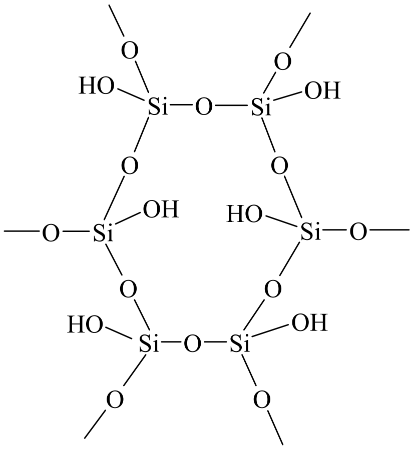
polymethacrylate	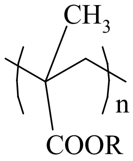
melamine resin	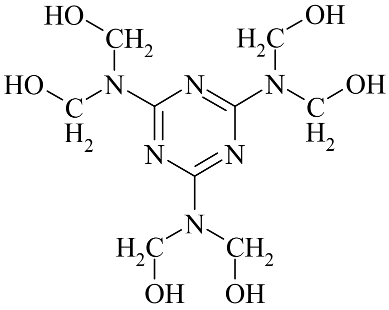

1.3.2. Elimination of background fluorescence

In addition to increasing luminescence intensity by using particles, as pointed out in chapter 1.3.1., the sensitivity of a label can be influenced by tampering with the luminescent background, as well. Since all background noise is shortwave and short-lived (i.e. fluorescent), two paths are possible to further enhance the intensity and thus the sensitivity of a luminescent label: (1) using long-wavelength or (2) long-lived luminophores.

1.3.2.1. Use of long-wavelength luminophores

By employing long-wavelength luminescent labels in order to avoid shortwave background fluorescence, analyte concentrations as low as 10^{-12} mol/L can be detected. Excitation close to the NIR region has a number of advantages: (1) Beyond 600 nm there is only negligible absorbance and fluorescence from cells and tissue in biological samples (compare the optical window of whole blood in the range of 650 – 700 nm in the schematized Figure 1.5.)[14-16]. (2) Inexpensive monochromatic and bright excitation light sources, such as diode lasers (at 635, 645, 650, 660 or 670 nm), are commercially available. (3) The damage to biological matter is proportional to the amount of energy E from the excitation light source penetrating the sample, which in turn is inversely proportional to the excitation wavelength λ_{exc} (Planck, equation 1.1.). (4) The intensity of scattered light I_S is inversely proportional to the fourth power of the excitation wavelength λ_{exc} (Rayleigh, equation 1.2.).

$$E = h \cdot \upsilon = h \cdot \frac{1}{\lambda_{exc}} \qquad 1.1.$$

$$I_S \sim \frac{1}{{\lambda_{exc}}^4} \qquad 1.2.$$

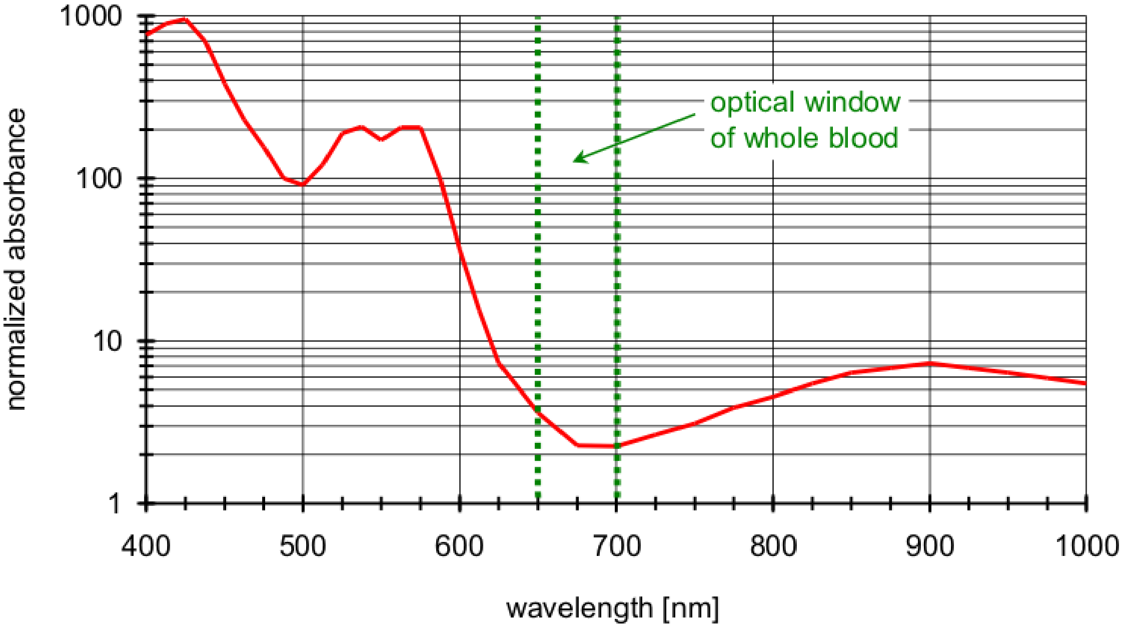

Figure 1.5. Absorbance spectrum of whole blood with the optical window in the range of 650 – 700 nm. Note that the y-axis is logarithmic.

1.3.2.2. Use of long-lived luminophores

In contrast to using long-wavelength luminophores, in this work the second possible approach with long-lived luminescent labels was taken. As is illustrated in Figure 1.6., any background noise is fluorescent in the low ns time regime and thus short-lived. By employing long-lived luminophores – in particular, phosphorescent labels – practically all background can be eliminated, leading to a much higher sensitivity of the respective assay.

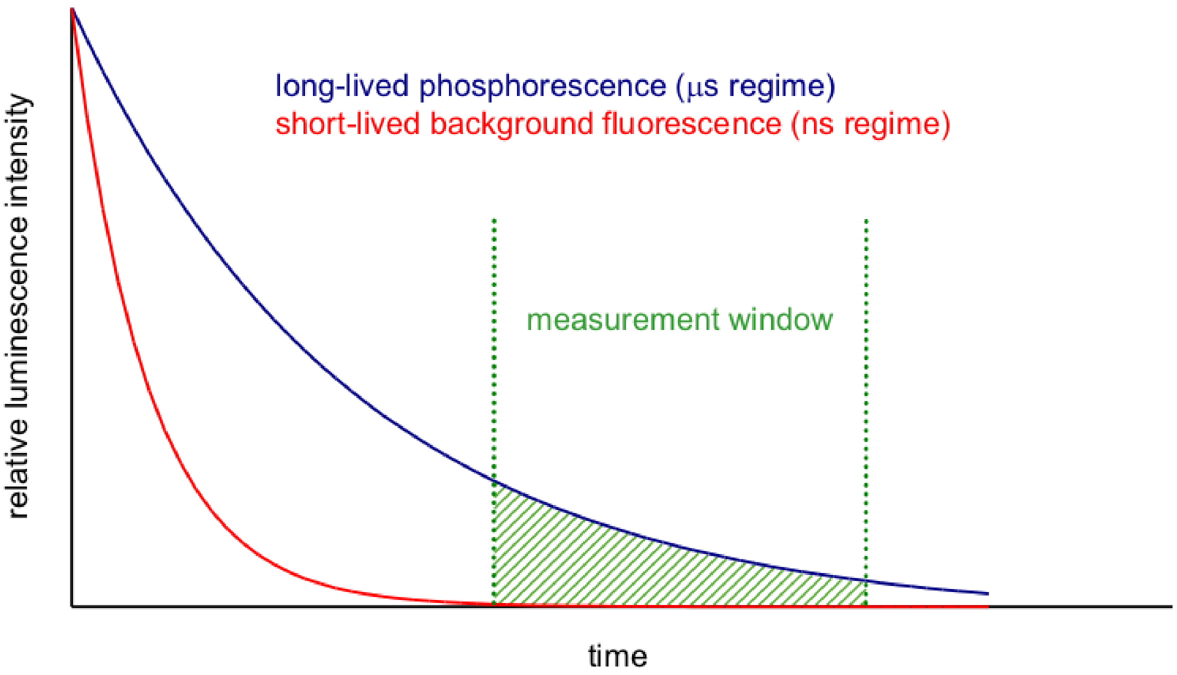

Figure 1.6. Elimination of short-lived background fluorescence (ns time regime) by measuring long-lived phophorescence (µs time regime).

Various types of probes exhibiting luminescence of long emission duration have been tested in assays, including probes emitting normal or delayed fluorescence, phosphorescent compounds, and a variety of chelates exhibiting intra-chelate energy transfer luminescence. A selection of long-lived dyes commonly used as labels is given in Table 1.3. in the order of rising decay times τ [17].

Table 1.3. Chemical structure and room temperature decay time of long-lived luminescent labels.

luminescent label	**chemical structure of exemplary compound**	τ
pyrene derivatives	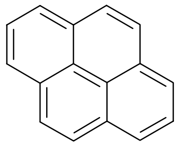	180 – 420 ns
ruthenium bipyridyl chelates	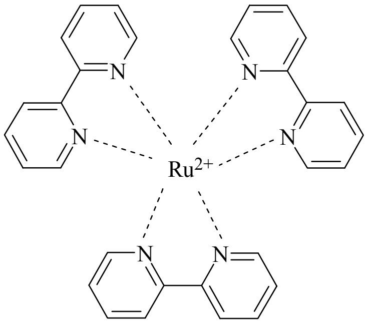	0.1 – 7 µs
lanthanoide chelates (e.g. europium)	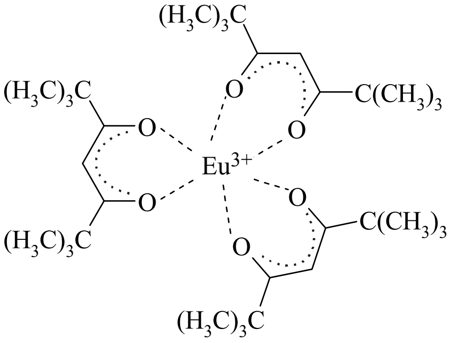 (H$_3$C)$_3$C (H$_3$C)$_3$C O C(CH$_3$)$_3$ O O Eu^{3+} O O O C(CH$_3$)$_3$ (H$_3$C)$_3$C (H$_3$C)$_3$C	1 µs – 2 ms
metalloporphyrins (e.g. palladium or platinum)	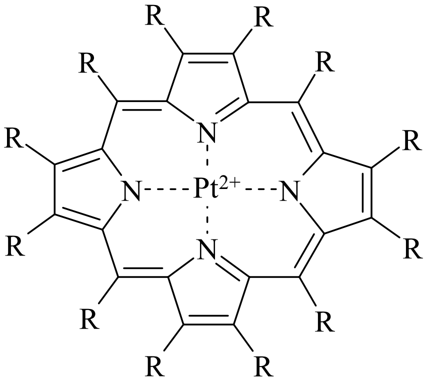 R R R R N R R N Pt^{2+} N R R N R R R R	20 µs – 1 ms
erythrosin	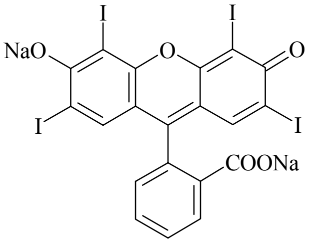 I I NaO O O I I COONa	250 µs

Many long-lived labels belong to the group of rare earth chelates. Yet, the excitation wavelength of most long-lived lanthanoide (e.g. europium) complexes[5], for instance, is in the UV region, with presently fewer commercially available semiconductor (SC) excitation light sources. The use of phosphorescent instead of fluorescent labels also goes along with disadvantageous spectrophysical properties, such as high rates of luminescence quenching by water or oxygen, for instance. This is also made clear by the fact that only very few molecules phosphoresce at room temperature.

Among the long-lived phosphorescent labels, two groups of chelates still meet the requirement of assays for a high sensitivity best: (1) porphyrins and (2) ruthenium bipyridyls. Yet, very importantly, they must be incorporated into a polymer matrix – such as particles – which shields them from external interfering species like quenchers[10].

Although palladium or platinum porphyrins are even more long-lived and long-wavelength than ruthenium bipyridyl chelates, their incorporation into particles is still difficult to achieve. In addition, those metalloporphyrins display an extremely large sensitivity towards oxygen or other interfering species.

The luminescent properties of certain ruthenium bipyridyl chelates are particularly well-suited for assays requiring high sensitivity. In such chelates, the wide absorbance of the excitation light by the organic ligand at the near UV region of the VIS spectrum ensures efficient light collection, whereas the chelated central ion collects the absorbed energy and produces a strong emission at long wavelength, well-distinguished from the main part of the disturbing short-wave background. Furthermore, the exceptionally long luminescence decay time of the ruthenium chelates (in the μs time regime) allows the effective elimination of the rapidly decaying background fluorescence, which in turn again contributes to a high specificity[18]. Another advantage of those ruthenium complexes is their stability and the large number of low-cost excitation light sources available.

All this leads to the conclusion that in order to create an assay of high sensitivity, any label – such as the ruthenium bipyridyl dyes in this work – must first be encapsulated into particles (spheres). Only this provides the important shielding effect against luminescence quenchers. So far, such bright phosphorescent particle systems are neither known nor characterized[10].

1.4. Aim of this thesis

The aim of this work (compare Figure 1.1.)[5] was to identify methods for reproducible preparation of such a new type of inert, brightly phosphorescent particles in order to reach the general objectives for assays: (1) a high sensitivity (which can be influenced by the binding constant or – as in this case – by the applied label), (2) reliability and (3) selectivity (which can be influenced by the receptor component).

The particles were to display a typical diameter of well below 100 nm. The photophysical and physical properties of those nanospheres were to be characterized in detail and a number of labelling applications were to be examined.

2. Physico-Chemical Background

2.1. Luminescence decay time

The luminescence decay time τ of a substance is defined as the average time during which an ensemble of molecules remains in the excited state prior to their return to the ground state[19-20]. In case of a monoexponential decay, it can also be described as the time after which $\frac{1}{e}$ (36.8 %) of the initially excited molecules are not deactivated yet (Figure 2.1.).

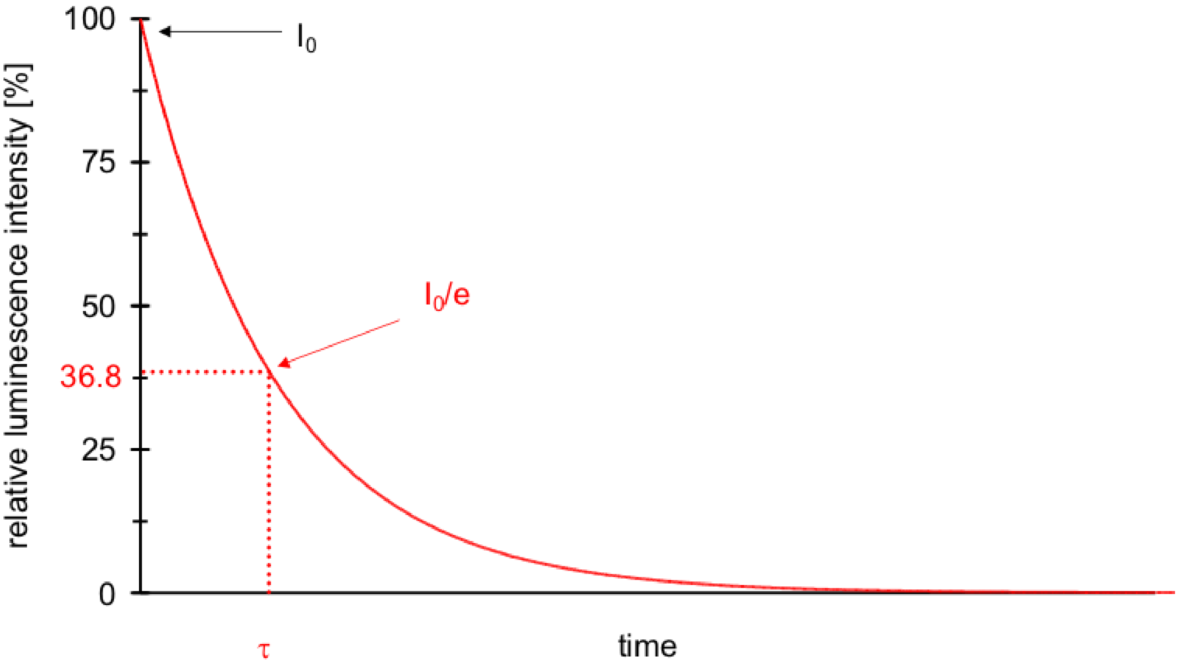

Figure 2.1. Scheme of a monoexponential decay. τ is the average decay time of the excited state.

The luminescence intensity $I(t)$ at the time t and the average decay time of the excited state τ are related, as shown in equation 2.1.

$$I(t) = I_0 \cdot e^{-\frac{t}{\tau}} \tag{2.1.}$$

where I_0 is the maximum luminescence intensity during excitation and t is the time after switching off the excitation light source.

Two methods are widely used for the measurement of the luminescence decay times, namely the pulse method (‘time domain measurement’) and the harmonic or phase modulation method (‘frequency domain measurement’).

TIME DOMAIN MEASUREMENT. In the time domain or pulse method[21], the sample is excited with short pulses of light and the time-dependent decay of luminescence intensity is measured. The photon counting method measures the decay of the luminescence by recording the first photon after very weak pulses, whereas the pulse sampling method measures different periods after each pulse to obtain the whole time-resolved decay. The pulse method has the advantage that disturbing fluorophores with lifetimes shorter than the incident light pulse are not measured. Short-lived background fluorescence can thus be easily separated. The disadvantage of the pulse method is the use of very sophisticated instrumentation. A detector with very short response time and a high band width is needed not to distort the signals by time. Another problem are the light sources available which can yield pulses of picosecond pulse width and constant intensity. The observed luminescence decay has to be corrected for the width of the lamp pulses which is called deconvolution.

FREQUENCY DOMAIN MEASUREMENT. In the frequency domain or phase modulation method, the sample is excited by sinusoidally modulated light[22]. The lifetime of the fluorophore causes a time lag between absorbance and emission, expressed by the phase shift θ and a decreased emission intensity relative to the incident light, called demodulation m (Figure 2.2.).

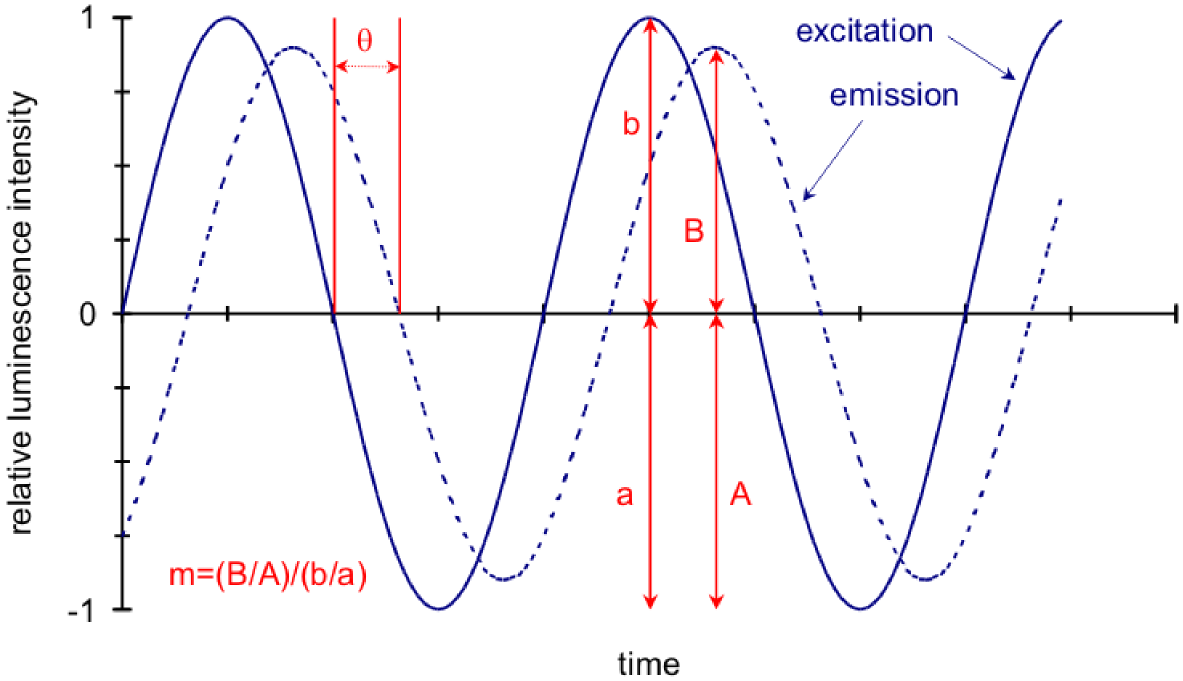

Figure 2.2. Scheme for frequency domain measurements. The sinusoidally modulated light is shifted (θ) and demodulated (m).

In this work, all average decay times were measured by the phase modulation method. Luminescence decay times τ were calculated by a simple mathematical formalism from the phase shifts (i.e. phase angles) θ obtained by a single frequency measurement via equation 2.2.

$$\tau = \frac{\tan\theta}{2 \cdot \pi \cdot \upsilon} \qquad 2.2.$$

where υ is the modulation frequency of the exciting light. τ is not the decay time of the measured luminophore but an average over all fluorescent species present. Monoexponential decay profiles were assumed. If the decay is multiexponential, then the calculated average decay times are only apparent values.

In contrast to direct detection methods, such as up-conversion (non-linear optical method), time-correlated single photon counting or using the storage oscilloscope or a streak camera, this phase fluorimetry is an indirect method for obtaining the decay time.

2.2. Quantum yield

Quantum yields Φ_x of an aqueous sample were calculated via equation 2.3.[23-24]. Corrected luminescence emission spectra were used throughout since the photomultiplier (PMT) is not equally sensitive over the entire wavelength range.

$$\Phi_x = \Phi_R \cdot \frac{A_R(\lambda_R)}{A_x(\lambda_x)} \cdot \frac{I(\lambda_R)}{I(\lambda_x)} \cdot \frac{{n_x}^2}{{n_R}^2} \cdot \frac{D_x}{D_R} \qquad 2.3.$$

where $A(\lambda)$ is the absorbance of the solution at the wavelength of excitation λ, $I(\lambda)$ the relative intensity of the exciting light at wavelength λ, n the average refractive index of the solution and D the integrated area of the corrected emission spectrum. Subscripts x and R refer to the sample and the ruthenium(II)-tris-2,2-bipyridyl chloride hexahydrate ($Ru(bipy)_3Cl_2 \cdot 6H_2O$) reference solutions, respectively. The quantum yield Φ_R for the reference complex is given in literature.

$$\Phi_R = 0.042$$

Due to the similarity of both sample and reference emission spectra, no conversion of wavelength to frequency was made for the calculation of quantum yields. Reference and sample were excited at the same wavelength. Since the voltage of the detector was kept constant during all quantum yield measurements and since all solutions were aqueous, the following two simplifications can be made (equations 2.4. and 2.5.).

$$I(\lambda_R) \approx I(\lambda_x) \qquad 2.4.$$

$$n_x \approx n_R \qquad 2.5.$$

Now, equation 2.3. simplifies to equation 2.6. and can be used to determine quantum yields Φ_x from experimental data $A(\lambda)$ and D.

$$\Phi_x = 0.042 \cdot \frac{A_R(\lambda_R)}{A_x(\lambda_x)} \cdot \frac{D_x}{D_R} \qquad 2.6.$$

2.3. Correction of amplitude and phase angle

In this work, any measured amplitude of a luminescence signal A and any measured phase angle θ was corrected in order to get rid of background noise. With the given data for amplitudes and phase angles A_{total}, θ_{total}, A_2 and θ_2 – assuming a modulation frequency of $\upsilon = 45\,kHz$ for Ru(dpp) – corrected values A_1 and θ_1 were calculated from the underlying basic equations 2.7. and 2.8. The subscripts refer to: total = measured data, 1 = corrected data, 2 = short-lived background (blind value).

$$A_{total} \cdot \sin(\theta_{total}) = A_1 \cdot \sin(\theta_1) + A_2 \cdot \sin(\theta_2) \qquad 2.7.$$

$$A_{total} \cdot \cos(\theta_{total}) = A_1 \cdot \cos(\theta_1) + A_2 \cdot \cos(\theta_2) \qquad 2.8.$$

This system of two equations can be solved, which was done using the computer program Maple V Release 5 by Waterloo Maple (Waterloo, Canada). The Maple algorithm used is given in Figure 2.3. This leads to the following solutions for the corrected values of amplitude and phase angle, presented in equations 2.9. for θ_1 and 2.10. for A_1.

$$\theta_1 = \arctan\left(\frac{A_2 \cdot \sin(\theta_2) - A_{total} \cdot \sin(\theta_{total})}{A_2 \cdot \cos(\theta_2) - A_{total} \cdot \cos(\theta_{total})} \right) \qquad 2.9.$$

$$A_1 = \left[A_{total} \cdot \cos(\theta_{total}) - A_2 \cdot \cos(\theta_2)\right] \cdot \sqrt{\frac{\left[A_2 \cdot \sin(\theta_2) - A_{total} \cdot \sin(\theta_{total})\right]^2}{\left[A_2 \cdot \cos(\theta_2) - A_{total} \cdot \cos(\theta_{total})\right]^2} + 1} \qquad 2.10.$$

Once a value for θ_1 is calculated, the corrected decay time τ_1 can be figured out by equation 2.11. (compare equation 2.2.).

$$\tau_1 = \frac{\tan(\theta_1)}{2 \cdot \pi \cdot \upsilon} \qquad 2.11.$$

```
> # given data: Atotal, Ptotal, A2, P2
> # wanted data: A1, P1
> # abbreviations: A = amplitude, P = phase angle (phase shift)
> # subscripts: total = measured data, 1 = corrected data, 2 = short-lived background (blind value)
> restart:
> readlib(readdata):
> values:=readdata(`a:\\Phase_Data_In.txt`,2):
> # input format for Phase_Data_In.txt (2 columns):
> # 1st line: phase angle (background), amplitude (background)
> # 2nd, 3rd, ... line: phase angle (measured), amplitude (measured)
> number:=nops(values)-1:
> equation1:=Atotal#sin(Ptotal)=A1#sin(P1)+A2#sin(P2):
> equation2:=Atotal#cos(Ptotal)=A1#cos(P1)+A2#cos(P2):
> A1:=solve(equation1,A1):
> equation3:=subs(A1=A1,equation2):
> P1:=solve(equation3,P1):
> A1:=A1:
> Digits:=5:
> Ptotal_degrees:=[seq(values[i][1],i=2..number+1)]:
> Ptotal_radian:=[seq(evalf(Ptotal_degrees[i]#Pi/180),i=1..number)]:
> P2_degrees:=values[1][1]:
> P2_radian:=evalf(P2_degrees#Pi/180):
> A2:=values[1][2]:
> P2:=P2_radian:
> Atotal_list:=[seq(values[i][2],i=2..number+1)]:
> Ptotal_list:=Ptotal_radian:
> P1_radian:=[seq(simplify(subs(Ptotal=Ptotal_list[i],Atotal=Atotal_list[i],P1)),i=1..number)]:
> A1:=[seq(simplify(subs(Ptotal=Ptotal_list[i],Atotal=Atotal_list[i],A1)),i=1..number)]:
> P1_degrees:=[seq(evalf(P1_radian[i]#180/Pi),i=1..number)]:
> tau_microseconds:=[seq(1e6#evalf(tan(P1_radian[i])/(2#Pi#45e3)),i=1..number)]:
> Data_Out:=[seq([Ptotal_degrees[i],Atotal_list[i],P1_degrees[i],A1[i],tau_microseconds[i]],i=1..number)]:
> writedata("a:\\Phase_Data_Out.txt",Data_Out,float):
> # output format of Phase_Data_Out.txt (5 columns):
> # phase angle (measured), amplitude (measured), phase angle (corrected), amplitude (corrected), decay
  time
```

Figure 2.3. Maple algorithm for solving the equation system of equations 2.7. and 2.8.

2.4. Fluorescence quenching

Fluorescence quenching refers to any process which decreases the intensity of the fluorescence emission of a sample[24-25]. Quenching by small molecules either in the solvent or bound to the examined molecule in close proximity to the fluorophore can largely decrease the quantum yield of the examined molecule. A variety of interactions can result in quenching. These mechanisms include collisional or dynamic quenching, static quenching, excited-state reactions, ground-state complex formation, molecular rearrangements, quenching by energy transfer and charge transfer reactions.

INNER-FILTER EFFECT. The presence of materials which absorb a significant proportion of the excitation or luminescent radiation will diminish the observed luminescence by a so-called inner-filter effect. When the luminophore itself is present in high concentrations, it should, of course, be diluted so as to yield little absorbance[26-30].

2.4.1. Dynamic quenching

A collision between a fluorophore in its excited state and the quencher results in radiationless deactivation and is called dynamic or collisional quenching (Figure 2.4.). When quenching occurs by a dynamic or collisional mechanism, the quencher must diffuse to the fluorophore during the lifetime of the excited state. Upon physical contact, the fluorophore returns to the ground state, without emission of a photon. Quenching occurs without any permanent change in the molecules, i.e. without a photochemical reaction.

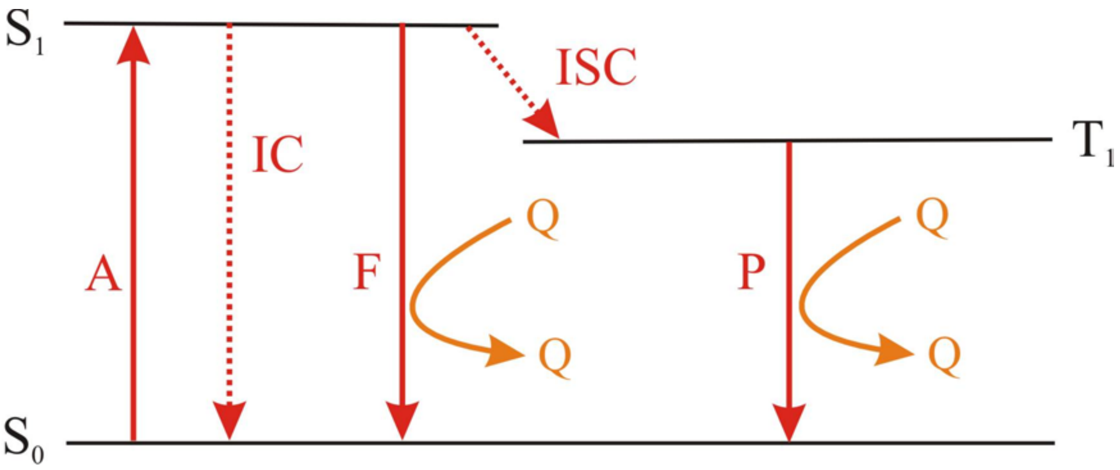

Figure 2.4. Simplified Jablonski diagram showing dynamic (collisional) quenching by a quencher Q. The following abbreviations are used: S_0/S_1 = singlet states, T_1 = triplet state, A = absorbance (10^{-15} s), F = fluorescence ($10^{-9} - 10^{-7}$ s), P = phosphorescence ($10^{-7} - 10^{2}$ s), IC = internal conversion, ISC = intersystem crossing. Dotted lines symbolize non-radiative decays, whereas solid lines terminating in the S_0 state represent radiative decays.

Quenching is an additional process that deactivates the excited state besides radiative emission. Because dynamic quenching depopulates the excited state without allowing fluorescence emission, the decrease in fluorescence intensity equates to the decrease in fluorescence lifetime. The dependence of the emission intensity F on quencher concentration $[Q]$ is given by the Stern-Volmer equation 2.12.

$$\frac{F_0}{F} = \frac{\tau_0}{\tau} = 1 + k_q \cdot \tau_0 \cdot [Q] = 1 + k_D \cdot [Q] \qquad 2.12.$$

where F_0, τ_0 and F, τ are the fluorescence intensities and lifetimes in the absence and presence of a quencher, respectively, k_q is the bimolecular quenching constant for the dynamic reaction of the quencher with the fluorophore and $[Q]$ is the quencher concentration. k_D is the Stern-Volmer constant (KSV) given by equation 2.13.

$$k_D = k_q \cdot \tau_0 \qquad 2.13.$$

Dynamic quenching can also be determined by fluorescence lifetime measurements of the fluorophore because there is an equivalent decrease in fluorescence intensity and lifetime (see equation 2.12., $\frac{F_0}{F} = \frac{\tau_0}{\tau}$).

Molecular oxygen is one of the best known dynamic quenchers. It quenches almost all known fluorophores since it is small. Iodide is also a commonly used quencher since it efficiently quenches surface groups because of its charged nature. With charged quenchers, electrostatic effects become important, which can be identified by dependence of quenching on ionic strength.

2.4.2. Static quenching

Static quenching occurs if a non-fluorescent ground state complex $(F-Q)$ is formed between the fluorophore F and the quencher Q (equation 2.14.). When this complex absorbs light, it immediately returns to the ground state without emission of a photon.

$$F + Q \rightleftharpoons (F-Q) \qquad 2.14.$$

The association constant K_S for the complex formation is given by equation 2.15.

$$K_S = \frac{[(F-Q)]}{[F][Q]} \tag{2.15.}$$

where $[(F-Q)]$ is the concentration of the complex $(F-Q)$, $[F]$ is the concentration of uncomplexed fluorophore F and $[Q]$ is the concentration of quencher Q. The total concentration of fluorophore $[F_0]$ is equal to the sum of complexed and uncomplexed fluorophore (equation 2.16.).

$$[F_0] = [F] + [(F-Q)] \tag{2.16.}$$

Solving equation 2.16. for $[(F-Q)]$ and substituting this in equation 2.15. leads to equation 2.17.

$$K_S = \frac{[F_0]-[F]}{[F][Q]} \tag{2.17.}$$

Substituting the fluorophore concentrations $[F_0]$ and $[F]$ with fluorescence intensities F_0 and F and rearranging equation 2.17. yields a Stern-Volmer like equation 2.18.

$$\frac{F_0}{F} = 1 + K_S[Q] \tag{2.18.}$$

Apparently, the system will follow the Stern-Volmer quenching law, but the quenching constant K_S is the equilibrium constant of the complex formation. It is important to mention that static quenching causes no change in the fluorescence lifetime of the fluorophore ($\tau = \tau_0$), because complex formation takes place in the ground state.

2.4.3. Comparison of dynamic and static quenching

Both dynamic and static quenching require molecular interaction between the fluorophore and the quencher. The measurement of fluorescence intensity cannot differentiate between dynamic and static quenching. The most effective way to distinguish between dynamic and static quenching is the measurement of luminescence decay times since in case of static quenching a fraction of fluorophores is removed by complex formation and this, of course, does not affect the fluorescence lifetime. Another possibility to distinguish between dynamic and static quenching is to record various Stern-Volmer plots (compare equation 2.18.) at different temperatures. With increasing temperature, the Stern-Volmer constant K_D is also rising, caused by the faster diffusion of the quenching molecules and thus the increased probability of collisional encounters between the fluorophore F and the quencher Q. The complex formation constant K_S, however, usually decreases with increasing temperature because the stability of the complexes decreases. Furthermore, the absorbance spectra of the fluorophore in the absence and presence of the quencher can be used for differentiation. Since dynamic quenching only has consequences on molecules in the excited state, no variation in the absorbance spectra can be observed. Static quenching, in contrast, affects the molecules in the ground state and thus the absorbance spectra as well.

2.5. Resonance energy transfer (RET)

In this work, resonance energy transfer (RET) – sometimes also referred to as fluorescence resonance energy transfer (FRET) – is the most important quenching method and implies the transfer of excited state energy from a donor to an acceptor[24, 31-33]. RET is a distance-dependent excited state interaction in which emission of one fluorohore is coupled to the excitation of another.

The excitation energy can be transferred by a radiationless process to a neighboring fluorophore if their energy level difference corresponds to the quantum of excitation energy. In this process, the quantum, or exciton, is transferred, which raises the electron in the acceptor to a higher energy state as the photo-excited electron in the donor returns to ground state. This mechanism requires resonance interaction between donor and acceptor over distances greater than interatomic. The conditions for this mechanism are that the fluorescent emission spectrum of the energy donor overlap the absorbance spectrum of the energy acceptor. Also, donor and acceptor transition dipole orientations must be approximately parallel. The probability that energy transfer will occur is inversely proportional to the sixth power of the distance between the fluorophores (compare equation 2.19.). This permits proximity to be measured up to a range of about 10 – 100 Å (1 – 10 nm). RET can detect even changes in distances ranging from 1 – 2 Å, hence it is a sensitive measure of conformational change, as well.

The energy received by the acceptor is less than that given by the donor. The rest of the energy is degraded and is spread over the environment. The acceptor can be fluorescent or non-fluorescent. If the acceptor also is fluorescent, the transferred energy can be emitted as a luminescence characterisic of the acceptor . If the acceptor is not fluorescent, the energy is lost through equilibration with the solvent.

When the donor and acceptor are different, RET can be detected by the appearence of luminescence of the acceptor or by quenching of donor luminescence. When the donor and acceptor are the same, RET can be detected by the resulting fluorescent depolarization. This energy transfer can be detected and used by measuring an emission of the acceptor fluorophore if it is excited at the donor fluorophore’s wavelength. This wavelength normally would not produce an emission from the acceptor, but does so if energy transfer is involved. This energy transfer can also be detected by measuring a decrease of donor emission at its wavelength in the presence of an acceptor. The acceptor has a quenching effect on the donor.

The two fluorophores need not necessarily be part of the same molecule. Energy transfer will take place between isolated molecules in solution as long as the average intermolecular distance is within 50 – 60 Å[34].

FÖRSTER RET CALCULATIONS. A quantitative theory for singlet-singlet energy transfer has been developed by Förster which assumes that the transfer occurs through dipole-dipole interactions of donor and acceptor[35]. To obtain useful structural information from energy transfer, the measured efficiency must be related to the distance between the two fluorophores. Unlike the Dexter theory of RET which includes transfer by means of forbidden transitions, the Förster theory involves only allowed transitions[36].

The rate of energy transfer depends on the overlap of the emission spectrum of the donor with the absorbance spectrum of the acceptor, the relative orientation of the donor and acceptor transition dipoles and the distance between these molecules. Förster developed a quantitative expression for the rate of energy transfer k_T due to dipole-dipole interactions in terms of experimentally accessible parameters (equation 2.19.):

$$k_T = \frac{1}{\tau_D} \cdot \left(\frac{R_0}{r} \right)^6 \qquad 2.19.$$

Here, τ_D is the decay time of the donor in the absence of acceptor, r the distance between the donor and acceptor molecule and R_0 is the Förster distance, i.e. the distance at which energy transfer is 50% efficient. In other words, R_0 is the distance where 50% of the excited donors are deactivated by RET. The magnitude of R_0 is dependent on the spectral properties of the donor and acceptor and can be calculated according to equation 2.20. (in nm).

$$R_0 = \frac{0.0211 \cdot \kappa^{1/3} \cdot \Phi_D^{1/6} \cdot J(\lambda)^{1/6}}{n^{2/3}} \qquad 2.20.$$

where κ is the orientation factor which equals $\sqrt{\frac{2}{3}}$ for a random distribution of donor and acceptor molecules, Φ_D is the luminescence quantum yield of the donor in the absence of acceptor, $J(\lambda)$ is the spectral overlap integral which represents the degree of overlap between the donor's luminescence spectrum and the acceptor's absorbance spectrum (equation 2.21.) and n is the refractive index of the medium.

$$J(\lambda) = \frac{\int_0^\infty F_D(\lambda) \cdot \varepsilon_A(\lambda) \cdot \lambda^4 \cdot d\lambda}{\int_0^\infty F_D(\lambda) \cdot d\lambda} \qquad 2.21.$$

where $F_D(\lambda)$ is the corrected fluorescence intensity of the donor over the total wavelength range, with the total intensity (i.e. the area under the curve) normalized to unity. With $\varepsilon_A(\lambda)$ being the molar absorbance of the acceptor at the wavelength λ, $J(\lambda)$ can be calculated from experimental data.

Substituting R_0 from equation 2.20. in equation 2.19. leads to a new expression for k_T given in equation 2.22.

$$k_T = \frac{8.82 \cdot 10^{-11} \cdot \kappa^2 \cdot J(\lambda) \cdot \lambda_D}{\mathrm{r}^6 \cdot n^4} \qquad 2.22.$$

where λ_D is the emissive rate of the donor, which is the quotient of the quantum yield Φ_D and the natural lifetime τ_D in the absence of the acceptor (equation 2.23.).

$$\lambda_D = \frac{\Phi_D}{\tau_D} \qquad 2.23.$$

The distance r is a critical parameter since no energy transfer will occur if r is too large. On the other hand, RET is too efficient if r is too small. Optimal distances range from 20 to 50 Å. Compare chapter 5.3.2. for practical RET calculations for the Ru(dpp)/bromophenol blue system.

2.6. Light scattering

To characterize dispersions of colloidal size particles, two of the most important parameters are the particle size and the zeta potential[37-38]. Particle sizes can be determined by light scattering studies, whereas zeta potentials can be determined by laser Doppler velocimetry (chapter 2.7.)[39-43]. Two different methods based on light scattering can be used to characterize nanospheres: static and dynamic light scattering[44].

2.6.1. Static light scattering

Static light scattering, also known as classical or Rayleigh scattering, provides a direct measure of molecular mass[45]. It is therefore very useful for determining whether the native state of a protein is a monomer or a higher oligomer and for measuring the masses of aggregates or other non-native species. It also can be used for measuring the stoichiometry of complexes between different proteins, e.g. receptor-ligand complexes or antibody-antigen complexes[46].

Static light scattering involves measurement of the amount of light scattered by a solution at a certain angle relative to the incident laser beam. For globular proteins smaller than about 500 kDa, the intensity of the scattered light is uniform in all directions, so it is only necessary to measure scattering at a single angle (usually 90°). The intensity of this scattered light is proportional to the product of the protein concentration (in mg/mL) multiplied by its molecular mass. For higher masses or rod-like or unfolded proteins, the efficiency of scattering varies significantly with angle. By measuring the scattering at additional angles, direct absolute measurements of masses can be made and the geometric size can also be determined. Since the signal from the light detector is directly proportional to the molecular mass of the protein times the concentration, by combining this signal with that from a concentration detector (refractive index or absorbance) it is possible to measure the molecular mass of each peak coming off the column.

2.6.2. Dynamic light scattering (DLS)

Dynamic light scattering (DLS), which is also known as photon correlation spectroscopy (PCS) or quasi-elastic light scattering (QELS), uses the scattered light to measure the rate of diffusion of the protein particles[45]. This motion data is conventionally processed to derive a size distribution for the sample, where the size is given by the Stokes' radius or hydrodynamic radius of the particle. This hydrodynamic size depends on both mass and shape (conformation). Dynamic scattering is particularly good at sensing the presence of very mall amounts of aggregated protein (< 0.01% by weight) and studying samples containing a very large range of masses. It forms one of the fundamentals of the widely applied nephelometric immunoassays.

In dynamic light scattering one measures the time dependence of the light scattered from a very small region of solution, over a time range from tenths of a microsecond to milliseconds. These fluctuations in the intensity of the scattered light are related to the rate of diffusion of molecules in and out of the region being studied (Brownian motion) and the data can be analyzed to directly give the diffusion coefficients of the particles doing the scattering. When multiple species are present, a distribution of diffusion coefficients is seen.

Traditionally, rather than presenting the data in terms of diffusion coefficients, the data are processed to give the size of the particles (radius or diameter). The relation between diffusion and particle size is based on theoretical relationships for the Brownian motion of spherical particles, originally derived by Einstein. The hydrodynamic diameter or Stokes radius, derived from this method, is the size of a spherical particle that would have a diffusion coefficient equal to that of the species investigated and the data is commonly presented as the fraction of particles as a function of their diameter.

Most particles are certainly not spherical and their apparent hydrodynamic size depends on their shape (conformation) as well as their molecular mass. Further, their diffusion is also affected by water molecules which are bound or entrapped by the particle. Therefore, this hydrodynamic size can differ significantly from the true physical size (e.g. that seen by NMR or x-ray crystallography) and this size is generally not a reliable measure of molecular mass.

While dynamic scattering is, in principle, capable of distinguishing whether a particle is a monomer or dimer, it is much less accurate for distinguishing small oligomers than is static light scattering or sedimentation velocity. The strength of dynamic scattering is its ability to analyze samples containing broad distributions of species of widely differing molecular masses (e.g. a native protein and various sizes of aggregates) and to detect very small amounts of the higher mass species. Furthermore, because there is no chromatographic separation involved, one does not have to be concerned that particle aggregates are being lost within a chromatographic column.

2.7. Zeta potential and laser Doppler velocimetry (LDV)

There are many aspects of a particle dispersion that need to be investigated to fully characterize a system. Particle size is often considered one of the most important parameters[47]. However, as particle size reduces, the surface area increases significantly in comparison with the volume, so surface properties increasingly determine the characteristics of the dispersion.

ZETA POTENTIAL. Surface charge is one of the significant surface properties. It is an important factor in determining the interactions between particles and hence dispersion characteristics, such as dispersion stability, flocculation, viscosity or film forming characteristics. The surface charge cannot be measured directly. Instead, the charge called the zeta potential is measured at a distance from the particle[48]. This potential is usually more of interest because particles interact according to the magnitude of this value, rather than the potential at the surface of the particle.

The zeta potential is increasingly being used to investigate fine particle systems. It is a consequence of the existence of surface charge and can give information on electrical interaction forces between the dispersed particles. A charged particle dispersed in a liquid containing ions will change the distribution of ions in its vicinity. The overall stability of a system depends on the interaction between individual particles in the dispersion. There are two mechanisms that affect this interaction. The first is due to the particle being charged. If the magnitude of this charge is great enough the repulsion between particles will ensure that the dispersion will resist flocculation. This is electrostatic stabilization. When this repulsion is not high enough, the attractive van der Waals forces always present in the dispersion can cause flocculation or coagulation to occur. A second mechanism, steric stabilization may be present. This is where a surface coating on the particles prevent them from approaching too closely.

Thus, the zeta potential is a measure of the magnitude of the repulsion or attraction between particles. Its measurement brings detailed insight into the dispersion mechanism and is the key to electrostatic dispersion control. Most particles in a polar medium, such as water, possess a surface charge. A charged particle will attract ions of the opposite charge in the dispersant, forming a strongly bound layer close to the surface of the particle. Those ions further away from the core particle make up a diffuse layer, more loosely bound to the particle. Within this diffuse layer is a notional boundary, inside which the particle and its associated ions act as a single entity, diffusing through the dispersion together. The plane at this boundary is known as the surface of hydrodynamic shear, or the slipping plane. The potential at this boundary is known as the zeta potential. It is important to note that the magnitude of the zeta potential is affected by both the nature of the surface of the particle and the composition of the dispersant.

The interaction of particles in polar liquids is not governed by the electrical potential at the surface of the particle, but by the potential that exists at the slipping plane. The zeta potential and surface charge can be entirely unrelated, so measurement of surface charge is not useful indication of particle interaction. Therefore, to utilize electrostatic control, it is the zeta potential of a particle that needs to be known rather than its surface charge.

LASER DOPPLER VELOCIMETRY (LDV). Laser Doppler anemometry (LDA) is a tool for fluid dynamic investigations in gases and liquids and is used to determine the zeta potential[49]. It is a well-established technique that gives information about flow velocity. The laser beam is divided into two and the focusing lens forces the two beams to intersect. The photodetector receives light scattered from tracer particles moving through the intersection volume and converts light intensity into an electrical current. The scattered light contains a Doppler shift (the Doppler frequency) which is proportional to the velocity component perpendicular to the bisector of the two laser beams. With a known wavelength of the laser light and a known angle between the intersecting beams, a conversion factor between the Doppler frequency and the velocity can be calculated. The tracer particles scatter light in all directions, with the highest intensity in forward scatter, i.e. away from the laser. Much less light is scattered in other directions, but direct backscatter is often used, because it allows integration of the transmitting and receiving optics in a single head.

2.8. Electron microscopy

Electron microscopes are instruments that use a beam of highly energetic electrons to examine objects on a very fine scale[50-52]. This examination can yield the following information: (1) Topography, i.e. the surface features of an object, its texture, or a direct relation between these features and materials properties (hardness, reflectivity). (2) Morphology, i.e. the shape and size of the particles making up the object, or a direct relation between these structures and materials properties (ductility, strength, reactivity). (3) Composition, i.e. the elements and compounds that the object is composed of and the relative amounts of them, or a direct relationship between composition and materials properties (melting point, reactivity, hardness). (4) Crystallographic information, i.e. how the atoms are arranged in the object, or a direct relation between these arrangements and materials properties (conductivity, electrical properties, strength).

Electron microscopes function exactly as their optical counterparts except that they use a focused beam of electrons instead of light to image the specimen and gain information as to its structure and composition[53-54]. There are four basic steps involved in all electron microscopes: (1) A stream of electrons is formed (by the electron source) and accelerated toward the specimen using a positive electrical potential. (2) This stream is confined and focused using metal apertures and magnetic lenses into a thin, focused, monochromatic beam. (3) This beam is focused onto the sample using a magnetic lens. (4) Interactions occur inside the irradiated sample, affecting the electron beam. These interactions and effects are detected and transformed into an image.

2.8.1. Transmission electron microscopy (TEM)

The transmission electron microscope (TEM) allows the user to determine the internal structure of materials, either of biological or non-biological origin[50-51]. Materials for TEM must be specially prepared to thicknesses which allow electrons to transmit through the sample, much like light is transmitted through materials in conventional optical microscopy. Because the wavelength of electrons is much smaller than that of light, the optimal resolution attainable for TEM images is many orders of magnitude better than that from a light microscope. Thus, TEMs can reveal the finest details of internal structure, in some cases as small as individual atoms. Magnifications of 350,000 times can be routinely obtained for many materials, whilst in special circumstances, atoms can be imaged at magnifications greater than 15 million times.

For biological samples, cell structure and morphology is commonly determined whilst the localization of antigens or other specific components within cells is readily undertaken using specialised preparative techniques. For non-biological materials, phase determination as well as defect and precipitate orientation are typical outcomes of conventional TEM experiments. Microstructural characterization of non-biological materials, including unit cell periodicities, can be readily determined using various combinations of imaging and electron diffraction techniques. Images obtained from a TEM are two-dimensional sections of the material under study, but applications which require three-dimensional reconstructions can be accommodated by these techniques.

The energy of the electrons in the TEM determine the relative degree of penetration of electrons in a specific sample, or alternatively, influence the thickness of material from which useful information may be obtained. Because of the high spatial resolution obtained, TEMs are often employed to determine the detailed crystallography of fine-grained, or rare, materials.

2.8.2. Scanning electron microscopy (SEM)

The scanning electron microscope (SEM) is one of the most versatile and widely used tools of modern science as it allows the study of both morphology and composition of biological and physical materials[50-51].

By scanning an electron probe across a specimen, high resolution images of the morphology or topography of a specimen, with great depth of field, at very low or very high magnifications can be obtained. Characterization of fine particulate matter in terms of size, shape and distribution as well as statistical analyses of these parameters, may be performed.

3. Preparation and Characterization of Inert Phosphorescent Nanospheres

A SIMPLE ENCAPSULATION TECHNIQUE IS PRESENTED TO PRODUCE HIGHLY PHOSPHORESCENT, INERT NANOSPHERES WHICH ARE SUITABLE LUMINESCENT LABELS. IT IS BASED ON THE CO-PRECIPITATION OF PHOSPHORESCENT RUTHENIUM(II)-TRIS(POLYPYRIDYL) COMPLEXES AND POLYACRYLONITRILE (PAN) DERIVATIVES FROM A SOLUTION IN N,N-DIMETHYLFORMAMIDE. THE BEADS PRECIPITATE IN THE FORM OF VERY SMALL AGGREGATES OF SPHERICAL SHAPE AND A TYPICAL PARTICLE DIAMETER OF LESS THAN 50 NM. THIS PROCESS ALLOWS THE ENCAPSULATION OF PHOSPHORESCENT AND FLUORESCENT DYES IN AN INDIVIDUAL NANOSPHERE PROVIDED THAT THEY ARE SUFFICIENTLY LIPOPHILIC. QUENCHING BY OXYGEN IS NEGLIGIBLE DUE TO THE USE OF PAN.

THE NANOSPHERES WERE CHARACTERIZED WITH RESPECT TO THEIR SPECTRAL PROPERTIES (QUANTUM YIELDS OF THE LUMINOPHORES, BRIGHTNESS, LUMINESCENCE DECAY TIME), STABILITY IN AQUEOUS BUFFERED SUSPENSIONS AND IN TERMS OF SIZE, SHAPE AND SURFACE CHARGE OF THE PARTICLES, AS WELL AS STORAGE STABILITY, QUENCHING BY OXYGEN AND DYE LEACHING.

3.1. Introduction

Micro- and nanospheres are popular tools for the use as labels in optical luminescence and bioanalysis to increase the sensitivity of assays[4, 55-60]. Intrinsic background fluorescence of samples is a problem often faced in optical analysis. When trying to eliminate background luminescence, two approaches are feasible. On the one hand, NIR dyes can be used since most samples show no fluorescence in this region[15-16, 61]. On the other hand, phosphorescent dyes with long decay times can be employed[62]. Here, the background fluorescence decays comparatively fast and can be eliminated by the measuring arrangement. The latter pathway shall be discussed here.

Basically, three groups of phosphorescent dyes are known that are potentially useful for labelling biomolecules. The first and most important group includes rare earth metal chelates, such as Eu(III)- or Tb(III)-complexes[63-72]. Such lanthanoide complexes are excitable in the UV-region only, for instance with a xenon flash lamp and their lifetimes can be as long as 1 ms. Despite the advantage that the phosphorescence of those chelates is hardly quenched by oxygen, they suffer from the fact that they must be excited by UV-light sources. Nevertheless, they are very useful in single-shot assays. The second group comprises the Pt- and Pd-complexes of porphyrins with lifetimes between 40 μs and 1 ms. Unfortunately, these are strongly quenched by oxygen and other notorious quenchers. The third type of long-lived luminescent dyes includes the ruthenium, osmium and rhenium complexes with polypyridyl ligands. Their lifetimes are between 100 ns and 10 μs[73-78]. The latter two groups of luminophores can be excited by semiconductor light sources in the visible region. The third group is cationic but their counter anions can easily be exchanged. However, those compounds are prone to luminescence quenching by both oxygen and oxidative or reductive quenchers, even though quenching in less crucial than for the Pt- or Pd-porphyrins.

One efficient way to prevent quenching consists in shielding the dyes from quenching gases or ions. This is accomplished by encapsulation of the dyes in micro- or nanospheres of a material that is impermeable to oxygen. Polystyrene and poly(methyl methacrylate) are common materials to produce micro- and nanospheres. However, they are permeable to oxygen so that some quenching still occurs.

It was shown recently that ruthenium(II) complexes dissolve in films of polyacrylonitrile (PAN) and these are not at all quenched by oxygen. Such materials were applied to design luminescent temperature sensors[79]. Thin films of polyacrylonitrile are also used as gas-impermeable barrier in food technology.

By taking advantage of those findings, luminescent transition metal complexes were encapsulated in beads made of polyacrylonitrile and various copolymers. A simple technique for manufacturing phosphorescent nanospheres in high quantities and in a reproducible manner is presented[80]. The resulting nanospheres are practically not quenched by oxygen. The spheres are characterized in terms of spectra, photophysical properties, storage stability in aqueous suspensions and in terms of particle size, shape and surface charge, quenching by oxygen and dye leaching.

3.2. Materials and methods

3.2.1. Chemicals and reagents

All chemicals and solvents used were of analytical grade and used without further purification. Doubly distilled water was used throughout. All polyacrylonitrile copolymers of Table 3.1. (polymers **2** – **9**) were obtained from Optosense (Wörth a. d. Isar, Germany). The films were prepared on a 125 µm thick 35 x 105 mm polyester support (Mylar) from Du Pont (Geneva, Switzerland). The names, net formulas, molecular weights and suppliers of all other reagents used in the experiments are listed in Table 3.2.

Table 3.1. Matrix composition of polyacrylonitrile copolymers.

polymer	**main monomer (= acrylonitrile, -CN) [% (w/w)]**	**type of comonomer (reactive groups)**	**comonomer [% (w/w)]**
1	100.0	-	-
2	95.0	acrylic acid (-COOH)	5.0
3	90.0	acrylic acid (-COOH)	10.0
4	87.0	acrylic acid (-COOH)	13.0
5	76.9	acrylic acid (-COOH)	23.1
6	95.0	ethylene glycol (-OH)	5.0
7	83.4	acrylic acid (-COOH), ethylene glycol (-OH)	8.3, 8.3
8	87.0	acrylic acid (-COOH), sulfonic acid ($-SO_3H$)	4.3, 8.7
9	90.0	primary amine ($-CONH(CH_2)_2NH_2$)	10.0

Table 3.2. Chemicals and solvents used in the experiments of chapter 3.

name	**net formula**	**MW [g/mol]**	**company**
3-(trimethylsilyl)-1-propane-sulfonic acid, sodium salt = Na-TMS	$(CH_3)_3Si(CH_2)_3SO_3Na$	218.33	Aldrich (Taufkirchen, Germany)
4,7-diphenyl-1,10-phenanthroline = bathophenanthroline	$C_{24}H_{16}N_2$	332.41	Lancaster (Mühlheim a. Main, Germany)
cetyltrimethylammonium bromide = CTAB	$C_{19}H_{42}BrN$	364.46	Merck (Darmstadt, Germany)
acetone	C_3H_6O	58.08	Merck
dimethyl sulfoxide, deuterated = DMSO	C_2H_6OS-d_6	84.18	Deutero (Kastellaun, Germany)
disodium hydrogen phosphate dihydrate	$Na_2HPO_4 \cdot 2H_2O$	177.99	Merck
ethanol	C_2H_6O	46.07	Merck
ethylene glycol	$C_2H_6O_2$	62.07	Merck
glycogen	$(C_6H_{10}O_5)_x$	-	Merck
hydrogen peroxide, 30%	H_2O_2	34.01	Merck
methanol, deuterated	CH_3OH-d_4	36.07	Deutero
N,N-dimethylformamide = DMF	C_3H_7NO	73.10	Merck
polyacrylonitrile	-	150,000	Polysciences (Warrington/PA, USA)
ruthenium (III) chloride	$RuCl_3$	207.43	Lancaster
ruthenium(II)-tris-2,2-bi-pyridyl chloride hexahydrate = $Ru(bipy)_3Cl_2 \cdot 6H_2O$	$RuC_{30}H_{24}N_6Cl_2 \cdot 6H_2O$	748.63	Aldrich
ruthenium(II)-tris-4,7-diphenyl-1,10-phenanthroline bis-trimethyl-silylpropane-sulfonate = $Ru(dpp)_3(TMS)_2$	$RuSi_2C_{84}H_{78}N_6S_2O_6$	1488.95	synthesis (chapter 3.2.3.)
ruthenium(II)-tris-4,7-diphenyl-1,10-phenanthroline dichloride = $Ru(dpp)_3Cl_2$	$RuC_{72}H_{48}N_6Cl_2$	1169.20	synthesis (chapter 3.2.3.) [a]
sodium azide	NaN_3	65.01	Merck
sodium chloride	$NaCl$	58.44	Merck

name	**net formula**	**MW [g/mol]**	**company**
sodium dihydrogen-phosphate monohydrate	$NaH_2PO_4 \cdot H_2O$	137.99	Merck
sodium hydroxide pellets	NaOH	40.00	Merck
sulfuric acid, 95-97%	H_2SO_4	98.08	Merck
TransFluoSpheres, carboxylate-modified microspheres	-	-	Molecular Probes (Eugene/OR, USA)
trehalose	$C_{12}H_{22}O_{11}$	342.30	Merck

[a] $Ru(dpp)_3Cl_2$ is now available from Fluka (Buchs, Switzerland)

3.2.2. Instrumentation and measurements

3.2.2.1. Buffers and ionic strength

Buffer compositions for all solutions were calculated according to Beynon and Easterby[81]. This theory is based on the Debeye-Hückel theory and allows the calculation of buffer composition at a defined pH, buffer concentration and ionic strength[82]. According to Lewis and Randall, the ionic strength (IS) is defined by equation 3.1.[83-84].

$$IS = \frac{1}{2} \cdot \sum_{i=1}^{n} c_i \cdot z_i^2 \qquad 3.1.$$

where c_i are the concentrations of the different ionic species in mM and z_i are their respective ionic valencies.

3.2.2.2. Absorbance measurements

Absorbance spectra were run on a UV/VIS scanning spectrophotometer U-3000 from Hitachi (Düsseldorf, Germany), shown in Figure 3.1., using a deuterium and a tungsten iodide lamp. Quartz cuvettes with a cell length of 1 cm and covered with a plastic lid in order to prevent evaporation of the solvents were used to measure the spectra of solutions. The baseline was determined against the applied solvents in the appropriate ratios as reference. Spectroscopic absorbance studies of sensor membranes were performed with a membrane fixing device against a blank polyester foil in the reference optical path.

Figure 3.1. Hitachi UV-VIS scanning spectrophotometer.

3.2.2.3. Luminescence measurements

Luminescence excitation and emission spectra were acquired on an Aminco-Bowman Series 2 luminescence spectrometer from SLM-Aminco (Rochester/NY, USA), shown in Figure 3.2. The spectrometer was equipped with a continuous wave 150-W xenon lamp as light source. Spectroscopic luminescence studies of sensor membranes were performed with a membrane fixing device.

Figure 3.2. SLM-Aminco luminescence spectrometer.

3.2.2.4. Fluorescence decay time measurements

Luminescence frequency spectra (1 – 1000 kHz) or fluorescence decay time measurements were acquired on a K2 multifrequency phase fluorometer from ISS (Champaign/IL, USA), using a 150-W continuous xenon lamp (PS 300-1) from ILC Technology (Sunnyvale/CA, USA) as excitation light source and two signal generators 2022D from Marconi Instruments (Dalgety Bay, UK). The light was passed through a Pockels' cell which provided modulated light. Emission was detected at 90° to the excitation through a blue bandpass filter (FTICA) from Schott (Mainz, Germany). Lifetimes were referenced against a dilute solution of glycogen (0.75 g/L).

3.2.2.5. Phosphorescence decay time measurements

All non-fluorescence decay time measurements were performed with a fiber-optic set-up pictured in Figure 3.3. The modulation frequency depends on the ruthenium metal-ligand complex used and is 45 kHz for Ru(dpp). Phosphorescent dyes were excited with sinusoidally modulated light. A dual-phase lock-in amplifier DSP 830 from Stanford Research (Gilching, Germany) was used for modulating the LED and for lock-in measurements of the phase shifts (i.e. phase angles) of luminescence[85].

Figure 3.3. Stanford Research lock-in amplifier.

The optical system consists of a blue LED NSPB 500 from Nichia (Nürnberg, Germany) as light source (λ_{max} 470 nm), combined with a blue bandpass filter (FTICA) from Schott or a HT141 Bright Blue filter from LEE P.P.V. Lighting (Brussels/Belgium), a bifurcated glass fiber bundle (NA 0.46, ∅ 2 mm) connected to a thermostated (25 °C) home made black cuvette holder and a red-sensitive photomultiplier tube (PMT, H5701-02) from

Hamamatsu (Herrsching, Germany). Emission light was filtered with convenient high pass filters, such as the 135 Deep Golden Amber filter from LEE P.P.V. Lighting, or an OG570 filter from Schott. The quartz cuvette containing the sample was fixed in a 90° angle to the excitation light source, as pointed out in Figure 3.4. With this set-up of a 90° detection angle, the highest possible sensitivity is achieved, i.e. a maximum signal with minimal background.

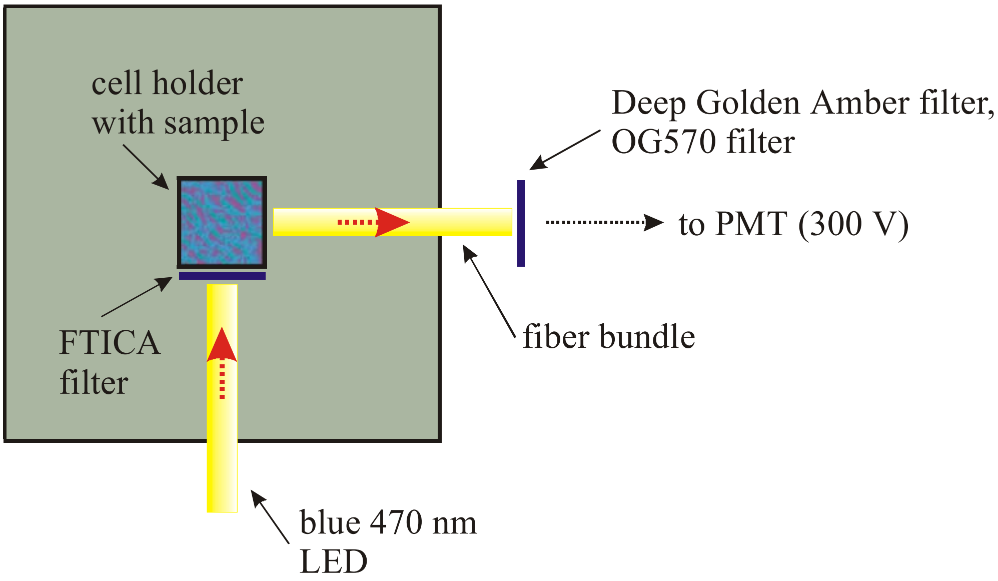

Figure 3.4. Cuvette holder with fiber-optic set-up for measurement of phase angles for calculation of decay times.

MEASUREMENT OF MEMBRANES. Decay time measurement of membranes in gases was carried out as follows. A flow of either oxygen (0.200 mbar), nitrogen (0.100 mbar) or air was passed first through a bubbler into a gas-washing bottle filled with water and then into an empty gas-washing bottle with the respective membrane attached with silicone grease to the inside wall of the glass bottle. Both gas-washing bottles were thermostated at 25 °C. Before each decay time measurement, the system was equilibrated for 20 min. For the measurement of membranes in gas-saturated water, the second gas-washing bottle containing the membrane was filled with water, as well.

3.2.2.6. pH measurements

The pH values were determined at 25 °C with a Calimatic digital pH meter from Knick (Berlin, Germany) calibrated to standard buffer solutions of pH 7.0 and pH 4.0 from Merck.

TITRATION OF CARBOXYLATED NANOSPHERES. In chapter 3.3.6.2., non-buffered aqueous suspension of carboxylated nanospheres were titrated with 10^{-4} N NaOH in order to determine the content of carboxy groups on the nanosphere surface. A mixed indicator, with a color change from purple (acidic) to green (basic), served as indicator dye.

3.2.2.7. Instruments for analyses of organic compounds

ELEMENTAL ANALYSES. Elemental analyses (C, H, N) were carried out on a CHN-Rapid analyzer from Heraeus (Hanau, Germany).

INFRARED SPECTRA. IR spectra were obtained with an Infrared Spectrophotometer 881 from Perkin-Elmer (Rodgau-Jügesheim, Germany). The wavenumbers $\bar{\nu}$ are given in cm^{-1} and the peak intensities are described by the following abbreviations: br = broad, s = strong, m = medium, w = weak.

FT-IR. Fourier transformation infrared spectra were acquired on a FTS 155 spectrophotometer from Bio-Rad (Munich, Germany).

MASS SPECTRA. Mass spectra were taken either with a MAT 311A Mass Spectrometer from Varian (Palo Alto/CA, USA) or a MAT 95 Mass Spectrometer from Finnigan (San Jose/CA, USA).

MAGNETIC NUCLEAR RESONANCE SPECTRA. ^{1}H-NMR and ^{13}C-NMR spectra were acquired either on a 250.13 MHz AC250 or on a 400.13 MHz ARX400 PFT-NMR Spectrometer from Bruker (Rheinstetten, Germany). Tetramethylsilane was used as an internal reference. The chemical shifts δ are given in ppm and the peaks are classed with the following abbreviations: s = singlet, d = doublet, dd = doublet of doublets, t = triplet, q = quartet, m = multiplet.

MELTING POINTS. Melting points are uncorrected and were measured with a melting point apparatus Thermogalen III from Leica (Bensheim, Germany). They were determined on a micro heating stage microscope with a temperature maximum of 350 °C.

3.2.2.8. Electron microscopy

TRANSMISSION ELECTRON MICROSCOPY (TEM). Transmission electron microscopic pictures were recorded on an EM208 S transmission electron microscope from Philips (Eindhoven, The Netherlands). Microscope support grids were prepared as follows: The copper grids were rinsed first with ethanol and then water, then dipped into a surfactant solution of 7.3 mg (0.02 mmol) CTAB in 20 mL water (1 mM) for 1 min and rinsed with water once. Now the positively charged grids were dipped into the respective suspensions of carboxylated nanospheres for 1 min and again rinsed with water. After this procedure the nanospheres are spatially fixed onto the grids and could be examined under the TEM.

SCANNING ELECTRON MICROSCOPY (SEM). Scanning electron microscopic pictures were recorded on a JSM-5600LV scanning electron microscope from JEOL (Peabody/MA, USA), shown in Figure 3.5. Microscope glass slides were prepared as follows: The slides were washed with a sulfuric acid (95 – 97%)/hydrogen peroxide (30%) mixture (70:30, v/v), then dipped into a surfactant solution of 7.3 mg (0.02 mmol) CTAB in 20 mL water (1 mM) for 1 min and rinsed with water once. Now the positively charged glass plates were dipped into the respective suspensions of carboxylated nanospheres for 1 min and again rinsed with water. After this procedure the nanospheres are spatially fixed onto the glass slides and could be examined under the SEM.

Figure 3.5. JEOL scanning electron microscope.

3.2.2.9. Light scattering

STATIC LIGHT SCATTERING. Static light scattering data were acquired with a KGS-2 compact goniometer system from ALV (Langen, Germany).

DYNAMIC LIGHT SCATTERING. Dynamic light scattering exeriments were also performed on a KGS-2 compact goniometer system from ALV.

3.2.2.10. Laser Doppler velocimetry

Laser Doppler velocimetry experiments to determine the zeta potential of nanospheres were done with a Zetasizer 3000 from Malvern (Herrenberg, Germany), shown in Figure 3.6.

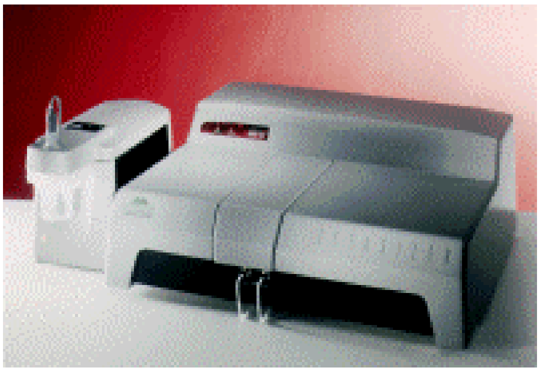

Figure 3.6. Malvern zeta potential measuring equipment.

3.2.2.11. Freeze drying

Freeze drying of nanosphere suspensions was accomplished with a Modulyo freeze dryer and an E2M8 high vacuum pump, both from Edwards (Crawley, UK), at -60 °C and $0.75 \cdot 10^3$ Pa. Before putting the aqueous suspensions into the lyophilizer, they were cooled in liquid nitrogen[86].

3.2.3. Preparation of ruthenium(II)-tris-4,7-diphenyl-1,10-phenanthroline bis-trimethylsilylpropanesulfonate [$Ru(dpp)_3(TMS)_2$] and ruthenium(II)-tris-4,7-diphenyl-1,10-phenanthroline dichloride [$Ru(dpp)_3Cl_2$]

1.78 g (8.6 mmol) of ruthenium (III) chloride were dissolved in 75 mL of ethylene glycol and 6.0 mL of water. The solution was heated to 120 °C. Then 10.0 g (30.1 mmol) of 4,7-diphenyl-1,10-phenanthroline were added at once and the solution was refluxed (~ 150 °C) for 70 min. After hot filtration the precipitate was discarded and 200 mL of ethanol were added to the remaining solution. This solution was separated in half and used for the following preparations of $Ru(dpp)_3(TMS)_2$ and $Ru(dpp)_3Cl_2$[87-89].

PREPARATION OF $RU(DPP)_3(TMS)_2$. The first half (approximately 140 mL) of the red solution were slowly poured to a solution of 2 g (9.2 mmol) of the sodium salt of 3-(trimethylsilyl)-1-propanesulfonic acid in 250 mL of water (36.8 mM), upon which the color turned to orange. The precipitate was filtered with suction and washed four times with water. Further purification was accomplished by recrystallization from an acetone/water mixture (80:20, v/v). Finally, the precipitate was washed with diethyl ether and dried in vacuum at 40 °C over night.

Yield: 5.72 g (3.84 mmol, 89.4%), orange powder, $RuSi_2C_{84}H_{78}N_6S_2O_6$ (1488.95 g/mol).

Elemental analysis: calculated/found for $RuSi_2C_{78}H_{66}N_6S_2O_6$: C: 67.76/67.46, H: 5.28/5.41, N: 5.64/5.89.

^{1}H-NMR (400 MHz, CH_3OH-d_4, 294 K): for numbering of atoms in the ligand see Figure 3.7.

identifier	δ_H **[ppm]**	**J [Hz]**	**multiplicity**	**number of H**
N-CH-2	8.39, 9.14	5.52, 4.60	dd	6
CH-5/6	7.91, 8.32	-	s, s	6
N-C-CH-3	7.73, 7.78	4.60, 5.52	dd	6
ArH-4	7.57-7.68	-	m	30
solvent (OH-d_1)	4.88	-	s	1
solvent (CH_3-d_3)	3.30	-	s	3
C-CH_2-SO_3	2.78	-	t	4
Si-C-CH_2-C	1.78	-	m	4
Si-CH_3	1.78	-	m	18
Si-CH_2-C	0.60	-	t	4

MS (ESI, solvent: CH_3OH): m/z = 549 (K^{2+}, calculated for K: 1098 Dalton), 1293 (K^{2+} + A^-, calculated for K: 1098 Dalton).

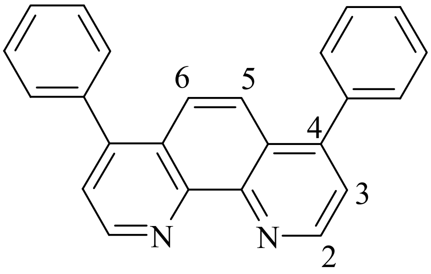

Figure 3.7. Numbering of atoms in the bathophenanthroline ligand for the ^{1}H-NMR identifier.

Preparation of Ru(dpp)$_3$Cl$_2$. The second half (approximately 140 mL) of the red solution were slowly poured to a solution of 1 g (17.1 mmol) of sodium chloride in 250 mL of water (68.4 mM), upon which the color turned to orange. The precipitate was filtered with suction and washed four times with water. Further purification was accomplished by recrystallization from an acetone/water mixture (80:20, v/v). Finally, the precipitate was washed with diethyl ether and dried in vacuum at 40 °C over night.

Yield: 4.53 g (3.88 mmol, 90.2%), orange powder, $RuC_{72}H_{48}N_6Cl_2$ (1169.20 g/mol).

Elemental analysis: calculated/found for $RuC_{72}H_{48}N_6Cl_2$: C: 73.96/73.21, H: 4.14/4.52, N: 7.19/7.04.

^{1}H-NMR (400 MHz, DMSO-d_6, 294 K):

identifier	δ_H **[ppm]**	**J [Hz]**	**multiplicity**	**number of H**
N-CH-2	8.36, 9.16	5.54, 4.49	dd	6
CH-5/6	7.86, 8.28	-	s, s	6
N-C-CH-3	7.73, 7.84	4.49, 5.54	dd	6
ArH-4	7.57-7.67	-	m	30
solvent (DMSO-d_6)	2.49	-	s	6

MS (ESI, solvent: CH_3OH): m/z = 549 (K^{2+}, calculated for K: 1098 Dalton), 1133 ($K^{2+} + Cl^-$, calculated for K: 1098 Dalton).

3.2.4. Preparation of nanospheres

3.2.4.1. Preparation of polyacrylonitrile nanospheres

118.5 mg of polymer **1** and 1.19 mg of $Ru(dpp)_3Cl_2$ were dissolved in 25 mL of DMF (ρ_{DMF} 0.948 kg/L). While stirring vigorously, 125 mL of water was added dropwise with a dropping funnel upon which the solution turned slightly opalescent due to the spontaneous formation of the nanospheres after addition of the initial roughly 20 mL of water. Then, 1 mL of a saturated aqueous solution of sodium chloride (360 g/L at 20 °C) was pipetted to the flask at once to precipitate the finely dispersed nanospheres. The DMF/water mixture was centrifuged at 3000 rpm for 15 min and the colored residue washed twice with 50 mL of a 5% (w/w) sodium chloride solution and then three times with 50 mL of water, the wash solutions always being colorless. The residue was taken up in 50 mL of water and heated to 70 °C for 15 min. They were centrifuged and then taken up in 50 mL of phosphate buffer (pH 7.0, IS 20 mM, 0.5% (w/w) sodium azide, 0.5% (w/w) trehalose). After sonification for 1 h, the suspensions were stored in the dark at 10 °C.

3.2.4.2. Preparation of poly-(acrylonitrile-co-polymer) nanospheres

118.5 mg of polymers **2** – **9** (for samples **2** and **5** – **11**), 59.3 mg of polymer **2** (for sample **3**) or 23.7 mg of polymer **2** (for sample **4**) and 1.19 mg (for samples **2** and **5** – **11**), 0.59 mg (for sample **3**) or 0.24 mg (for sample **4**) $Ru(dpp)_3Cl_2$ were dissolved in 25 mL of DMF. While stirring vigorously, 125 mL of a 1 mM solution of sodium hydroxide (for samples **2** – **7** and **9** – **10**), 125 mL of water (for sample **8**) or 125 mL of 1 mM hydrochloric acid (for sample **11**) were added dropwise with a dropping funnel. After addition of roughly 20 mL of either sodium hydroxide (samples **2** – **7** and **9** – **10**), water (sample **8**), or hydrochloric acid (sample **11**), spontaneous formation of nanospheres occurred. Except for samples **8** and **11** where the suspensions turned turbid, all other solutions remained clear. Then, hydrochloric acid was added to samples **2** – **10** and sodium hydroxide solution to sample **11** until the pH was 4.0 for samples **2** – **10** and 9.0 for sample **11**. This caused the precipitation of finely dispersed nanospheres. The DMF/water mixtures were centrifuged at 3000 rpm for 15 min, the colored residues washed twice with 50 mL of 10^{-5} M hydrochloric acid (for samples **2** – **10**) or 50 mL of 10^{-5} M sodium hydroxide (for sample **11**) and finally three times with 50 mL of water. All washing solutions remained colorless. The residues were taken up in 50 mL of water and heated to 70 °C for 15 min. They were centrifuged and then taken up in 50 mL of phosphate buffer (pH 7.0, IS 20 mM, 0.5% (w/w) sodium azide, 0.5% (w/w) trehalose). After sonification for 1 h, the suspensions were stored in the dark at 10 °C.

3.2.5. Preparation of membranes

MEMBRANE COCKTAILS. Eleven different membrane cocktails for the samples **1** – **11** (compare Table 3.4.), using the polymers **1** – **9** (compare Table 3.1.), were prepared by dissolving 1.42 mg $Ru(dpp)_3Cl_2$ and 142.2 mg of the respective polymer matrix in 3.0 mL DMF each. This is equivalent to the following concentrations: $c_{matrix/DMF}$ 5.0% (w/w) and $c_{Ru(dpp)/matrix}$ 1.0% (w/w).

KNIFE COATING DEVICE. A home made knife coating device, as shown in a schematic view in Figure 3.8., was used for the preparation of membranes. A strip of polyester (Mylar) foil was cleaned with ethanol. Then about 0.2 mL of the viscous DMF cocktail solution was dropped onto the membrane and knife-coated to a layer thickness of 200 µm before solvent evaporation and curing of the membrane. Afterwards the film was exposed to ambient air at 25 °C and dried over night without further treatment. Assuming equal densities and taking into consideration the thickness of the spacers, this gave an actual thickness of the foil of about 20.0 µm after evaporation of the solvent.

The cocktail mixture adhered well on the polyester support and resulted in an orange, homogeneous sensor membrane. The membranes were stored in the dark in a desiccator under ambient air. They were stable for several days.

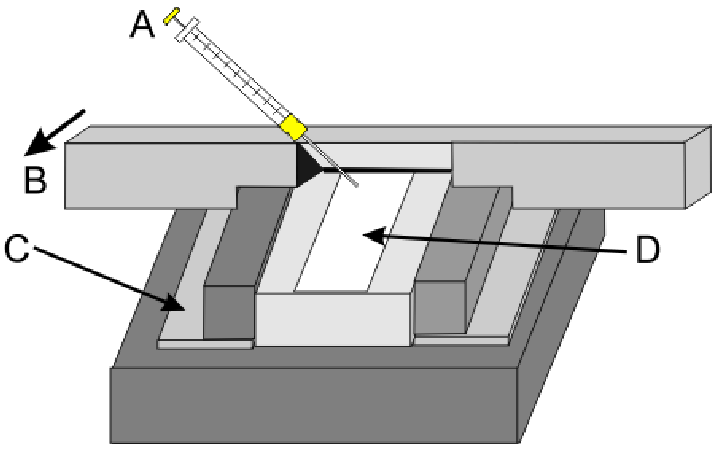

Figure 3.8. Schematic view of the knife coating device, with A = pipette containing the membrane cocktail, B = coating knife, C = spacer and D = polyester support for membrane (Mylar).

3.3. Results and discussion

3.3.1. Choice of polymer matrix

Polyacrylonitrile and its derivatives are attractive polymeric matrices for the encapsulation of phosphorescent dyes in micro- and nanospheres[90-93]. They display an extraordinarily poor permeability for gases and ionic as well as neutral chemical species. Hence, they can protect luminescent dyes against potential luminescence quenchers, such as oxygen. Polyacrylonitrile polymers are soluble in DMF, swell in DMF/water mixtures and themselves act as solvents for lipophilic dyes. In addition to plain polyacrylonitrile, funtional copolymers, such as the ones listed in Table 3.1., were employed. Both anionic and cationic charges were introduced into the polymer and no significant change was observed in the permeability of the copolymers for oxygen.

Polyacrylonitrile is amphiphilic in a sense that it is both hydrophilic and lipophilic. This makes polyacrylonitrile and its functional copolymers soluble in DMF and in turn opens the way to produce nanospheres by the precipitation process. On dropwise addition of water to a diluted solution of polyacrylonitrile in DMF, a stable dispersion of nanoscale polyacrylonitrile aggregates is formed. Surprisingly, the nanospheres do not tend to aggregate and sediment.

If the spheres are precipitated from DMF solutions containing Ru(dpp), the dye is co-precipitated with the spheres. This is an elegant way to stain nanospheres in a defined manner. Solvents other than water may also be used to precipitate the polyacrylonitrile nanospheres provided (a) that the solvent is miscible with DMF and (b) that the polymer is not soluble in the binary mixture. Since polyacrylonitrile and its copolymers are soluble in DMF only (they swell in DMSO), the nanospheres may be suspended in almost any other solvent.

3.3.1.1. Choice of polyacrylonitrile copolymer

Among the various polyacrylonitrile-based copolymers investigated as encapsulation matrices (polymers **2** – **9**), polyacrylonitrile with an acrylic acid content of 5% (w/w) proved to be the best choice as far as a preferable combination of low oxygen quenching, high quantum yields, long decay times and a small nanosphere diameter is concerned.

Carboxy groups are introduced via the copolymerization of acrylic acid into the PAN polymer chains from which the nanospheres are generated by the precipitation process. Upon neutralization with a base, the polyacrylic acid regions swell due to electrostatic repulsion between different carboxy groups to yield pores.

Figure 3.9. shows a plot of the ratio of the area of the nitrile band (centered at 2247 cm^{-1}) and the carboxy band (centered at 1737 cm^{-1}) in the FT-IR against the content of acrylic acid in the respective poly-(acrylonitrile-co-acrylic acid) copolymer[94-95]. This confirms the approximate percentage composition of the acrylic acid copolymers.

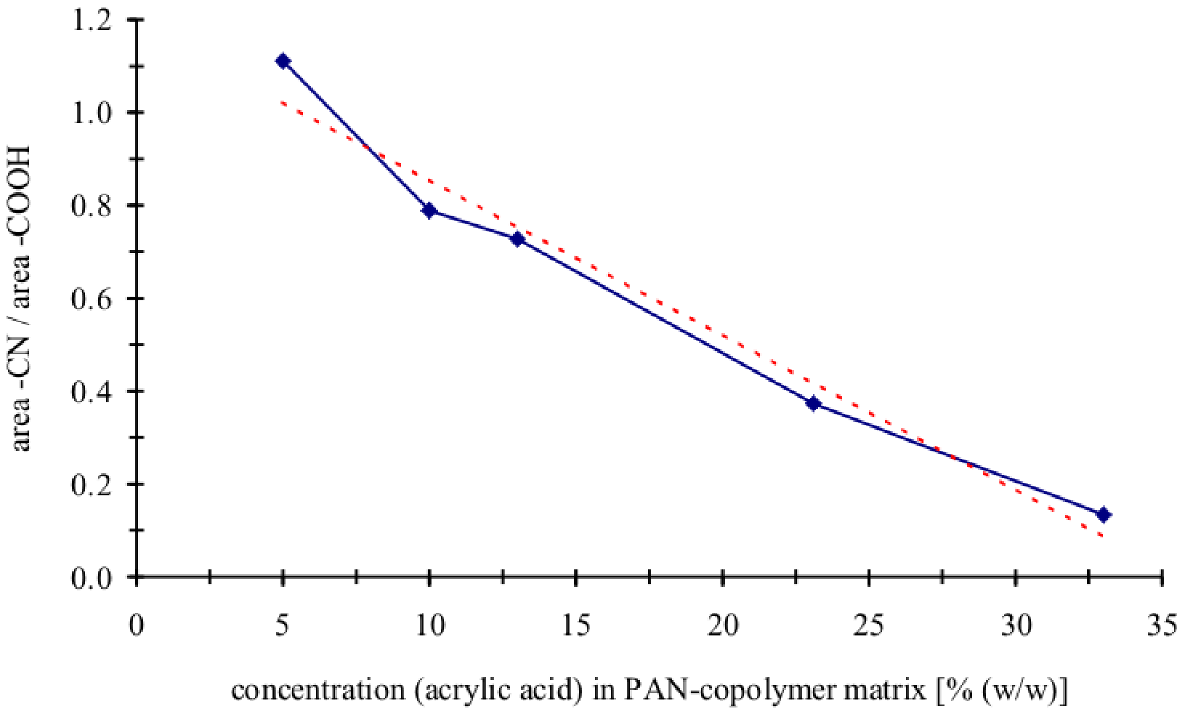

Figure 3.9. Plot of the ratio of the area of the nitrile band (centered at 2247 cm^{-1}) and the carboxy band (centered at 1737 cm^{-1}) in the FT-IR against the content of acrylic acid in the respective poly-(acrylonitrile-co-acrylic acid) copolymer. The dotted red line is a linear fit of the blue curve.

With increasing amount of acrylic acid comonomer, the apparent decay time gets shorter and the quantum yield gets smaller as a result of a more polyelectrolyte character of the nanospheres. When still decreasing the content of acrylic acid, the nanosphere suspensions become more instable due to too little electrostatic repulsion of the surface of the nanospheres. Using other copolymers than acrylic acid-containing ones in order to introduce active groups, such as hydroxyl, sulfonic acid or primary amine groups (polymers **6** – **9**), goes along with a higher oxygen quenching and less stable nanosphere suspensions. The active groups on the surface of the nanospheres (-COOH, -OH, $-SO_3H$, $-NH_2$), depending on the different comonomers used, enable the covalent coupling of biomolecules by conventional methods, as shown in chapter 5.2.4.

3.3.1.2. Matrix concentration

The maximum amount of matrix with respect to its organic solvent that still yields clear solutions is 1.0% (w/w) matrix/DMF but a concentration of 0.5% (w/w) proved to be the optimal choice (compare samples **2** – **4** with 0.50%, 0.25% and 0.10% (w/w) matrix/DMF, respectively). A lower matrix concentration leads to shorter apparent decay times, higher oxygen cross-sensitivity, lower quantum yields and a higher consumption of DMF. A higher percentage, in contrast, results in larger nanosphere diameters and finally makes the precipitation impossible since larger, jelly-like aggregates are formed at the dropping location that cannot be redissolved anymore.

3.3.2. Choice of dye

The requirements to meet for ideal dyes are an extremely good solubility in both PAN (copolymer matrix) and DMF (solvent), insolubility in water for precipitation of the nanospheres and a positive charge to cross-link them with the negatively charged matrix. The long-lived phosphorescent ruthenium(II)-tris-polypyridyl complexes were selected as dyes since they exhibit those positive features[73-74, 88-89, 96]. They yield bright luminescent nanospheres with a large Stokes' shift of about 150 nm (λ_{exc} 465 nm, λ_{em} 613 nm). Due to their positive charge it is possible to cross-link them with copolymers containing negatively charged groups. Furthermore, the dyes can be made lipophilic by using proper ligands. The lipophilic dyes are then extracted quantitatively into the nanospheres during the preparation process because they are very well soluble in the polymer. Even in a lipophilic environment, e.g. if proteins are present in the sample, no dye leaching in aqueous solutions is occurring. The high quantum yields ($\Phi > 40\%$) and the large molar absorbances ($\varepsilon \approx 30{,}000$ L mol^{-1} cm^{-1}) of the ruthenium dyes are further advantages. They are excitable with an argon ion laser at 488 nm or cheap blue light emitting diodes (LEDs) at 450 nm or 470 nm. The use of phosphorescent nanospheres eliminates background fluorescence, leading to a higher sensitivity. Last but not least, the complexes are stable against the loss of ligands and its emission spectrum is broad enough to overlap with the absorbance spectra of various luminescence acceptor dyes.

Among the several ruthenium(II)-tris-polypyridyl complexes, the ruthenium(II)-tris-4,7-diphenyl-1,10-phenanthroline complex Ru(dpp), displayed in Figure 3.10., is most suitable as dye since it is very easily prepared and when incorporated into a PAN-matrix, its quantum yield is the highest and its decay time is the longest, even though the free dye has the highest oxygen quenching of all ruthenium complexes. This shows the superb shielding effect of the matrix. Figure 3.11. shows a photograph of aqueous buffered suspensions of carboxylated nanospheres with incorporated phosphorescent Ru(dpp) dye, when excited with a UV-lamp at 366 nm.

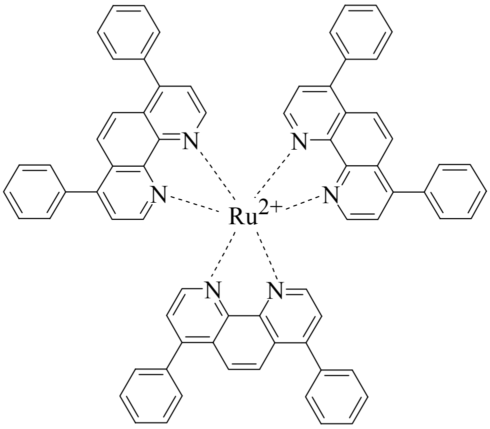

Figure 3.10. Chemical structure of the Ru(dpp) complex.

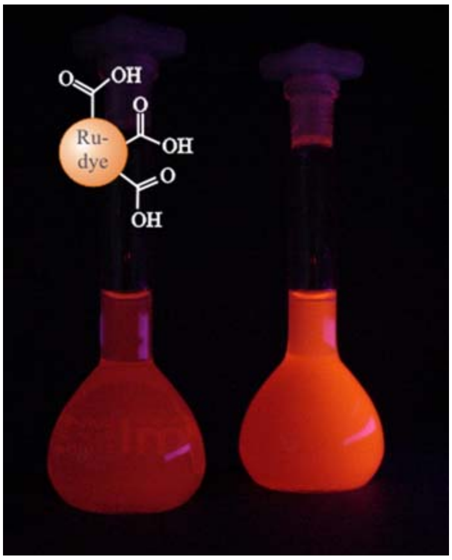

Figure 3.11. Aqueous buffered stock (right flask) and diluted (left flask) suspension of carboxylated nanospheres with incorporated phosphorescent Ru(dpp) dye. The nanospheres were excited with a UV-lamp at 366 nm.

3.3.2.1. Ligand

When using transition metal complexes other than $Ru(dpp)_3$, the apparent decay time does not cover the desired long µs-range anymore. Exchanging the diphenyl-phenanthroline (dpp) ligand against phenanthroline (phen) or bipyridyl (bipy) makes the resulting complexes $Ru(phen)_3$ and $Ru(bipy)_3$ water-soluble. Consequently they cannot be extracted into the polymer matrix. Actually, ruthenium complexes with ligands, such as diphenyl-bipyridyl, show an even lower oxygen cross-sensitivity than diphenyl-phenanthroline but unfortunately a shorter apparent decay time, as well.

3.3.2.2. Counterion

In the application in chapter 4.2.3., trimethylsilylpropanesulfonate (TMS) was used as counterion for $Ru(dpp)^{2+}$. Its chemical structure is pictured in Figure 3.12.

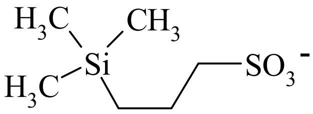

Figure 3.12. Chemical structure of the trimethylsilylpropanesulfonate (TMS) counterion.

However, chloride is preferred as counterion for $Ru(dpp)_3^{2+}$ since the resulting nanosphere suspensions are much more stable due to a cross-linking of the matrix. The chloride ions easily exchange with the carboxy groups on the copolymer surface and thus build a three-dimensional network with the double positive charged ruthenium dye by electrostatic interaction (compare Ca^{2+} as cross-linking agent in alginate fibers). Otherwise individual polymer chains might be washed out.

3.3.2.3. Dye loading

The concentration of incorporated phosphorescent dye is aimed to be as high as feasible in order to yield higher luminescence intensities. The amount of ruthenium complex within the nanospheres can be up to 10% (w/w) dye/matrix for polymer **2**. If this is exceeded, the apparent decay time becomes shorter and the nanosphere suspensions become instable. This is due to a compensation of the repulsing negative carboxy groups on the surface by the double positively charged ruthenium dye. Then aggregates are formed immediately and no dispersions are obtained anymore.

3.3.3. Precipitation details

There are a number of important details in the preparation process of the phosphorescent nanospheres that need to be mentioned. The size, surface charge and reactive groups of the nanospheres can be varied distinctively by the preparation process.

In contrast to the widely used emulsion polymerization, the particles made from polymers **1** – **9** were prepared by a precipitation technique (see Figure 3.13. for the copolymer approach). By using prepolymerized PAN particle systems (long, randomly arranged chains) it is provided that all nanospheres can be made of the same stock polymer which leads to reproducible properties of the nanospheres.

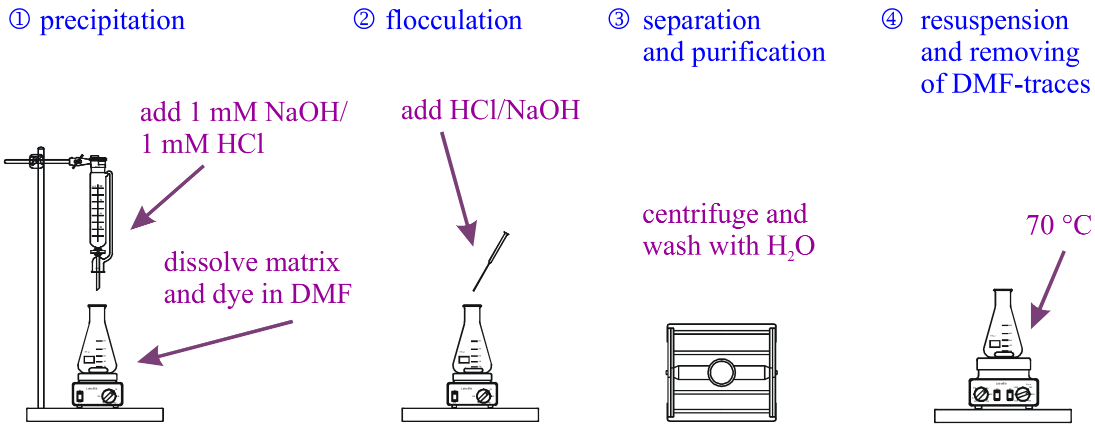
① precipitation
② flocculation
③ separation and purification
④ resuspension and removing of DMF-traces
add 1 mM NaOH/ 1 mM HCl
dissolve matrix and dye in DMF
add HCl/NaOH
centrifuge and wash with H2O
70 °C

Figure 3.13. Schematic of the process for making poly-(acrylonitrile-co-polymer) nanospheres.

Precipitation is a simple and convenient method for the fabrication of nanospheres. Unlike other methods of immobilizing dye molecules into polymer spheres, such as covalent binding of dyes to the outside of polystyrene spheres, the matrix noncovalently traps the luminescent dye into pores inside the matrix. To incorporate a new dye, the process can easily be modified by the addition of that dye into the copolymer solution before precipitation. Since the dye is being trapped into the pores of the matrix during the precipitation process, the leaching out of the dye from the pores during sensor use is minimized, as well.

The amount of doubly distilled water (when starting with polymers **1** and **6**), 10^{-3} M sodium hydroxide (for polymers **2** – **5** and **7** – **8**) or 10^{-3} M hydrochloric acid (for polymer **9**) added to the DMF solution of the matrix and the dye has to be present in at least the five-fold amount compared with the volume of organic solvent in order to extract all of the DMF out of the nanospheres. Adding a 1 mM solution of sodium hydroxide to polymers with acidic comonomer components or 1 mM hydrochloric acid to polymers with basic comonomer components leads to a higher concentration of those reactive comonomer groups on the surface of the nanospheres. This way the hydrophilic parts (e.g. carboxy or amine groups) are primarily on the outside and the PAN main monomer mostly on the inside of the nanospheres. The resulting suspensions are more stable due to electrostatic repulsion of the deprotonated carboxy groups and the protonated amine groups.

The reason for using doubly distilled water is to avoid flocculated systems which would form immediately in the presence of electrolytes. In contrast to other solvents, such as ethanol, for example, water has the advantage that the ruthenium dyes are insoluble here and a complete extraction of the lipophilic dyes into the nanospheres is guaranteed.

The system PAN/DMF/water allows the precipitation of the nanospheres at a defined point of time, controlled by the amount of water in the DMF solution. Moreover, stable dispersions are obtained without any content of emulsifiers, such as sodium dodecyl sulfate (SDS), that would otherwise have to be removed in a complicated process (e.g. by dialysis). During the precipitation process, at a characteristic concentration of between 10 - 20% (w/w) 10^{-3} M sodium hydroxide solution in the DMF solution of the copolymer matrix, the apparent decay time increases sharply (Figure 3.14. for polymer **2**). This is due to the completion of the formation of the nanospheres and a subsequent extraction of DMF out of the nanospheres. Since the decay time measurement was performed in an air-saturated solution what is actually seen is the oxygen quenching which decreases drastically after that point. Now the polymer gets more and more rigid with more water added. Only up to this concentration of roughly 10 – 20% (w/w) water/DMF, depending on the copolymers used, the polymers are soluble in the water/DMF mixture. Afterwards, when adding more water, the nanospheres precipitate which can be observed by the slightly opalescent appearance of the solution. Continuously measuring the apparent decay time of the solution allows to monitor the preparation process and to quantify the amount of water needed to precipitate a specific polymer.

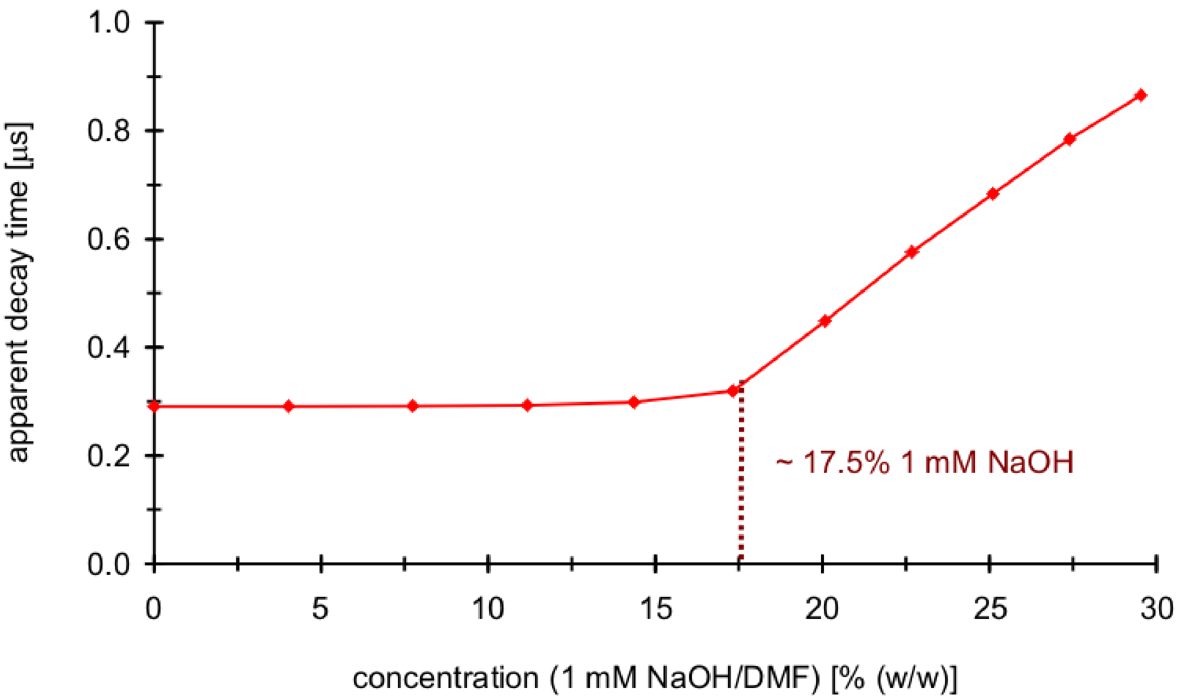

Figure 3.14. Dependance of the apparent decay time on the addition of sodium hydroxide solution to a DMF solution of the matrix during the precipitation process (sample **2**).

When precipitating the nanospheres with hydrochloric acid (polymers **1** – **8**) or sodium hydroxide solution (polymer **9**), the pH should be lowered to approximately 4.0 for the flocculation of the nanospheres with acidic surface groups (polymers **1** – **8**) and to a pH of roughly 9.0 for nanospheres with basic surface groups (polymer **9**). Only then it is provided that the carboxy groups (polymers **1** – **5** and **7** – **8**) on the surface of the nanospheres are all protonated and the amine groups (polymer **9**) are deprotonated. Associates are then formed due to the neutral surface. Since this process is fully reversible, when adjusting the pH back to 7.0, the nanospheres can be suspended once again due to electrostatic repulsion. This shows the importance of the pH value at all preparation stages and the possibility to precipitate or resuspend the nanospheres as needed. It should be mentioned that the nanospheres can be only resuspended from freshly prepared associates. After several days there is a tendency to irreversibly form large and stable aggregates. During the washing steps, no leaching of the dye out of the polymer matrix was be observed.

In order to resuspend the nanospheres, it is sufficient to treat them in an ultrasonic bath for 1 h. The heating of the aqueous suspensions to about 70 °C is meant to remove traces of DMF that might still be present in the suspensions even after the washing steps. Residues of DMF in the nanospheres result in a higher gas permeability and therefore a higher level of oxygen quenching.

3.3.4. Buffer composition and storage conditions

The tendency of the nanospheres to aggregate and their stability in general was also examined. This is of importance for the use of the nanospheres as labels. Nanospheres from pure PAN show a strong tendency to form aggregates. It was found that when kept in phosphate buffer solution (pH 7.0, 100 mM > $\mathrm{IS}_{\text{adjusted with NaCl}}$ > 20 mM, 0.5% (w/w) sodium azide, 0.5% (w/w) trehalose), the nanospheres made of PAN copolymers were stable over a period of several months. No sedimentation in buffered systems was observed. The higher the ionic strength gets, the more repulsion among the nanospheres is created in addition to the one originating from the deprotonated acidic groups (polymers **1** – **8**) or the protonated amine groups (polymer **9**) on the surface, leading to even more stable solutions. An ionic strength of up to 100 mM was successfully applied, as well. The resulting suspensions are clear and stable over months if stored in the dark at 10 °C and thus prove the superb dispersibility of the nanospheres in an aqueous buffered environment. Even storage of freeze-dried nanospheres is possible[86], if stored in the dark at 10 °C, since the nanospheres can be fully resuspended after freeze drying due to the preceding addition of trehalose.

SODIUM AZIDE. The addition of 0.5% (w/w) sodium azide to the buffered suspensions is necessary in order to prevent bacteria growth which would otherwise release carbon dioxide. As a result of the lowered pH value the nanospheres would then start to aggregate over time.

TREHALOSE. α,α-Trehalose (α-D-glucopyranosyl-α-D-glucopyranoside) is a disaccharide with the chemical structure given in Figure 3.15. The addition of 0.5% (w/w) trehalose to the buffered suspensions enables the complete resuspenion of the nanospheres after freeze drying. It prevents an aggregation of the nanospheres while subliming the water during freeze drying[97]. Figure 3.16. shows the size distribution of PAN nanospheres (sample **1**) before freeze drying and after freeze drying and resuspension. Even though the distribution is more polydispers after freeze drying/resuspension, the suspension is still totally clear.

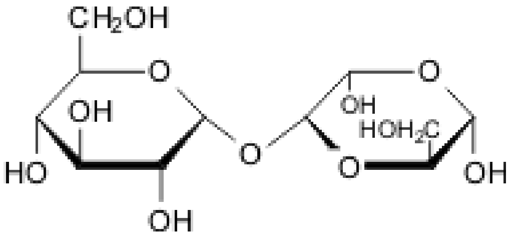

Figure 3.15. Chemical structure of α,α-trehalose.

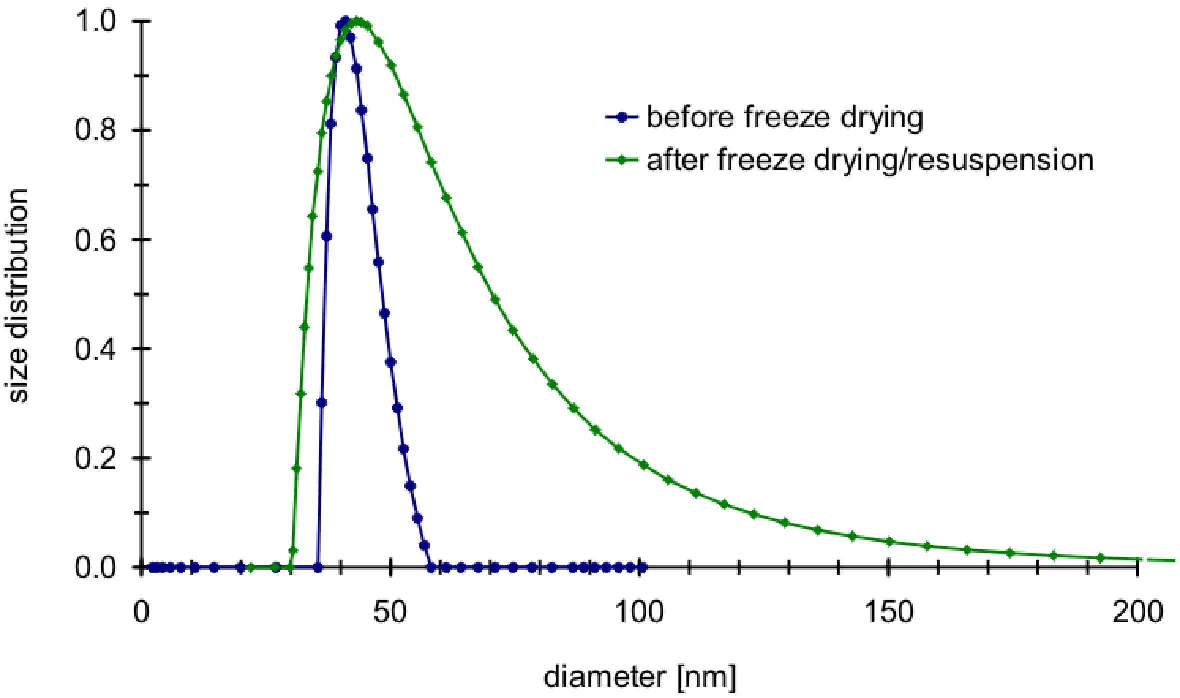

Figure 3.16. Diameter of nanospheres (sample **1**) by dynamic light scattering at a detection angle of 90°, before freeze drying (●) and after freeze drying/ resuspension (♦).

3.3.5. Photophysical characterization of nanospheres (suspensions)

3.3.5.1. Excitation and emission spectra

Figure 3.17. shows the excitation and emission (air/N_2) spectra of the incorporated ruthenium dye $Ru(dpp)_3Cl_2$ in a buffered aqueous suspension. Since the excitation spectrum is very broad, various excitation light sources can be applied. Ru(dpp) can be excited with a blue (470, 450 nm) and blue-green (505 nm) LED or with the argon ion laser at 488 nm. Even the violet diode lasers (404 nm) are a potential light source. The excitation and emission spectra show almost no overlapping and a very large Stokes' shift of about 150 nm (λ_{exc} 465 nm, λ_{em} 613 nm). In the emission spectra in Figure 3.17. one can also notice the negligible amount of quenching caused by oxygen.

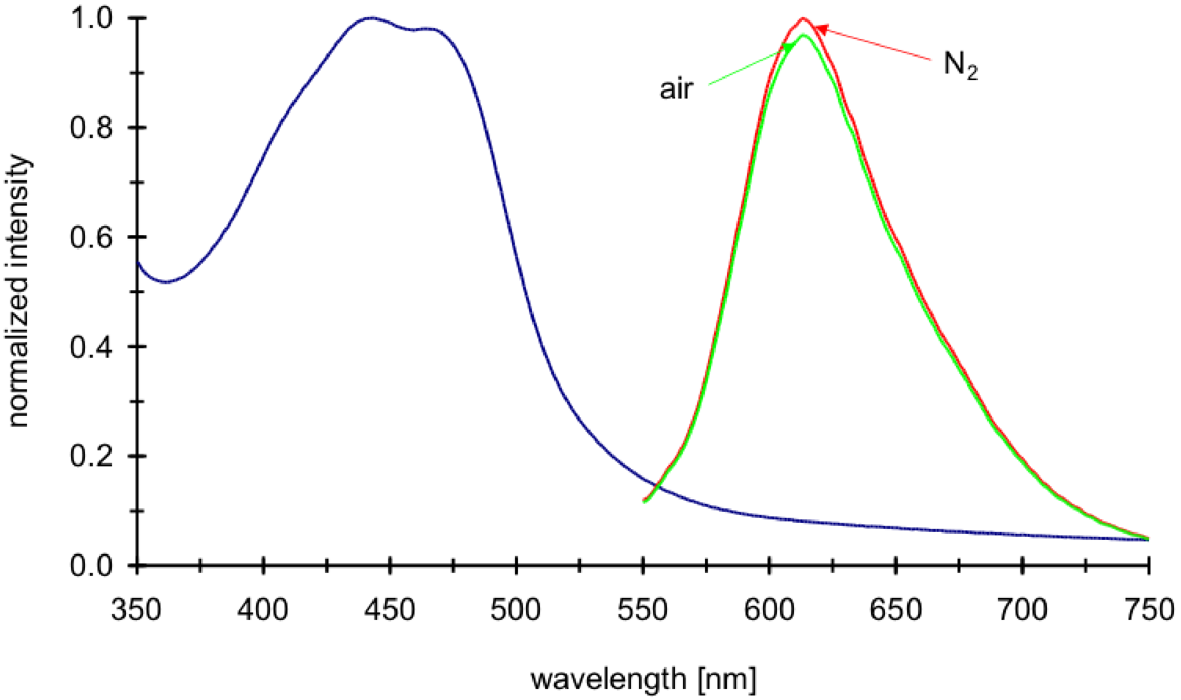

Figure 3.17. Spectral characteristics (absorbance and emission spectra, λ_{exc} 488 nm) of encapsulated Ru(dpp) (sample **2**).

3.3.5.2. Brightness

The brightness of the nanospheres (compare Figure 3.11.) was compared to the luminescence intensity of the carboxylate modified microspheres (TransFluoSpheres T-8865, λ_{em} 605 nm) from Molecular Probes (Table 3.3.). Those TransFluoSpheres have comparable spectral properties to the Ru(dpp) dye and are known to be extremely strong fluorescent[4]. In order to examine the luminescence intensity, an aqueous solution of both micro- and nanospheres of identical polymer concentration (w/w) was measured. It can be seen that when excited with the blue diode laser (at 404 nm) or blue LEDs (at 450 nm or 470 nm), the nanospheres have an up to fourfold intensity compared to the TransFluoSpheres microspheres due to their broad excitation spectrum. Only at the longer wavelengths of the argon ion laser (488 nm), for which the TransFluoSpheres were specifically designed, or the blue-green LED (505 nm), the TransFluoSpheres show a higher brightness. Nevertheless, if the blue LEDs are the preferred light source, the presented nanospheres are much brighter.

Table 3.3. Brightness of the nanospheres (sample **2**) compared to the TransFluoSpheres T-8865 (λ_{em} 605 nm).

light source	λ_{exc} **[nm]**	**luminescence intensity** [a]
blue diode laser	404	4.1
blue LED	450	3.4
blue LED	470	1.4
argon ion laser	488	0.7
blue-green LED	505	0.2

[a] TransFluoSpheres = 1.0

3.3.5.3. Luminescence frequency spectra

In the luminescence frequency spectra (Figure 3.18.) for sample **2**, one can see the dependance of the phase angle and the modulation on the applied modulation frequency. An evaluation of the data points to a biexponential fit as the best choice (and not a monoexponential one) which is typical for incorporated dyes. The apparent decay time varies between 6 – 7 µs for the main component (~ 95%) and 1 – 2 µs for a second component (~ 5%). The minor component results from surface-bound dye which can be quenched by oxygen. Even though ξ^2 (7.1) is relatively high, a systematic error can be ruled out since the errors are evenly distributed over the whole frequency range.

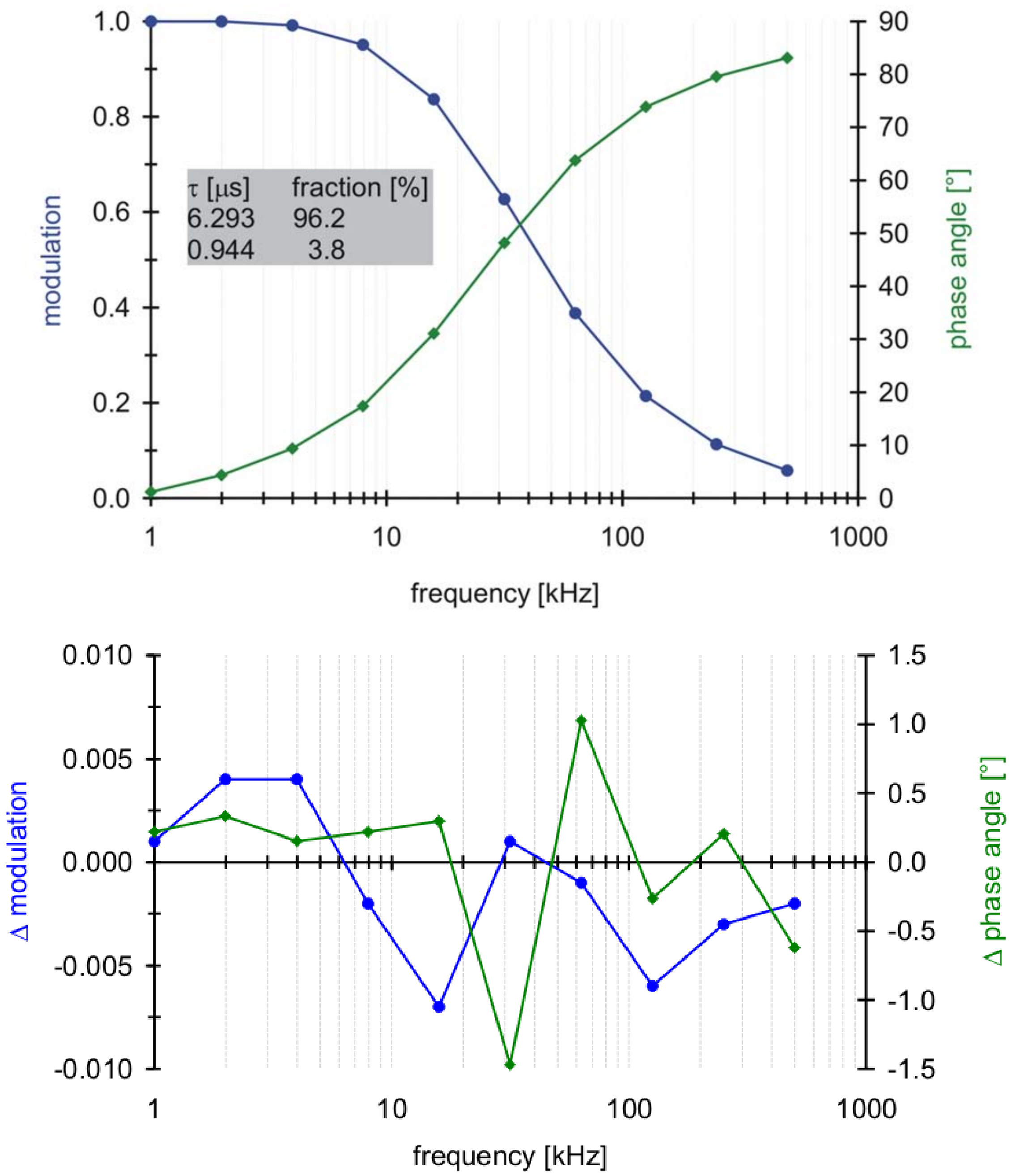

Figure 3.18. Luminescence frequency spectra (top) and error distribution (bottom, ξ^2 7.1) displaying the modulation (●) and phase angle (♦) for sample **2**.

3.3.5.4. Dilution behavior

As expected, no change in the decay behavior of the dyes was observed with increasing dilution of the nanosphere suspensions. This also indicates that the dye is not washed out of the matrix. In quartz cuvettes, the decay time stayed constant to a nanosphere concentration of 0.2 mg/L, i.e. a Ru(dpp) concentration of 2.8 nmol/L (for more details see chapter 3.3.6.4. with Figure 3.22.).

3.3.6. Physical characterization of nanospheres (suspensions)

Table 3.4. summarizes the type of suspension, the average diameter d (by dynamic light scattering at 90°), the apparent decay time τ (air/N_2), the oxygen cross-sensitivity $\Delta\tau$ (change of τ air/N_2) and the quantum yield Φ for all of the nanospheres investigated.

Table 3.4. Characterization of polyacrylonitrile nanospheres (suspensions).

sample	**polymer**	**c (matrix/DMF)** [a] **[% (w/w)]**	**d [nm]**	**τ, air [µs]**	**τ, N_2 [µs]**	**$\Delta\tau$ [%]**	**Φ**
0 [b]	-	-	-	1.20	4.70	74.5	0.30
1	**1**	0.50	43.4	6.01	6.20	3.0	0.39
2	**2**	0.50	29.8	5.78	6.11	5.5	0.32
3	**2**	0.25	19.8	5.57	6.08	8.5	0.31
4	**2**	0.10	21.7	4.22	4.63	9.0	0.26
5	**3**	0.50	32.3	5.70	6.10	6.5	0.43
6	**4**	0.50	6.1	5.46	5.91	7.5	0.39
7	**5**	0.50	2.8	5.32	5.93	10.5	0.38
8	**6**	0.50	instable	6.01	6.24	4.0	-
9	**7**	0.50	18.7	5.79	6.18	6.5	-
10	**8**	0.50	18.5	5.36	5.98	10.5	0.34
11	**9**	0.50	instable	5.55	5.84	5.0	-

[a] $c_{Ru(dpp)/matrix}$ = 1.0% (w/w) for all samples
[b] free Ru(dpp) in water

3.3.6.1. Diameter and shape

Transmission electron microscopic pictures of four different types of nanospheres showed a nearly circular shape and a diameter of roughly 5 – 30 nm (Figure 3.19. for samples **2**, **3**, **6** and **7**). Scanning electron microscopic pictures of four different types of nanospheres confirmed this diameter of about 5 – 30 nm (Figure 3.20. for samples **2**, **3**, **6** and **7**). Static and dynamic light scattering experiments (Figure 3.21. for samples **1** and **2**) revealed a polydisperse coil with a diameter of the nanospheres of down to about 5 nm (for sample **7**).

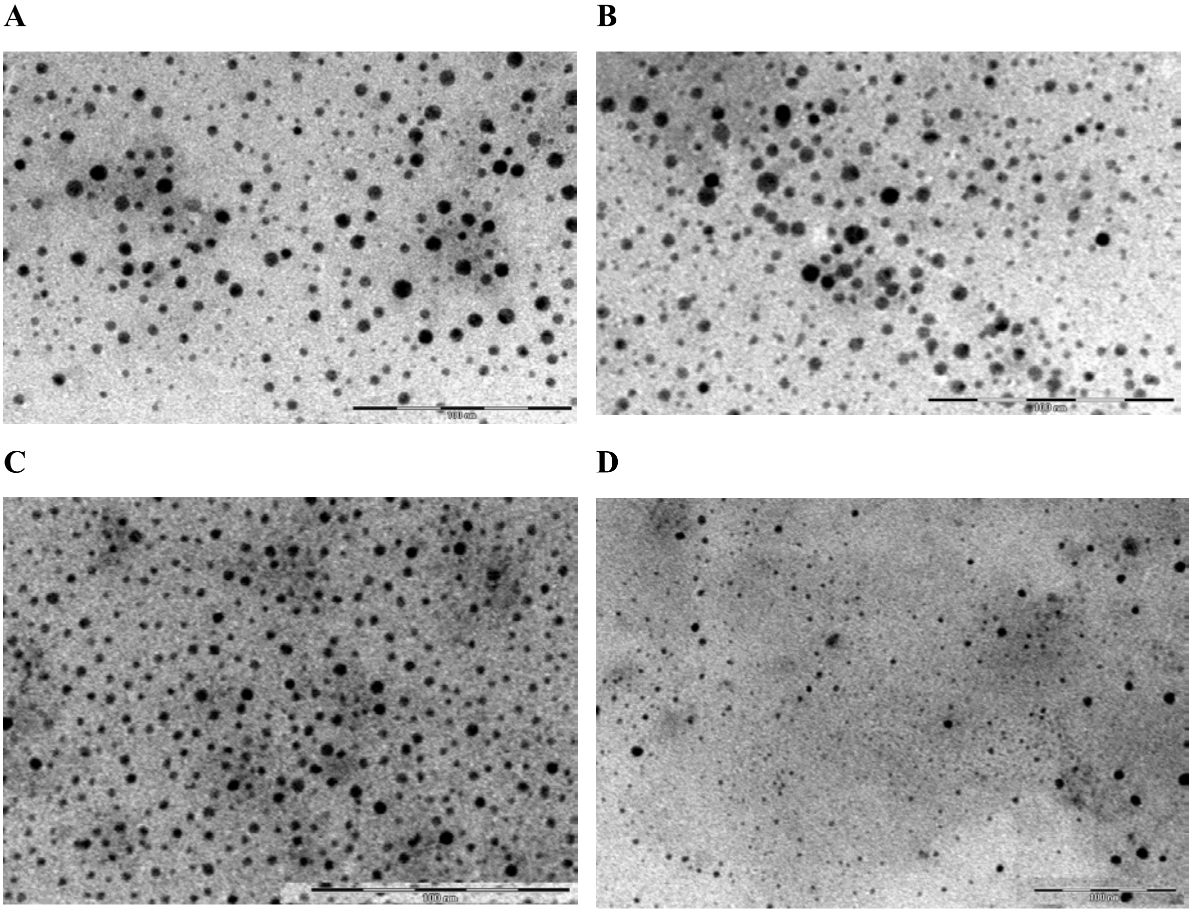

Figure 3.19. Transmission electron microscopic pictures (TEM) of different nanospheres: (A) sample **2**, (B) sample **3**, (C) sample **6** and (D) sample **7**. The total scale bar always corresponds to 100 nm.

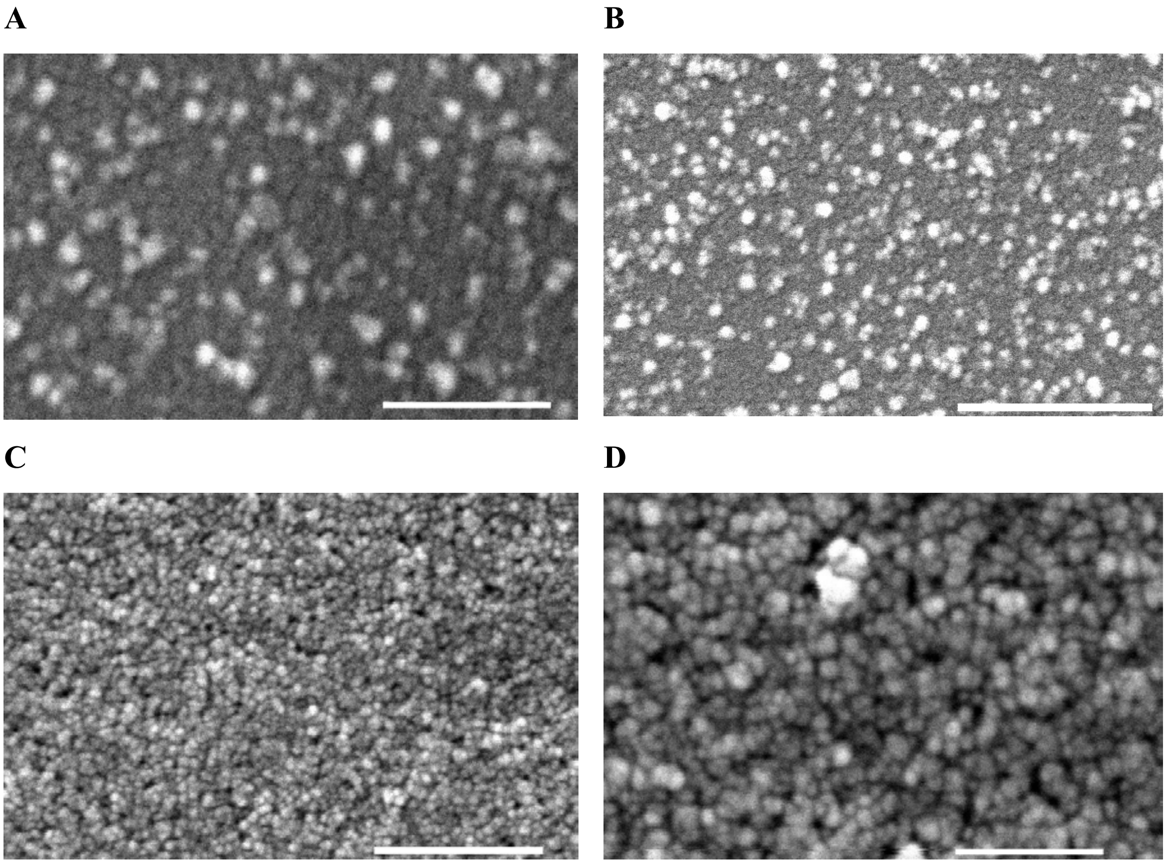

Figure 3.20. Scanning electron microscopic pictures (SEM) of different nanospheres: (A) sample **2**, (B) sample **3**, (C) sample **6** and (D) sample **7**. The total scale bar always corresponds to 100 nm.

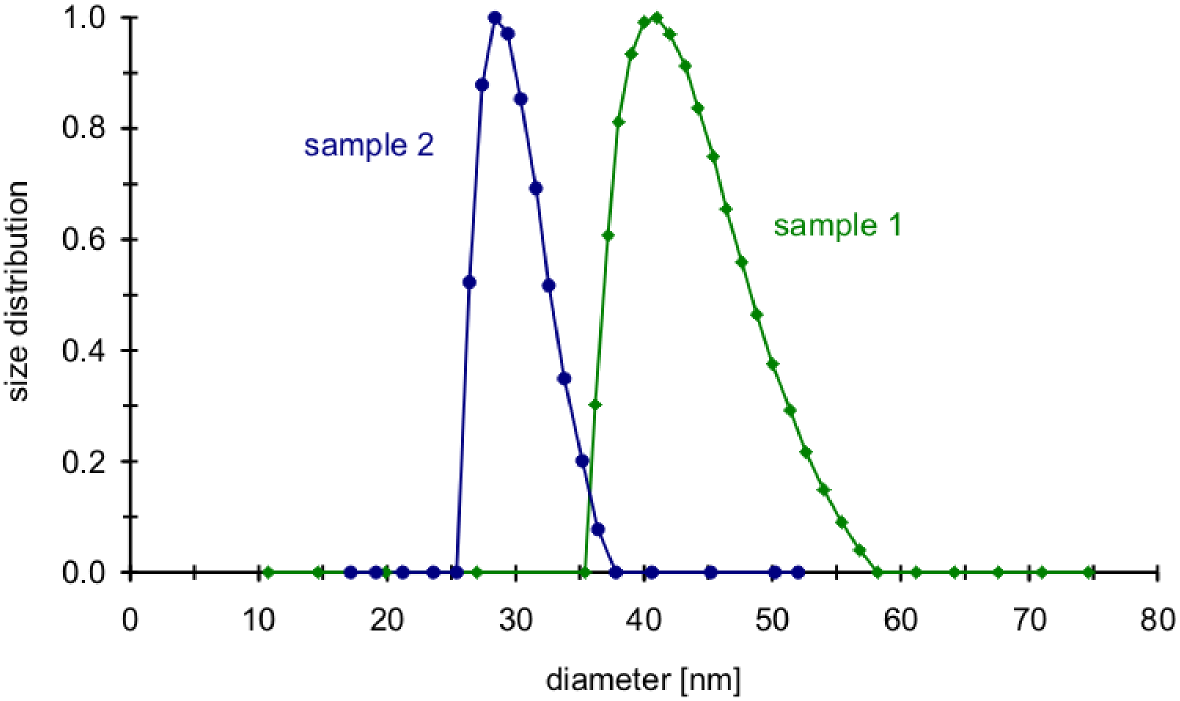

Figure 3.21. Diameter of nanospheres (samples **1** and **2**) by dynamic light scattering at a detection angle of 90°.

Even though the light scattering distributions (Figure 3.21.) point to a not extremely monodispers shape of the nanospheres, the very simple preparation technique fully compensates this handicap. The nanosphere diameter can be influenced by the preparation process. Both increasing the amount of carboxy groups in the copolymer and increasing the concentration of the matrix in DMF leads to larger nanospheres. Some matrices (e.g. polymers **6** and **9**) show a higher tendency to aggregate and a rather polydispers size distribution.

3.3.6.2. Surface charge

ZETA POTENTIAL. Laser Doppler velocimetry experiments revealed a negative zeta potential (e.g. $\zeta = -54.0$ mV for sample **2**) confirming the negative surface charge resulting from the carboxy groups.

TITRATION OF CARBOXYLATED NANOSPHERES. Two types of carboxylated nanospheres with different sizes were titrated with NaOH (compare chapter 3.2.2.6.) in order to determine the content of carboxy groups on the nanosphere surface when compared to the total number of carboxy groups in the nanosphere (equations 3.2. and 3.3.; $c_{carboxy\,groups}$ in mol/g, $c_{suspension}$ in g/L, $c_{acrylic\,acid\,/\,matrix}$ in %, $M_{acrylic\,acid}$ 72.06 g/mol) and the ratio of carboxy groups to Ru(dpp) dye in the nanospheres (equation 3.4.; $c_{Ru(dpp)/\,matrix}$ in %). The calculations are based on the assumption that only those carboxy groups located on the nanosphere surface can be titrated with the base. The results are summarized in Table 3.5.

$$carboxy\,groups\,on\,surface = \frac{c_{carboxy\,groups} \cdot M_{Ru(dpp)}}{c_{Ru(dpp)/\,matrix} \cdot 0.01} \qquad 3.2.$$

$$c_{carboxy\,groups} = \frac{\dfrac{c_{NaOH} \cdot V_{NaOH}}{V_{suspension}}}{c_{suspension}} \qquad 3.3.$$

$$ratio_{carboxy\,groups\,/\,Ru(dpp)} = \frac{c_{carboxy\,groups} \cdot M_{acrylic\,acid} \cdot 100}{c_{acrylic\,acid\,/\,matrix} \cdot 0.01} \qquad 3.4.$$

Table 3.5. Characterization of two types of carboxylated nanospheres by a titration experiment.

sample	**2**	**3**	**5**
polymer	**2**	**2**	**3**
d [nm]	29.8	19.8	32.3
$c_{\text{matrix/DMF}}$ [% (w/w)]	0.50	0.25	0.50
$c_{\text{acrylic acid/matrix}}$ [% (w/w)]	5.0	5.0	10.0
$c_{\text{Ru(dpp)/matrix}}$ [% (w/w)]	1.0	1.0	1.0
ratio carboxy groups/Ru(dpp)	6.4	9.5	14.7
carboxy groups on surface [%]	5.2	7.7	23.8

Equation 3.5. shows that the nanosphere diamter ($2 \cdot r$) is indirectly proportional to the ratio of nanosphere surface A_{sphere} to nanosphere volume V_{sphere}.

$$\frac{A_{sphere}}{V_{sphere}} = \frac{4 \cdot r^2 \cdot \pi}{4/3 \cdot r^3 \cdot \pi} = \frac{3}{r} \qquad 3.5.$$

This explains both the decrease of the ratio of carboxy groups to Ru(dpp) dye from 9.5 to 6.4 and the decrease of the content of carboxy groups on the nanosphere surface from 7.7 to 5.2%, when increasing the nanosphere diameter from 19.8 nm (sample **3**) to 29.8 nm (sample **2**). It is important that samples **2** and **3** both have a content of acrylic acid of only 5% (w/w) in the copolymer.

The larger ratio of carboxy groups to Ru(dpp) dye (14.7) and the larger content of carboxy groups on the surface (23.8%) in sample **5**, in spite of the even larger nanosphere diameter, is due to the higher content of acrylic acid in the copolymer, here 10% (w/w).

3.3.6.3. Apparent decay time, quantum yield and cross-sensitivity to oxygen

The most important characteristic of the new nanospheres is their very low oxygen cross-sensitivity as can be seen in Table 3.4. Whereas free $Ru(dpp)_3Cl_2$ dye in water (sample **0**) has a tremendously high oxygen quenching $\Delta\tau$ of about 75% and a quantum yield Φ of below 0.30 in nitrogen, the incorporated dye in the proper polymers (e.g. polymer **2**) has a quenching rate of only 3 – 5% and a quantum yield of over 0.40.

The apparent decay time of the free ruthenium complex in water varies between 1.20 µs in air and 4.70 µs in nitrogen, but can be as high as 6.20 µs in apolar organic solvents. The extremely low oxygen quenching of the incorporated dye proves the excellent shielding effect of the PAN copolymers and thus shows that the matrix itself does not act as a quencher. With decreasing nanosphere diameter, the oxygen quenching increases due to a higher surface-to-bulk ratio. Increasing the amount of carboxy groups in the polymer by using more acrylic acid comonomer unfortunately leads to a higher quenching, as well, since the nanospheres become more hydrophilic and can take up more water. But since carboxy functional groups are essential for stabilizing the suspensions, for cross-linking the nanospheres with the positive ruthenium dye and for the covalent coupling of biomolecules to the nanosphere surface, a compromise is necessary.

3.3.6.4. Luminescence detection limit

The luminescence detection limit was determined by measuring the apparent decay times of nanosphere suspensions at various dilutions, both in 96-well microtiter plates from Greiner (Frickenhausen, Germany) and in quartz cuvettes (Figure 3.22.). The sensitivity was always less for measurements in microtiter plates due to the slightly fluorescent material (polystyrene) of the plates. Yet, in both cases the detection limit was very low, with constant decay times down to a nanosphere concentration of 0.2 mg/L in cuvettes and 12.2 mg/L in microtiter plates, i.e. a Ru(dpp) concentration of 2.8 nmol/L in cuvettes and 173.2 nmol/L in microtiter plates.

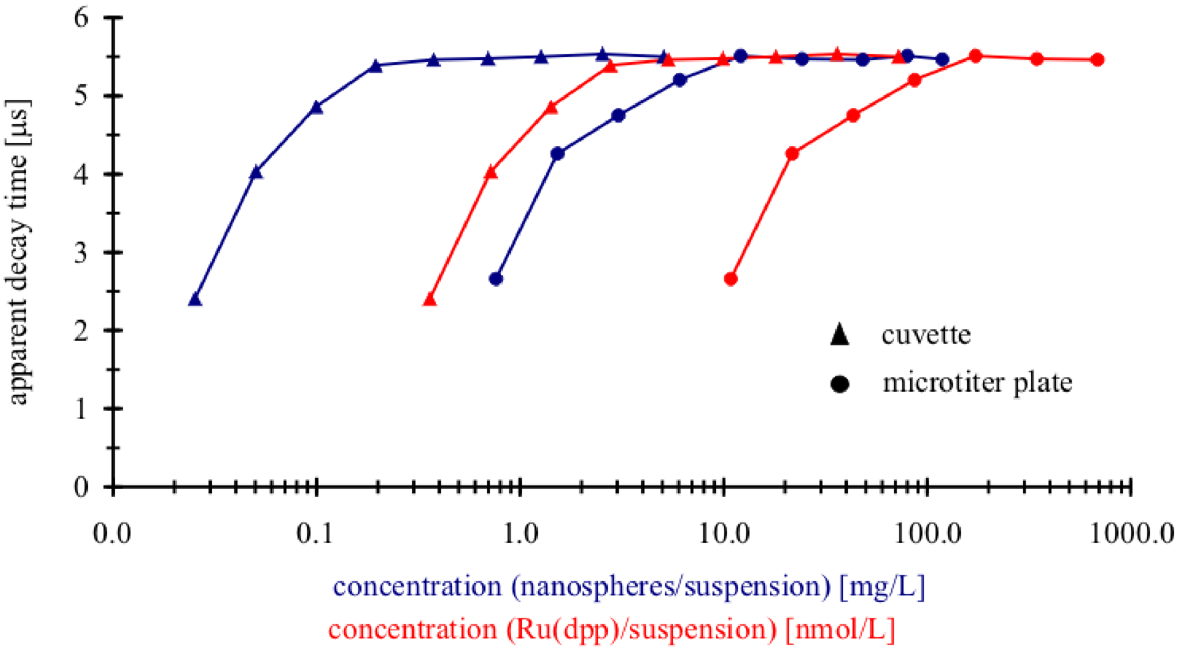

Figure 3.22. Luminescence detection limit for phosphorescent nanospheres when measured in a quartz cuvette (▲) or a microtiter plate (•).

3.3.7. Physical characterization of nanospheres (membranes)

For the polyacrylonitrile polymers **1** – **3** and **6** – **9**, membranes (200 µm films on Mylar polyester foils) were measured. The oxygen cross-sensitivity, both in gases and gas-saturated water, was always less than 2.0%. The gases applied were O_2, air and N_2. Table 3.6. summarizes the decay times τ and the dynamic quenching constants k_D (Stern-Volmer constant KSV, compare chapter 2.4.1.) of the membranes in gases, whereas Table 3.7. lists the decay times τ in gas-saturated water. k_D was calculated according to equation 3.6.

$$k_D = \frac{\frac{\tau_{nitrogen}}{\tau_{oxygen}} - 1}{p_{oxygen}(oxygen)} = \frac{\tau_{nitrogen} - \tau_{oxygen}}{\tau_{oxygen} \cdot 1013.25 hPa} \qquad 3.6.$$

Table 3.6. Characterization of polyacrylonitrile nanospheres (membranes in gases). Gases applied were O_2, air and N_2.

sample	**polymer** [a]	**τ, O_2 [μs]**	**τ, air [μs]**	**τ, N_2 [μs]**	**$\Delta\tau$, air/N_2 [%]**	**k_D, air [hPa^{-1}]**
1	**1**	5.57	5.75	5.81	1.0	$4.25 \cdot 10^{-5}$
2	**2**	5.72	5.87	5.92	0.8	$3.45 \cdot 10^{-5}$
3	**2**	5.75	5.90	5.97	1.2	$3.78 \cdot 10^{-5}$
4	**2**	5.76	5.88	5.92	0.7	$2.74 \cdot 10^{-5}$
5	**3**	5.84	5.91	5.94	0.5	$1.69 \cdot 10^{-5}$
8	**6**	5.51	5.68	5.75	1.2	$4.30 \cdot 10^{-5}$
9	**7**	5.50	5.66	5.69	0.5	$3.41 \cdot 10^{-5}$
10	**8**	5.57	5.78	5.85	1.2	$4.96 \cdot 10^{-5}$
11	**9**	5.54	5.78	5.89	1.9	$6.24 \cdot 10^{-5}$

[a] for polymer composition see Table 3.1.

Table 3.7. Characterization of polyacrylonitrile nanospheres (membranes in gas-saturated water). Gases applied were O_2 and N_2.

sample	**polymer** [a]	**τ, O_2 [μs]**	**τ, N_2 [μs]**	**$\Delta\tau$, air/N_2** [b] **[%]**
1	**1**	5.33	5.63	1.1
2	**2**	5.41	5.70	1.1
3	**2**	5.43	5.81	1.4
4	**2**	5.48	5.69	0.8
5	**3**	5.27	5.49	0.8
8	**6**	5.17	5.56	1.5
9	**7**	5.31	5.50	0.7
10	**8**	5.09	5.44	1.3
11	**9**	5.17	5.70	2.0

[a] for polymer composition see Table 3.1.

[b] $\tau_{air} = \tau_{oxygen} \cdot 0.2093$

3.4. Conclusion

Polyacrylonitrile derivatives are attractive matrices for the encapsulation of organic phosphorescent dyes since they have a poor permeability for gases and dissolved ionic and neutral chemical compounds. Thus they are shielded efficiently against luminescence quenching, e.g. caused by molecular oxygen and therefore they show constant decay times and quantum yields in samples of variable and unknown composition. In addition, many lipophilic dyes are well soluble in these materials and will not be washed out into the sample.

The nanospheres have a very high surface-to-bulk ratio which is an evidence for a highly branched, porous structure[98-99]. Polyacrylonitrile with an acrylic acid content of 5% proved to be the best choice as encapsulation matrix. Suspensions of such phosphorescent nanospheres are only poorly quenchable by oxygen, show no tendency to sedimentation and have an activated surface for the coupling of biomolecules or chemically responsive indicators. In case of using the ruthenium(II)-tris(4,7-diphenyl-1,10-phenanthroline) complex as phosphorescent dye, bright luminescent nanospheres with a large Stokes shift were obtained. No dye leaching was observed in aqueous solutions. They can be excited with either the argon ion laser or blue LEDs.

The new nanospheres can be used as bright phosphorescent labels in immunoassays or as nanoprobes to measure intracellular chemical parameters. Furthermore, they are excellent phosphorescence standards and are useful to design phosphorescent chemical sensors.

4. Phosphorescent Nanospheres for Use in Advanced Time-Resolved Multiplexed Bioassays

A new concept to design phosphorescent nanospheres is presented. The spheres are distinguishable by their individual decay time and spectral distribution of their emission spectra. They are composed of a phosphorescent ruthenium metal ligand complex (MLC) which is dissolved along with certain strongly fluorescent cyanine dyes, in modified polyacrylonitrile-based nanospheres. Since the emission spectrum of the MLC overlaps the absorbance spectrum of the cyanine and both the MLC (the donor) and the cyanine (the acceptor) are in close spatial proximity, efficient resonance energy transfer (RET) does occur. Thus, the nanospheres emit dual luminescence, one from the acceptor dye, the other from the donor MLC. Variation of the concentrations of the acceptor dye results in a varying efficiency of RET, thus making the spheres distinguishable. Hence, a set of multiplexable sphere labels is obtained by using one MLC (acting as the phosphorescent donor and present in constant concentration) and one acceptor dye (which varies in terms of both spectral properties and concentration). The nanospheres can be identified by the emission maximum (reflecting the kind of acceptor dye) and by decay time (reflecting its concentration). Since the same donor MLC is used throughout, all nanospheres can be excited with the same light source.

4.1. Introduction

Reactive luminescent dyes are widely used labels for biomolecules. However, numerous features are crucial for making a dye an efficient label. These include high light efficiency (large quantum yields, high molar absorbance), a large Stokes’ shift in order to separate the excitation and emission signal without loss of light and also to eliminate background luminescence, photostability, luminescence characteristics that are unaffected by the sample, the presence of reactive groups for the covalent coupling to biomolecules, solubility in water and, preferably, nontoxicity. Even though a number of fluorescent dyes are known as viable labels, only a few fulfill all of the above criteria[100]. Problems mainly arise from limited photostability and insufficient brightness, especially in case of samples containing a high background fluorescence.

Furthermore, there is a tremendous need for so-called multiplexing dyes with clearly distinguishable optical properties. Such dyes enable the separation of large numbers of species, such as oligonucleotides or proteins[101-102]. Ways to increase sensitivity of luminescence assays and thus to eliminate background fluorescence of the sample are: the use of longwave emitting dyes, the use of phosphorescent dyes and incorporation of fluorescent dyes into polymer matrices to yield micro- or nanospheres[54, 103-105].

Various schemes are used in fluorescent multiplexing: (1) In the first, a series of individual dyes with different absorbance and emission spectra as well as different luminescence decay times is employed. (2) In another, micro- or nanospheres with encapsulated dyes of the same absorbance spectra but different emission spectra are used and identification is accomplished by measurement of luminescence decay time. If various dyes are combined – as for example in the TransFluoSpheres of Molecular Probes – a resonance enery transfer cascade can occur[4]. (3) Thirdly, micro- or nanospheres can be used containing two dyes that differ in the ratio of concentrations and thus can be identified by ratiometric measurement of the two respective luminescence intensities[106]. (4) A final possibility for multiplexing consists in the use of dyes with different decay characteristics even if identical in terms of spectra.

All of these schemes suffer from the same restrictions: Only a limited number of different and identifiable labels – 30 to 50 at the most – can be produced. With five distinctive dyes, each in 10 different concentrations, only 50 different labels can be obtained. Using more than 10 different dyes is difficult due to wavelength limitations. Also, schemes (1), (2) and (4) require individual fluorescent dyes for each label. Concept (3) has the attractive feature that two dyes are needed only in order to obtain a series of labels.

However, for multi-analyte detection which is becoming more and more important in immunoassays and gene assays, a much larger number of clearly and quickly distinguishable labels is needed, 100 probably being the minimum. This is particularly true for applications such as cell separation, flow cytometry, DNA- and immunochips and fluorescence microscopy[101, 107-108].

TWO-DIMENSIONAL ASSAY. In a first approach, the above methods were combined in order to reach the goal of creating well over 100 different labels. Instead of using single dyes, schemes (2) and (3) were combined and this leads to a vast number of two-dimensional labels that can be differentiated in terms of both emission wavelength and decay time. Figure 4.1. shows such a two-dimensional dot plot of luminescence labels that can be clearly assigned by both the emission wavelength of the cyanine acceptor (x-axis) and the apparent decay time of the nanospheres (y-axis). In fact, the dot plot is more of an ellipse plot spread in the decay time axis and not in the spectral axis since the y-axis is the one measurable variable that can have a certain error. The emission of the cyanine acceptor (x-axis) is only measured at one specific wavelength.

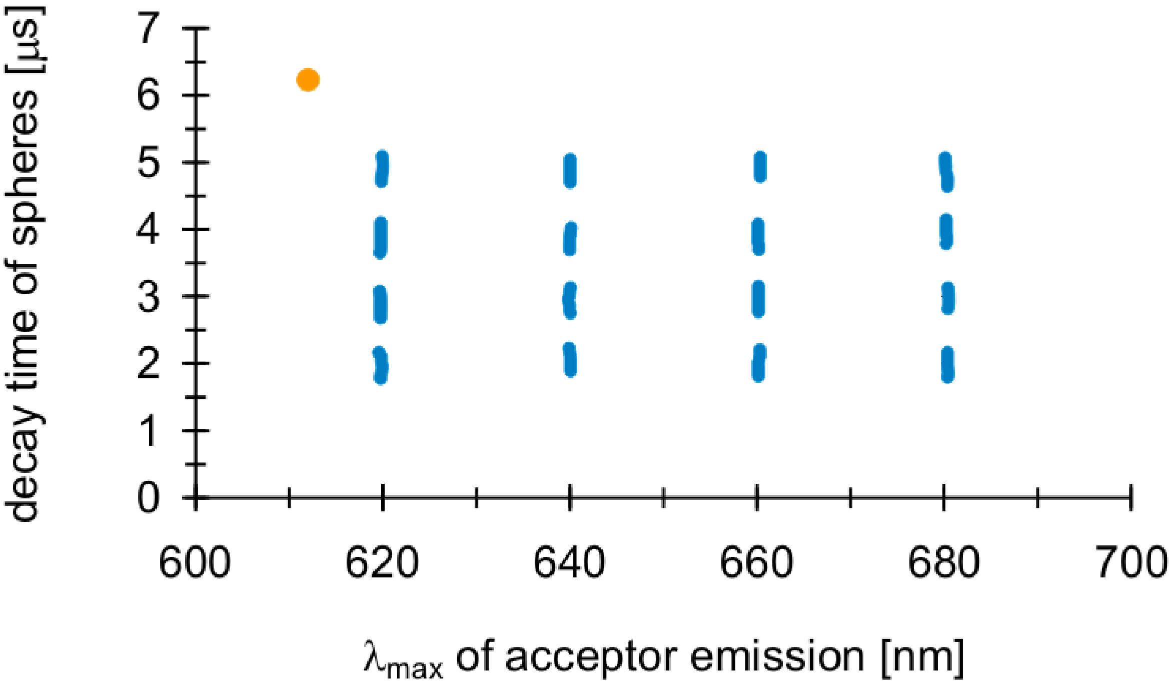

Figure 4.1. Two-dimensional field showing classification of 16 nanosphere labels (blue ellipses) based on simultaneous analysis of both emission wavelength of cyanine acceptor and apparent decay time of spheres (compare Figure 4.9. for experimental data). The orange circle represents the Ru(dpp) donor. Using one specific acceptor, thus at a certain emission wavelength, with increasing acceptor concentration the extent of RET increases, as well, leading to decreasing decay times of the nanospheres.

THREE-DIMENSIONAL ASSAY. The general formula for the number of different nanosphere labels z that can be obained is given by equation 4.1.

$$z = \binom{n}{k} \cdot c^k \qquad 4.1.$$

where n is the number of available acceptor dyes, k the number of acceptor dyes used within one nanosphere and c the number of concentrations (including 0) in which a given acceptor dye is incorporated into different nanospheres. The binomial coefficient $\binom{n}{k}$ is calculated according to equation 4.2.

$$\binom{n}{k} = \frac{n!}{k!(n-k)!} \qquad 4.2.$$

Table 4.1. gives a selection of possible combinations of n, k, c and the resulting value for z. It can be seen that in a two-dimensional multiplexing set-up with four different acceptor dyes available (n = 4), always one acceptor dye in each nanosphere (k = 1) and four different concentrations in which an acceptor dye is incorporated into different nanospheres (c = 4), a set of 16 labels can be created (compare Figure 4.1.). Yet, applying four acceptors (n = 4) with two acceptors within a nanosphere at a time (k = 1) and ten different acceptor concentrations (c = 4), already 600 different labels are obtained. The number of labels can even reach up to approximately 100,000 with n = 10, k = 3 and c = 10.

Table 4.1. Possible combinations of n (number of available acceptor dyes), k (number of acceptor dyes used within one nanosphere) and c (number of concentrations in which a given acceptor dye is incorporated into different nanospheres). z (number of different nanosphere labels) was calculated according to equation 4.1.

n	4	4	4	4	4	4	10	10	10	10	10	10
k	1	1	2	2	3	3	1	1	2	2	3	3
c	4	10	4	10	4	10	4	10	4	10	4	10
z	16	40	96	600	256	4000	40	100	720	4,500	7,680	120,000

In a three-dimensional multiplexing set-up with four different acceptor dyes available ($n = 4$), always two acceptor dyes in each nanosphere ($k = 2$) and four different concentrations in which an acceptor dye is incorporated into different nanospheres ($c = 4$), a set of 96 different labels can be created (compare Figure 4.2.).

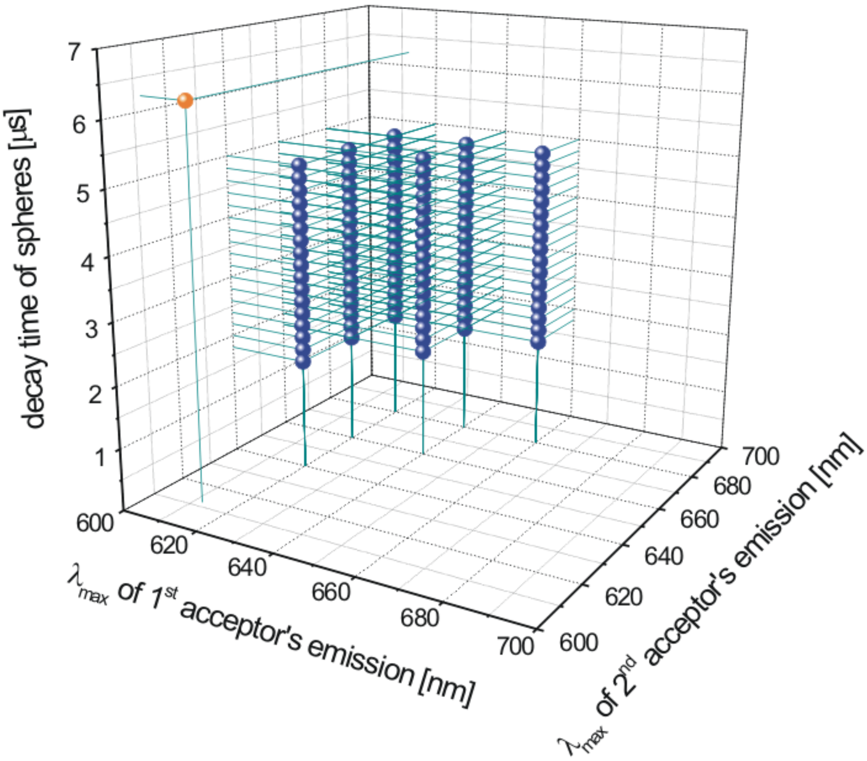

Figure 4.2. Three-dimensional field showing classification of 96 nanosphere labels (blue spheres) based on simultaneous analysis of emission wavelengths of cyanine acceptors and apparent decay time of spheres (compare Figure 4.14. for experimental data; $n = 4$, $k = 2$, $c = 4$; $z = 96$). The orange sphere represents the Ru(dpp) donor.

4.2. Materials and methods

4.2.1. Chemicals and reagents

All chemicals and solvents used were of analytical grade and used without further purification. Doubly distilled water was used throughout. The preparation of ruthenium(II)-tris-4,7-diphenyl-1,10-phenanthroline bis-timethylsilylpropanesulfonate [$Ru(dpp)_3(TMS)_2$] is described in chapter 3.2.3. Poly-(acrylonitrile-co-acrylic acid) containing 5% (w/w) of acrylic acid (PAN-COOH5, equivalent to polymer **2** in Table 3.1.) and poly-(acrylonitrile-co-acrylic acid) containing 10% (w/w) of acrylic acid (PAN-COOH10, equivalent to polymer **3** in Table 3.1.) were obtained from Optosense. The names, net formulas, molecular weights and suppliers of all other reagents used in the experiments are listed in Table 4.2.

Table 4.2. Chemicals and solvents used in the experiments of chapter 4.

name	**net formula**	**MW [g/mol]**	**company**
1,1’-diethyl-2,2’-carbocyanine chloride = pinacyanol chloride, CY604	$C_{25}H_{25}ClN_2$	388.94	Aldrich
1,1’-diethyl-4,4’-carbocyanine iodide = CY703	$C_{25}H_{25}IN_2$	480.39	Aldrich
2-morpholinoethansulfonic acid monohydrate = MES	$C_6H_{13}NO_4S \cdot H_2O$	213.25	Fluka
3,3’-diethyloxadicarbocyanine iodide = CY582	$C_{23}H_{23}IN_2O_2$	486.36	Aldrich
3,3’-diethylthia-dicarbocyanine iodide = CY655	$C_{23}H_{23}IN_2S_2$	518.48	Aldrich
disodium hydrogen phosphate dihydrate	$Na_2HPO_4 \cdot 2H_2O$	177.99	Merck
N,N-dimethylformamide = DMF	C_3H_7NO	73.10	Merck
ruthenium(II)-tris-2,2-bipyridyl chloride hexahydrate = $Ru(bipy)_3Cl_2 \cdot 6H_2O$	$RuC_{30}H_{24}N_6Cl_2 \cdot 6H_2O$	748.63	Aldrich
ruthenium(II)-tris-4,7-diphenyl-1,10-phenanthroline bis-trimethylsilylpropane-sulfonate = $Ru(dpp)_3(TMS)_2$	$RuSi_2C_{84}H_{78}N_6S_2O_6$	1488.95	synthesis (chapter 3.2.3.)
ruthenium(II)-tris-4,7-diphenyl-1,10-phenanthroline dichloride = $Ru(dpp)_3Cl_2$	$RuC_{72}H_{48}N_6Cl_2$	1169.20	synthesis (chapter 3.2.3.)
sodium azide	NaN_3	65.01	Merck
sodium chloride	$NaCl$	58.44	Merck
sodium dihydrogenphosphate monohydrate	$NaH_2PO_4 \cdot H_2O$	137.99	Merck
sodium hydroxide pellets	$NaOH$	40.00	Merck
trehalose	$C_{12}H_{22}O_{11}$	342.30	Merck

4.2.2. Instrumentation and measurements

A detailed description of all apparatus used in this chapter is given in chapter 3.2.2. All formulas needed in connection with calculations of luminescence decay times, quantum yields and their corrections are given in chapters 2.1. – 2.3.

4.2.3. Preparation of dye solutions

TWO-DIMENSIONAL ASSAY. A ruthenium donor stock solution **A** was prepared by dissolving 7.02 mg $Ru(dpp)_3(TMS)_2$ and 1.00 g PAN-COOH5 in 100 mL of N,N-dimethylformamide (DMF, ρ_{DMF} 0.948 kg/L). The cyanine acceptor stock solutions $\mathbf{B_i}$ (with i = 1 to 4) were prepared according to Table 4.3. The solutions $\mathbf{C_ia}$, $\mathbf{C_ib}$, $\mathbf{C_ic}$, $\mathbf{C_id}$ and $\mathbf{C_ie}$ (with i = 1 to 4) were prepared according to Table 4.4., to a total volume of 10.0 mL and equivalent to 0.7% (w/w) Ru(dpp) dye/matrix and 0.5% (w/w) matrix/DMF. Figure 4.3. shows photographs of nanosphere suspensions $\mathbf{C_1b}$ – $\mathbf{C_1e}$, $\mathbf{C_2b}$ – $\mathbf{C_2e}$, $\mathbf{C_3b}$ - $\mathbf{C_3e}$ and $\mathbf{C_4b}$ – $\mathbf{C_4e}$.

Table 4.3. Two-dimensional assay. Preparation of the cyanine acceptor stock solutions $\mathbf{B_i}$ (with i = 1 to 4).

name of solution	**cyanine acceptor**	**m (acceptor) [mg]**	**V (DMF) [mL]**
$\mathbf{B_1}$	CY582	5.0	50
$\mathbf{B_2}$	CY604	5.0	50
$\mathbf{B_3}$	CY655	5.0	50
$\mathbf{B_4}$	CY703	13.3	50

Table 4.4. Two-dimensional assay. Preparation of solutions $\mathbf{C_ia}$, $\mathbf{C_ib}$, $\mathbf{C_ic}$, $\mathbf{C_id}$ and $\mathbf{C_ie}$ (with i = 1 to 4).

name of solution	**V (A) [mL]**	**V ($\mathbf{B_i}$) [mL]**	**V (DMF) [mL]**
$\mathbf{C_ia}$	5.0	0	5.0
$\mathbf{C_ib}$	5.0	0.5	4.5
$\mathbf{C_ic}$	5.0	1.0	4.0
$\mathbf{C_id}$	5.0	2.5	2.5
$\mathbf{C_ie}$	5.0	5.0	0

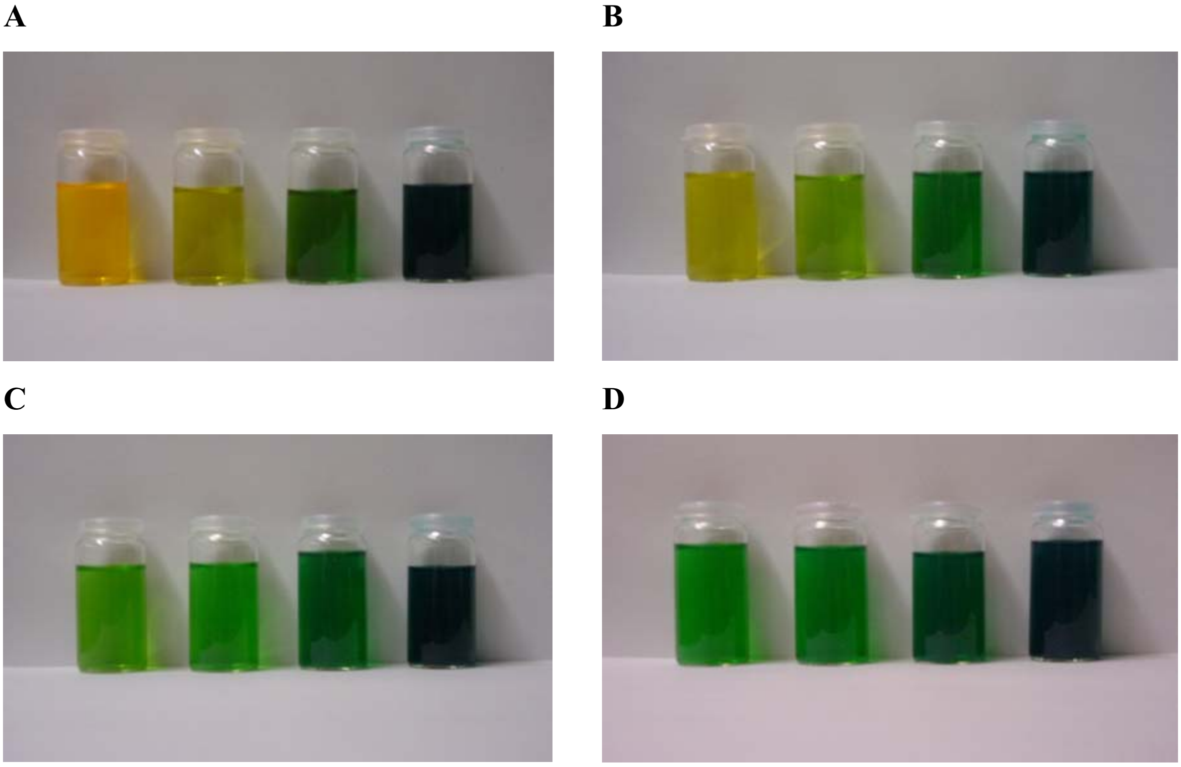

Figure 4.3. Two-dimensional assay. Photographs of nanosphere suspensions: (A) $\mathbf{C_1b}$ – $\mathbf{C_1e}$, (B) $\mathbf{C_2b}$ – $\mathbf{C_2e}$, (C) $\mathbf{C_3b}$ – $\mathbf{C_3e}$ and (D) $\mathbf{C_4b}$ – $\mathbf{C_4e}$.

THREE-DIMENSIONAL ASSAY. A ruthenium donor stock solution **D** was prepared by dissolving 9.99 mg Ru(dpp)$_3$Cl$_2$ and 1.00 g PAN-COOH10 in 211 mL of N,N-dimethylformamide (DMF, ρ_{DMF} 0.948 kg/L). The cyanine acceptor stock solutions $\mathbf{E_1}$ and $\mathbf{E_2}$ were prepared according to Table 4.5. The solutions $\mathbf{F_1}$ – $\mathbf{F_{16}}$ were prepared according to Table 4.6., to a total volume of 10.0 mL and equivalent to 1.0% (w/w) Ru(dpp) dye/matrix and 0.5% (w/w) matrix/DMF.

Table 4.5. Three-dimensional assay. Preparation of the cyanine acceptor stock solutions $\mathbf{E_1}$ and $\mathbf{E_2}$.

name of solution	**cyanine acceptor**	**m (acceptor) [mg]**	**V (A) [mL]**
$\mathbf{E_1}$	CY655	4.03	17.0
$\mathbf{E_2}$	CY703	24.27	51.2

Table 4.6. Three-dimensional assay. Preparation of solutions $\mathbf{F_1}$ – $\mathbf{F_{16}}$.

name of solution	**V (D) [mL]**	**V (E_1) [mL]**	**V (E_2) [mL]**
$\mathbf{F_1}$	10.0	0.0	0.0
$\mathbf{F_2}$	9.9	0.1	0.0
$\mathbf{F_3}$	9.6	0.4	0.0
$\mathbf{F_4}$	8.8	1.2	0.0
$\mathbf{F_5}$	9.6	0.0	0.4
$\mathbf{F_6}$	9.5	0.1	0.4
$\mathbf{F_7}$	9.2	0.4	0.4
$\mathbf{F_8}$	8.4	1.2	0.4
$\mathbf{F_9}$	8.0	0.0	2.0
$\mathbf{F_{10}}$	7.9	0.1	2.0
$\mathbf{F_{11}}$	7.6	0.4	2.0
$\mathbf{F_{12}}$	6.8	1.2	2.0
$\mathbf{F_{13}}$	6.0	0.0	4.0
$\mathbf{F_{14}}$	5.9	0.1	4.0
$\mathbf{F_{15}}$	5.6	0.4	4.0
$\mathbf{F_{16}}$	4.8	1.2	4.0

4.2.4. Preparation of luminescent nanospheres

Two-dimensional assay. While stirring vigorously, 25 mL of a 1 mM solution of sodium hydroxide were added dropwise to each of the solutions $\mathbf{C_ia}$ – $\mathbf{C_ie}$ (with i = 1 to 4). Then, 1 M hydrochloric acid was pipetted to the flasks until a pH of 4.0 was reached. This caused the precipitation of finely dispersed nanospheres. The DMF water mixtures were centrifuged at 3000 rpm for 15 min and the colored residues washed twice with 20 mL of 0.01 mM hydrochloric acid and then three times with 20 mL of water. All washing solutions remained colorless. The residues were suspended in 25 mL of water, heated to 70 °C for 10 min., centrifuged and then taken up in 25 mL of phosphate buffer (pH 7.0, IS 50 mM, 0.5% (w/w) sodium azide, 0.5% (w/w) trehalose). After sonification for 1 h, the suspensions were stored in the dark at 10 °C.

Three-dimensional assay. While stirring vigorously, 40 mL of a 1 mM solution of sodium hydroxide were added dropwise to each of the solutions $\mathbf{F_1}$ – $\mathbf{F_{16}}$. Then, 1 M hydrochloric acid was pipetted to the flasks until a pH of 4.0 was reached. This caused the precipitation of finely dispersed nanospheres. The DMF water mixtures were centrifuged at 3000 rpm for 15 min and the colored residues washed twice with 20 mL of 0.01 mM hydrochloric acid and then three times with 20 mL of water. All washing solutions remained colorless. The residues were suspended in 25 mL of water, heated to 70 °C for 10 min., centrifuged and then taken up in 25 mL of 2-morpholinoethanesulfonic acid (MES) buffer (pH 7.0, IS 30 mM, 0.5% (w/w) sodium azide, 0.5% (w/w) trehalose). After sonification for 1 h, the suspensions were stored in the dark at 10 °C.

4.3. Results and discussion

4.3.1. Choice of dyes

4.3.1.1. Phosphorescent donor dye

The phosphorescent ruthenium(II) complex Ru(dpp) has a luminescence decay time in the order of several µs (τ 6.23 µs) and was selected as label because it is well soluble in DMF and in the polymer matrix, but not in water[109]. The dye yields bright luminescent nanospheres with a Stokes' shift as large as 150 nm (λ_{exc} 465 nm, λ_{em} 613 nm). Strictly spoken, it is not a typical Stokes' shift since it does not involve a singlet state transmission. But for simplification purposes the term Stokes' shift is used throughout.

Due to its positive charge, it strongly interacts with polymers containing negatively charged groups. It is extracted quantitatively into the nanospheres during the preparation process. Even in a lipophilic environment, e.g. if proteins are present in the sample, no dye leaching in aqueous solutions is occurring.

The quantum yield Φ of 0.38 and the relatively large molar absorbance ($\varepsilon \approx 30{,}000$ L mol^{-1} cm^{-1}) of the ruthenium complex is a further advantage. The possibility to encapsulate this dye in large quantities in a polymer matrix is responsible for the high quantum yield. The ruthenium complex is excitable with an argon ion laser at 488 nm or blue light-emitting diodes (LEDs) at 450 nm or 470 nm (compare Figure 4.4.). Due to the very broad phosphorescence emission spectrum of the ruthenium complex, only one type of donor is sufficient to overlap with and thus to excite a large number of acceptor dyes.

The use of phosphorescent nanospheres eliminates background fluorescence, leading to a higher sensitivity. Last but not least, the donor complex is stable against loss of ligands.

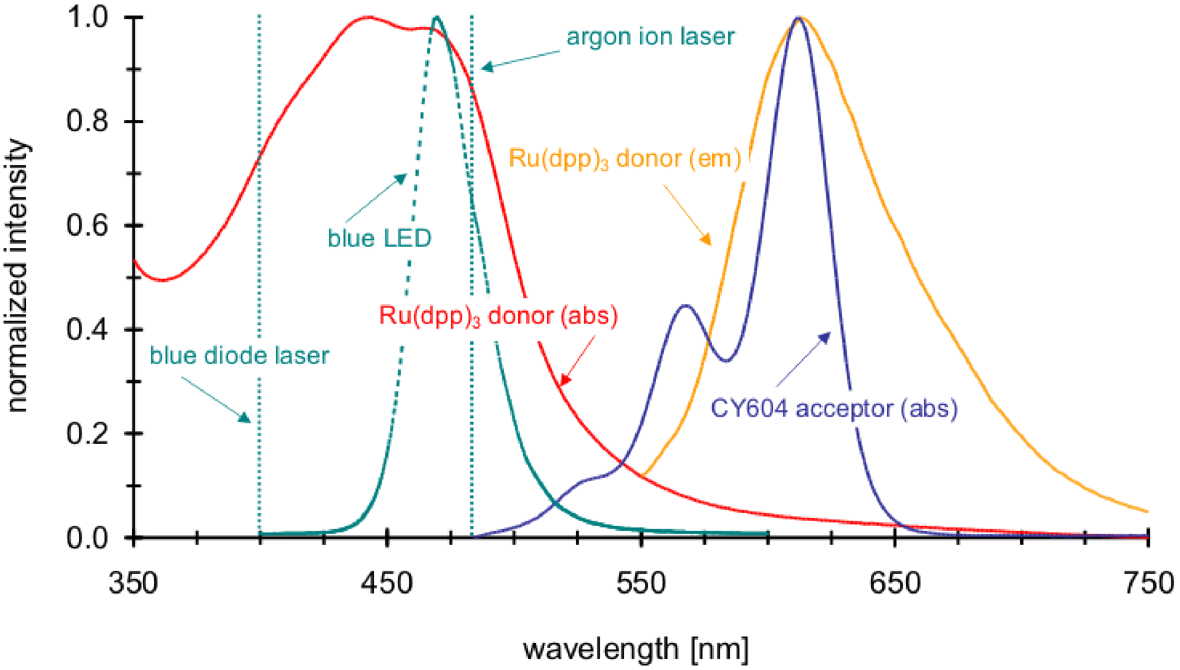

Figure 4.4. Phosphorescence excitation and emission spectra (λ_{exc} 488 nm) of the ruthenium donor complex and, exemplary, the absorbance spectrum of the cyanine acceptor CY604. Three conceivable excitation light sources for the ruthenium complex are included: the blue diode laser line (404 nm), the blue LED spectrum (maximum at 470 nm) and the argon ion laser line (488 nm).

4.3.1.2. Fluorescent acceptor dyes

Four highly fluorescent cyanines (see Figure 4.5. for chemical structures and Table 4.7. for spectral data) were selected as acceptor dyes for the following reasons[110]. They show almost no intrinsic absorbance at wavelengths shorter than 500 nm. This guarantees a selective excitation of the phosphorescent donor with the 488 nm line of the argon ion laser. Their absorbances range from approximately 570 to 750 nm but since even the shortwave shoulder peaks can be used for excitation purposes, dyes with an absorbance of well above 750 nm can be used as well. The cyanines have molar absorbances exceeding 200,000 L mol^{-1} cm^{-1} and large quantum yields. Their lipophilic character along with the positive charge which results in a strong interaction with the carboxylic groups of the copolymer simplifies the incorporation into nanospheres. The large overlap with the absorbance spectra of the ruthenium phosphorescence and the small fluorescence emission peaks of the cyanines are further attractive qualities for RET applications. The cyanines have a good photostability. All in all, those features make the cyanines ideal energy acceptors.

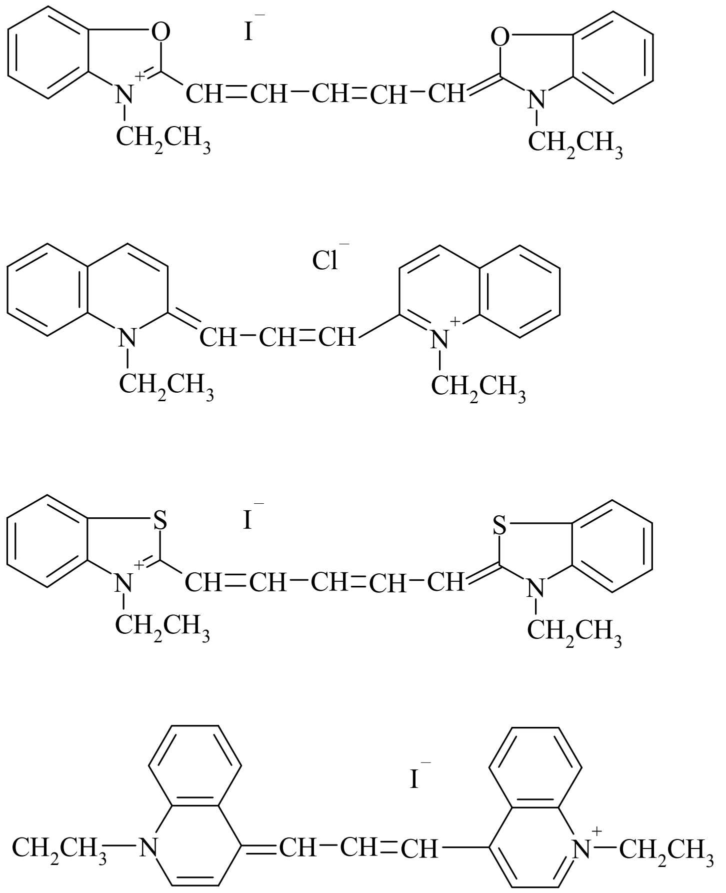

CY582

CY604

CY655

CY703

Figure 4.5. Chemical structures of the foure fluorescent cyanines (CY582, CY604, CY655, CY703) used as acceptor dyes.

Table 4.7. Spectral data of the ruthenium complex (donor) and cyanines (acceptors).

dye	**solvent**	λ_{max} **[nm]**	λ_{em} **[nm]**	$\Delta\lambda$ **[nm]**	ε **[L mol^{-1} cm^{-1}]**
Ru(dpp) [a]	phosphate buffer	465	612	147	28,100
CY582	DMF	587	608	21	224,700
CY604	DMF	612	633	21	238,300
CY655	DMF	659	678	19	245,400
CY703	DMF	713	731	18	324,500

[a] encapsulated in PAN-COOH5 or PAN-COOH10 nanospheres (suspensions **C_1a** or **F_1**)

When varying the concentration of the acceptor dye, the luminescence decay time of the donor is changed and, hence, the decay behavior of the stimulated fluorescence of the acceptor dye. It therefore is possible to use the phosphorescence decay time of the micro- and nanospheres as a parameter for identification along with the spectral properties.

Consequently, a two-dimensional field of luminescence labels is created (compare Figure 4.1.).

Table 4.7. summarizes the spectral data of the donor and acceptor dyes applied. Figure 4.6. shows the absorbance spectra of the cyanines in DMF. The hatched areas indicate the overlap of the ruthenium MLC phosphorescence with the cyanine absorbance spectra. In fact, up to seven or eight different cyanines can serve as luminescence energy acceptors, provided that their excitation wavelengths cover the ruthenium donor emission wavelength range between approximately 550 and 750 nm. Figure 4.7. shows the luminescence emission spectra of the cyanines in DMF.

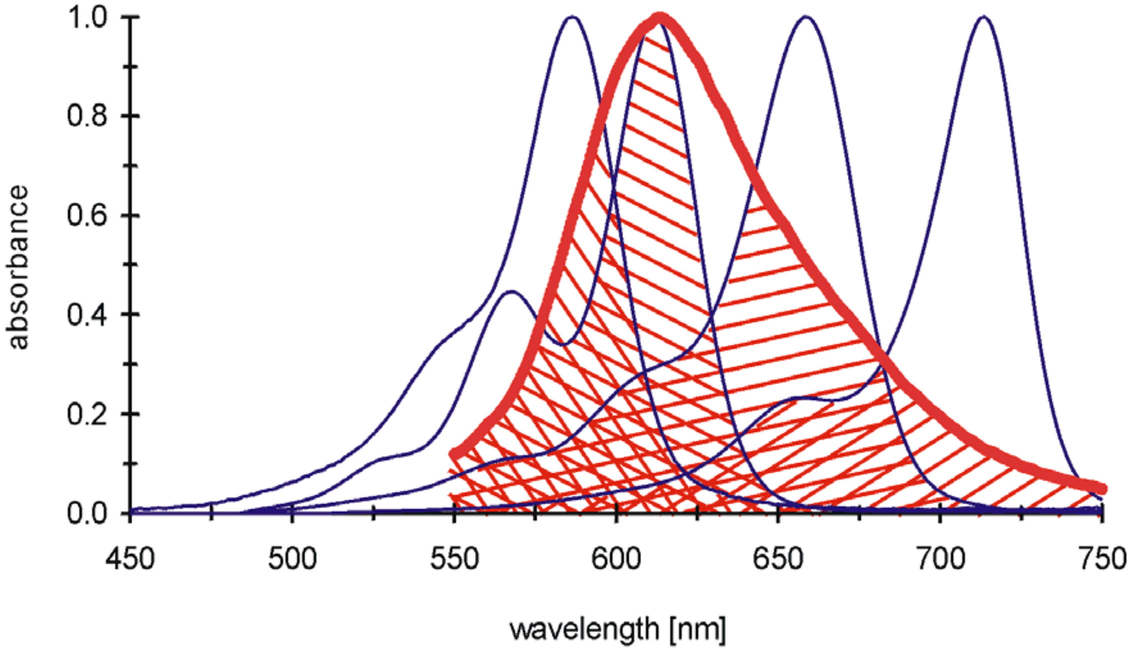

F

Figure 4.6. Normalized absorbance spectra of the cyanines in DMF, from left to right: CY582, CY604, CY655, CY703. The hatched areas indicate the overlap of the ruthenium donor phosphorescence emission spectrum (bold red line) with the four cyanine acceptor absorbance spectra, respectively.

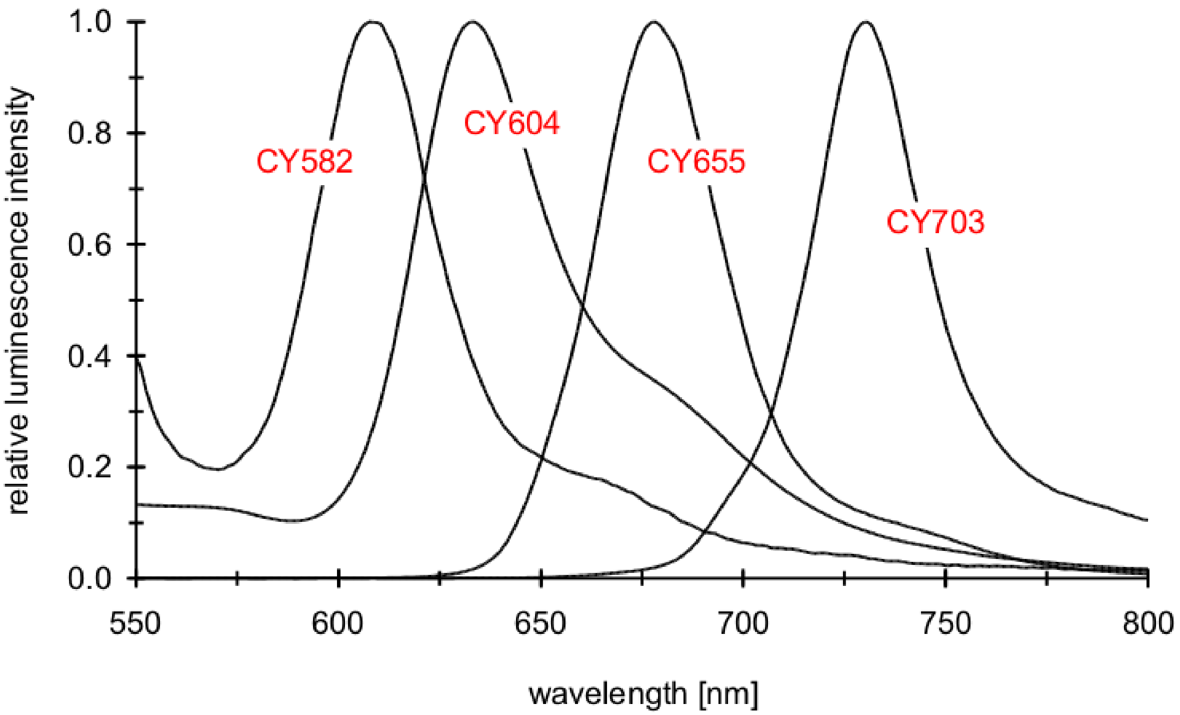

Figure 4.7. Luminescence emission spectra of the cyanines, from left to right: CY582, CY604, CY655, CY703.

4.3.2. Choice of encapsulation matrix

Polyacrylonitrile and its derivatives are attractive polymeric matrices for the encapsulation of phosphorescent dyes in micro- and nanospheres[90-91, 109, 111]. They display an extraordinarily poor permeability for gases and ionic as well as uncharged chemical species. Hence, they can protect luminescent dyes against potential luminescence quenchers, such as oxygen. Polyacrylonitrile polymers are soluble in DMF, swell in DMF/water mixtures and act themselves as good solvents for many lipophilic dyes.

On dropwise addition of water to a diluted solution of polyacrylonitrile in DMF, a stable dispersion of nanoscale polyacrylonitrile aggregates is formed. Surprisingly, the nanospheres do not aggregate or sediment. If the spheres are precipitated from DMF solutions containing Ru(dpp), the dye is co-precipitated with the spheres. This is an elegant way to stain nanospheres in a defined manner. Solvents other than water may also be used to precipitate the polyacrylonitrile nanospheres provided (a) that the solvent is miscible with DMF and (b) that the polymer is not soluble in the binary mixture. Since polyacrylonitrile and its copolymers are soluble in DMF only, the nanospheres may be suspended in almost any other solvent.

Polyacrylonitrile with an acrylic acid content of 5 – 10% (w/w) proved to be the best choice to obtain stable suspensions due to electrostatic repulsion of the surface of the nanospheres and to provide for active groups on the surface of the nanospheres for the covalent coupling of biomolecules by conventional methods, as shown in chapter 5.2.4.[109].

4.3.3. Photophysical characterization of nanospheres

A schematic view of a typical flow cytometric set-up is shown in Figure 4.8. A light source emits light at the excitation wavelength of the ruthenium donor complex which passes the sample containing the labelled nanospheres. It is then diverted (a) to a fluorimeter and (b) to a phase detection system. The first one serves to record an emission spectrum of the sample and the latter one to measure the phase angle which can subsequently be converted into an average luminescence decay time.

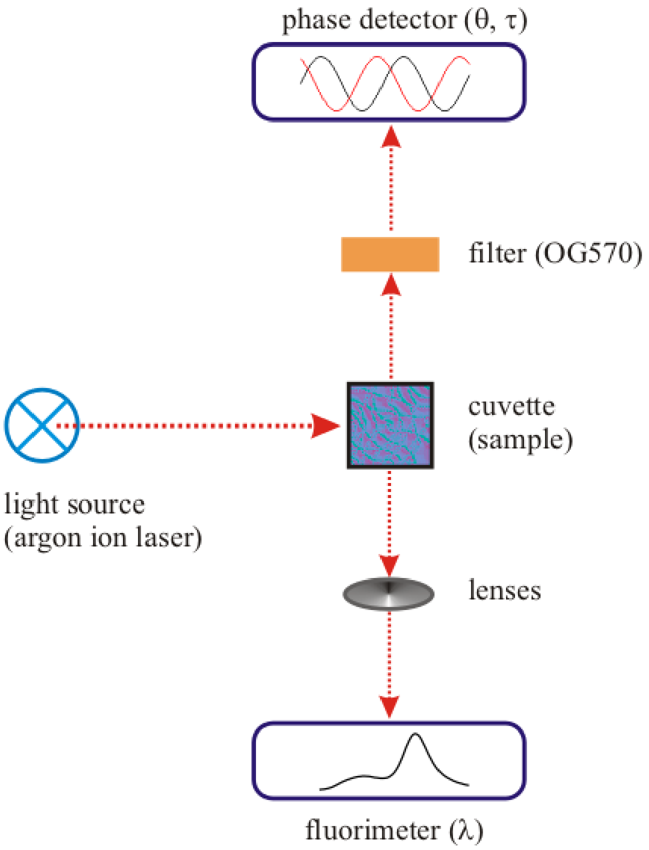

Figure 4.8. Schematic flow cytometry set-up to record luminescence emission spectra and measure luminescence decay times.

A state-of-the-art phase detection system can easily resolve phase angles down to 1°. Such a differentiation allows a variation of the phase angle from 60° (no RET) down to

20° (highest RET). In the two-dimensional assay, with 10 different acceptor dyes, the setting up of an array of 400 labels is possible. In the three-dimensional assay, with 100 different accetor pairs, an array of 4000 labels becomes feasible.

4.3.3.1. Absorbance and emission spectra

TWO-DIMENSIONAL ASSAY. In each of the four arrays, the cyanine absorbance at the appropriate wavelength increases with dye concentration at a constant level of donor concentration (Figure 4.9.). The acceptor concentrations were calculated from those absorbance spectra using the known molar absorbances of the donor and acceptor dyes and assuming that the donor was quantitatively extracted into the polymer matrix during sphere precipitation.

Figure 4.10. shows the luminescence emission spectra (at λ_{exc} 488 nm) of those nanospheres normalized to 1 at the emission wavelength of the ruthenium complex (611.5 nm).

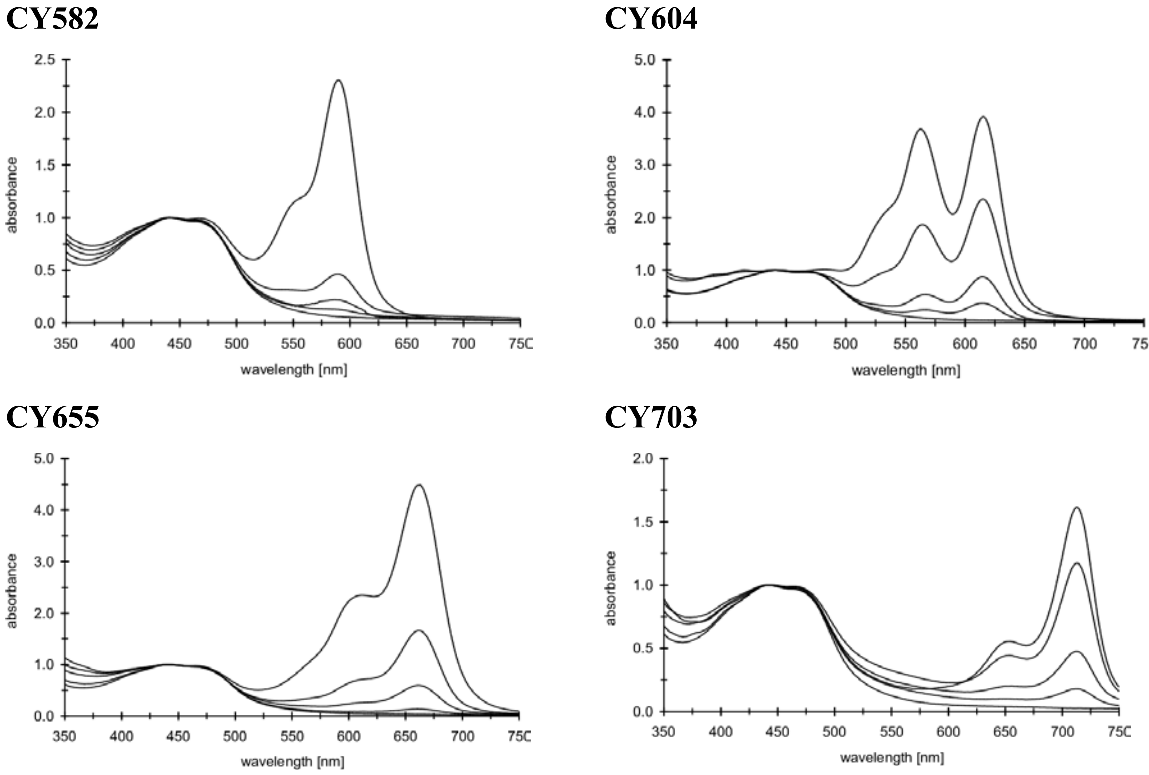

Figure 4.9. Two-dimensional assay. Absorbance spectra in phosphate buffer [acceptor concentrations from top to bottom]: (top left) CY582 [1.30, 0.27, 0.14, 0.08, 0 mmol/kg], (top right) CY604 [1.82, 1.09, 0.40, 0.18, 0 mmol/kg], (bottom left) CY655 [2.43, 0.89, 0.32, 0.08, 0 mmol/kg], (bottom right) CY703 [0.58, 0.43, 0.18, 0.07, 0 mmol/kg].

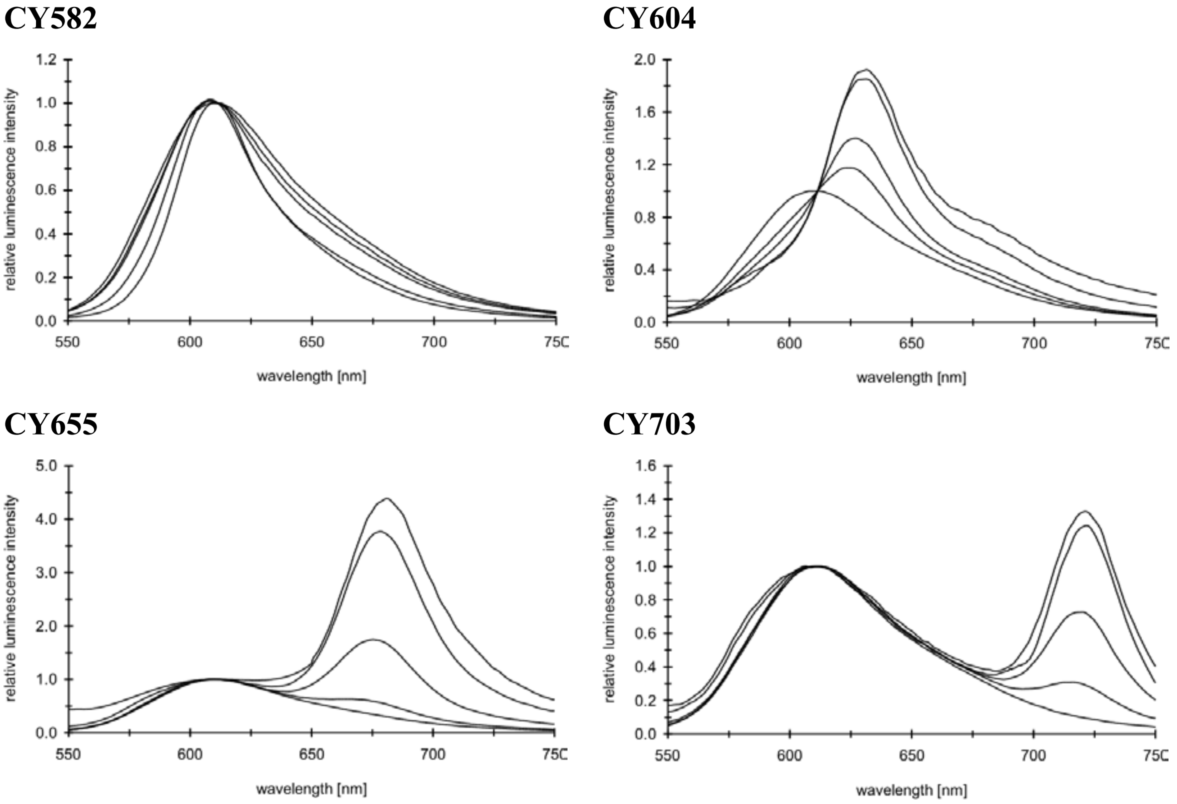

Figure 4.10. Two-dimensional assay. Luminescence emission spectra in phosphate buffer [acceptor concentrations from top to bottom]: (top left) CY582 [1.30, 0.27, 0.14, 0.08, 0 mmol/kg], (top right) CY604 [1.82, 1.09, 0.40, 0.18, 0 mmol/kg], (bottom left) CY655 [2.43, 0.89, 0.32, 0.08, 0 mmol/kg], (bottom right) CY703 [0.58, 0.43, 0.18, 0.07, 0 mmol/kg].

The underlying principle of all arrays is that the luminescence emission of the ruthenium complex decreases due to resonance energy transfer to the cyanine acceptor within the same nanosphere. Figure 4.11. shows a scheme to illustrate intra-particular RET from Ru(dpp) donor (λ_{em} 612 nm, constant concentration) to a cyanine acceptor (here λ_{em} 678 nm for CY655, five different concentrations) within one nanosphere. The measured decay times of all 16 nanosphere labels, at the respective emission wavelength of the cyanine acceptor, are plotted in a two-dimensional field in Figure 4.12.

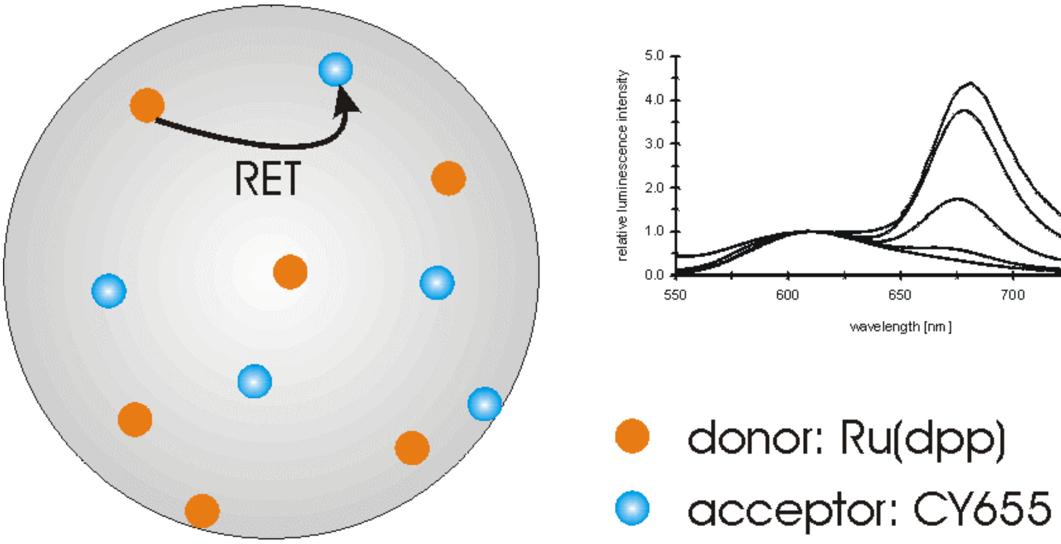

Figure 4.11. Two-dimensional assay. Scheme to illustrate intra-particular RET from Ru(dpp) donor (λ_{em} 612 nm, constant concentration) to cyanine acceptor (λ_{em} 678 nm for CY655, five different concentrations) within one nanosphere.

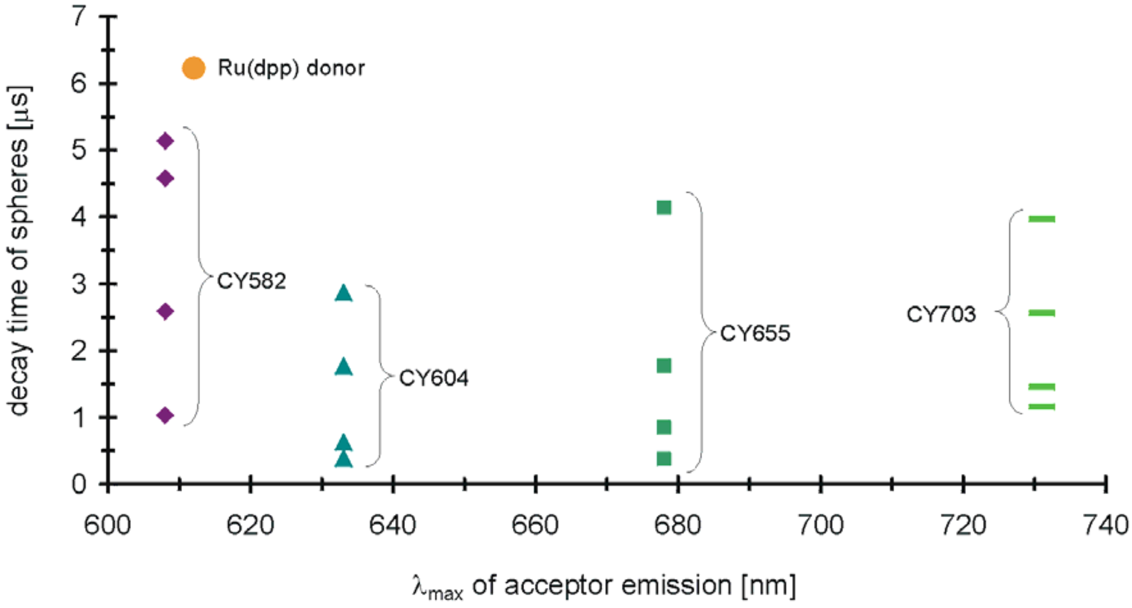

Figure 4.12. Two-dimensional field showing classification of 16 nanosphere labels based on simultaneous analysis of both emission wavelength of cyanine acceptor and apparent decay time of spheres (compare Figure 4.1. for theoretical approach).

The relative luminescence intensity of the nanospheres rises with the increase of the acceptor concentration in the four different luminescence emission arrays (Figure 4.10.). Since the excitation of the cyanines cannot result directly from the argon ion laser light source due to negligible absorbance at 488 nm, it must result from the emission of the excited ruthenium complex. Thus, one can clearly observe the phenomenon of RET. As can be seen in Table 4.9., the apparent decay time in air consecutively decreases from

6.23 µs (no acceptor) to 0.38 – 1.16 µs (maximal acceptor concentration) depending on the applied cyanine and its concentration. Along with it, the quantum yield in air also decreases from 0.38 to 0.03 – 0.27, once again depending on the acceptor characteristics. The levels of oxygen quenching are very low throughout all arrays with always below 3.5% cross-sensitivity (change of Φ between air and N_2).

THREE-DIMENSIONAL ASSAY. In this array of 16 labels, the cyanine absorbance at the appropriate wavelength (659 nm for CY655 and 713 for CY703) increases with dye concentration at a constant level of donor concentration (Figure 4.13.). The acceptor concentrations were calculated from those absorbance spectra using the known molar absorbances of the donor and acceptor dyes and assuming that the donor was quantitatively extracted into the polymer matrix during sphere precipitation.

Figure 4.14. shows the luminescence emission spectra (at λ_{exc} 488 nm) of those nanospheres normalized to 1 at the emission wavelength of the ruthenium complex (613 nm). Table 4.8. lists the ratios of the emission maxima of Ru(dpp)/CY655 and Ru(dpp)/CY703, while Figure 4.15. gives a plot of a selection of those ratios against the respective acceptor concentrations in the nanospheres.

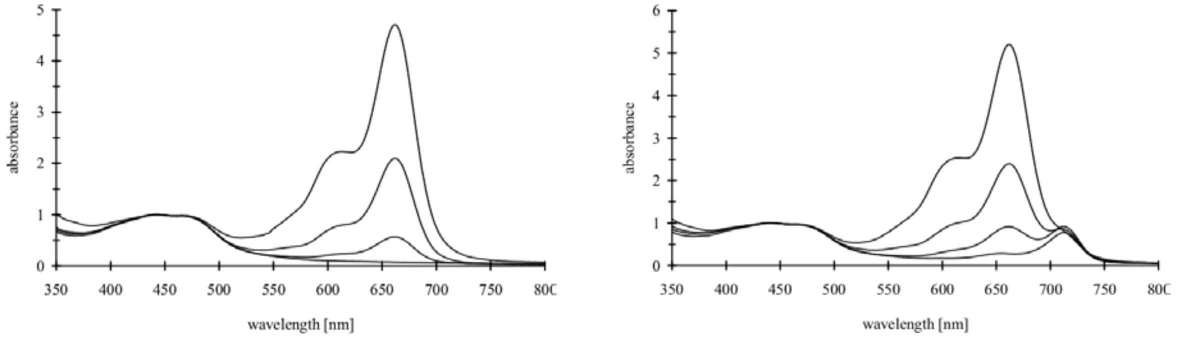

(I) **F_1, F_2, F_3, F_4**

(II) **F_5, F_6, F_7, F_8**

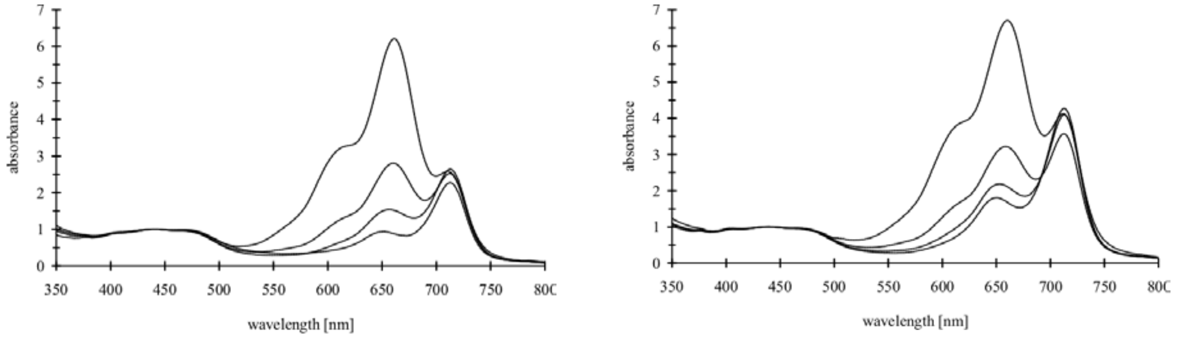

(III) **F_9, F_{10}, F_{11}, F_{12}**

(IV) **F_{13}, F_{14}, F_{15}, F_{16}**

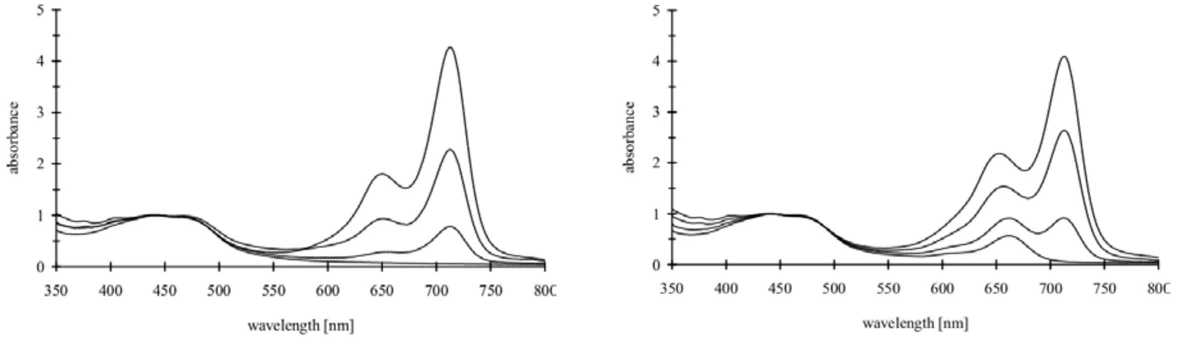

(V) **F_1, F_5, F_9, F_{13}**

(VI) **F_2, F_6, F_{10}, F_{14}**

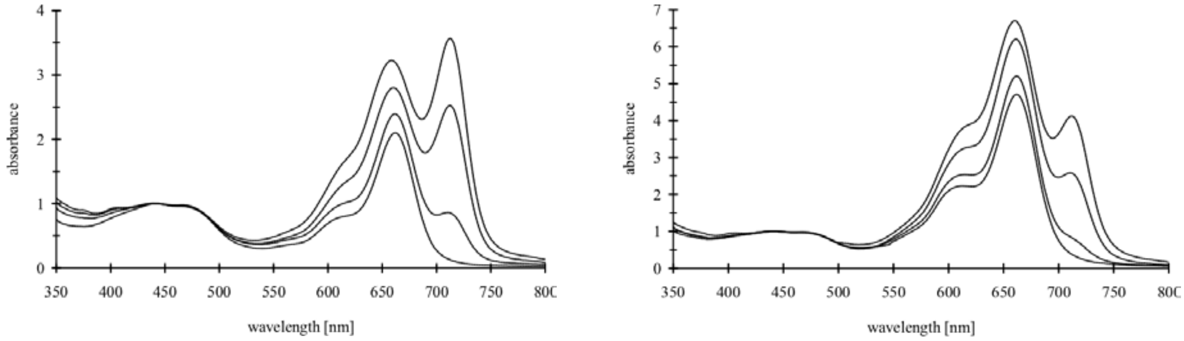

(VII) **F_3, F_7, F_{11}, F_{15}**

(VIII) **F_4, F_8, F_{12}, F_{16}**

Figure 4.13. Three-dimensional assay. Absorbance spectra of eight combinations (I) – (VIII) of always four different suspensions in MES buffer [for acceptor concentrations see Table 4.10.]: (I) **F_1**, **F_2**, **F_3**, **F_4**; (II) **F_5**, **F_6**, **F_7**, **F_8**; (III) **F_9**, **F_{10}**, **F_{11}**, **F_{12}**; (IV) **F_{13}**, **F_{14}**, **F_{15}**, **F_{16}**; (V) **F_1**, **F_5**, **F_9**, **F_{13}**; (VI) **F_2**, **F_6**, **F_{10}**, **F_{14}**; (VII) **F_3**, **F_7**, **F_{11}**, **F_{15}**; (VIII) **F_4**, **F_8**, **F_{12}**, **F_{16}** [always arranged from bottom to top].

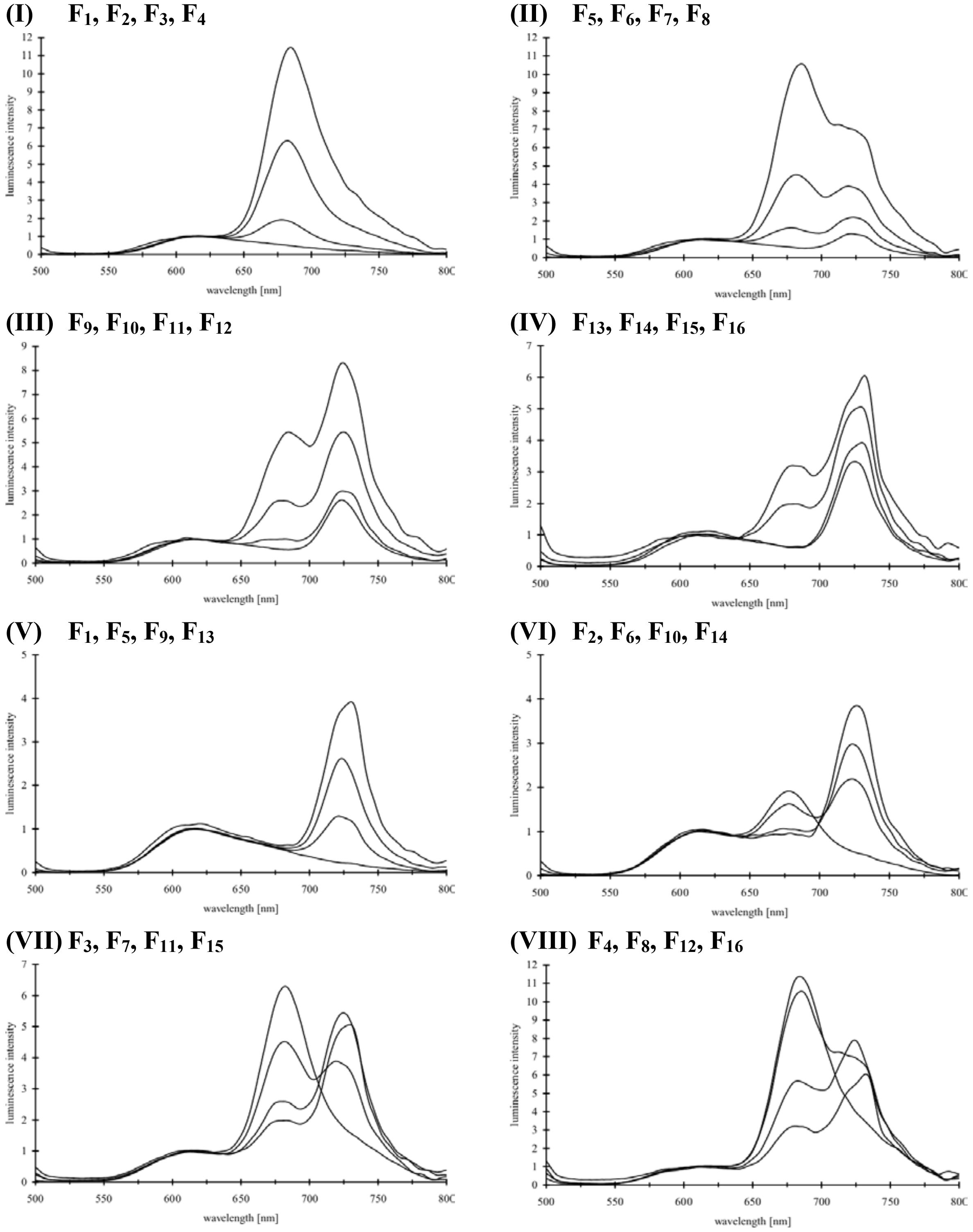
(I) F_1, F_2, F_3, F_4

(II) F_5, F_6, F_7, F_8

(III) F_9, F_{10}, F_{11}, F_{12}

(IV) F_{13}, F_{14}, F_{15}, F_{16}

(V) F_1, F_5, F_9, F_{13}

(VI) F_2, F_6, F_{10}, F_{14}

(VII) F_3, F_7, F_{11}, F_{15}

(VIII) F_4, F_8, F_{12}, F_{16}

Figure 4.14. Three-dimensional assay. Luminescence emission spectra of eight combinations (I) – (VIII) of always four different suspensions in MES buffer [for acceptor concentrations see Table 4.10.]: (I) **F_1**, **F_2**, **F_3**, **F_4**; (II) **F_5**, **F_6**, **F_7**, **F_8**; (III) **F_9**, **F_{10}**, **F_{11}**, **F_{12}**; (IV) **F_{13}**, **F_{14}**, **F_{15}**, **F_{16}**; (V) **F_1**, **F_5**, **F_9**, **F_{13}**; (VI) **F_2**, **F_6**, **F_{10}**, **F_{14}**; (VII) **F_3**, **F_7**, **F_{11}**, **F_{15}**; (VIII) **F_4**, **F_8**, **F_{12}**, **F_{16}** [always arranged from bottom to top].

Table 4.8. Three-dimensional assay. Ratios of the emission maxima of Ru(dpp)/CY655 and Ru(dpp)/CY703.

name of suspension	**ratio of emission maxima of Ru(dpp)/CY655**	**ratio of emission maxima of Ru(dpp)/CY703**
F_1	1.90	4.42
F_2	0.53	1.77
F_3	0.16	0.53
F_4	0.09	0.23
F_5	1.83	0.77
F_6	0.62	0.46
F_7	0.22	0.26
F_8	0.10	0.15
F_9	1.92	0.37
F_{10}	1.00	0.34
F_{11}	0.41	0.18
F_{12}	0.19	0.12
F_{13}	1.61	0.27
F_{14}	1.20	0.28
F_{15}	0.51	0.22
F_{16}	0.31	0.19

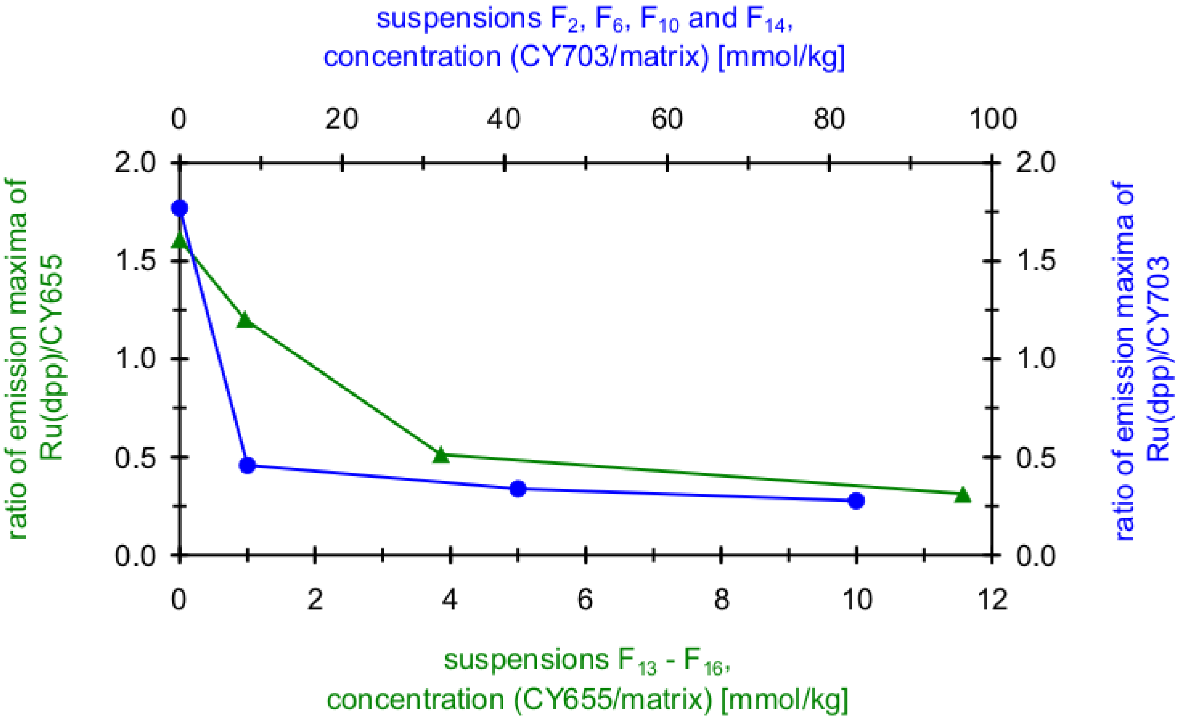

Figure 4.15. Plot of a selection of ratios of the emission maxima of Ru(dpp)/CY655 [▲, from left to right: suspensions **F13** – **F16**, $c_{CY703/matrix}$ 83.28 mmol/kg (constant)] and Ru(dpp)/CY703 [●, from left to right: suspensions **F2**, **F6**, **F10** and **F16**, $c_{CY655/matrix}$ 0.96 mmol/kg (constant)] against the respective acceptor concentrations in the nanospheres.

4.3.3.2. Luminescence frequency spectra

TWO-DIMENSIONAL ASSAY. Figure 4.16. shows the phase angles and modulations at a frequency range from 1 kHz to 1 MHz, respectively. The apparent decay time is composed of both the ruthenium donor as well as the delayed cyanine acceptor decay times. Since the decay behavior is rather multiexponential than monoexponential, the apparent decay times were not determined by those multifrequency measurements but were calculated from phase angles obtained by a single frequency measurement at a modulation frequency of 45 kHz.

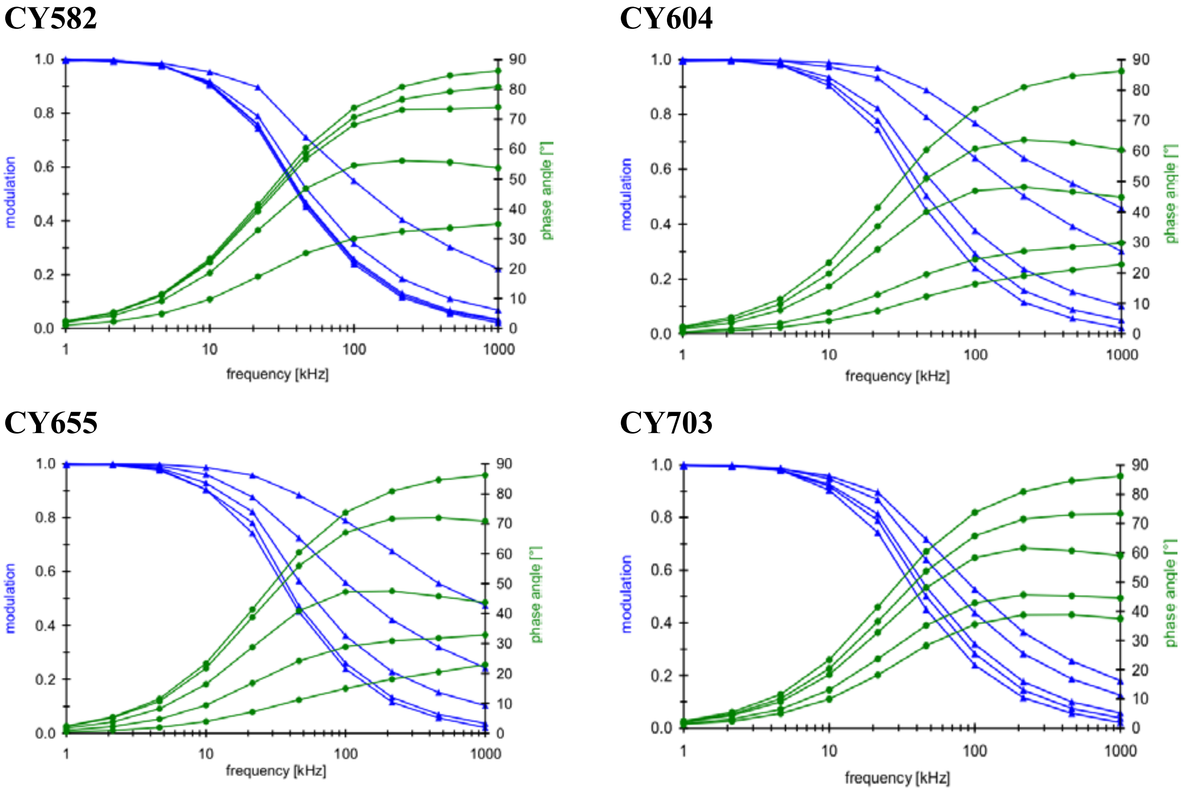

Figure 4.16. Two-dimensional assay. Frequency spectra in phosphate buffer [acceptor concentrations – modulation (▲) from top to bottom / phase angles (●) from bottom to top]: (top left) CY582 [1.30, 0.27, 0.14, 0.08, 0 mmol/kg], (top right) CY604 [1.82, 1.09, 0.40, 0.18, 0 mmol/kg], (bottom left) CY655 [2.43, 0.89, 0.32, 0.08, 0 mmol/kg], (bottom right) CY703 [0.58, 0.43, 0.18, 0.07, 0 mmol/kg].

In the frequency spectra, with rising modulation frequencies the modulation goes down from 1 to almost 0 and, simultaneously, the phase angle increases from 0° to approximately 90°. The slight decrease of the phase angles at frequencies close to 1 MHz is caused by a small fraction of direct excitation of the cyanines at those high frequencies. If a monoexponential fit is applied (which is only justifiable for suspensions **C_1a** – **C_4a** with an acceptor concentration of 0 mmol/kg), the intersection of the modulation and phase angle curves lead to the proper modulation frequency for the ruthenium complex of about 45 kHz.

THREE-DIMENSIONAL ASSAY. Figures 4.17. and 4.18. show the phase angles and modulations at a frequency range from 1 – 100 kHz, respectively. The apparent decay time is composed of both the ruthenium donor as well as the delayed cyanine acceptors decay times. Since the decay behavior is rather multiexponential than monoexponential, the apparent decay times were not determined by those multifrequency measurements but were calculated from phase angles obtained by a single frequency measurement at a modulation frequency of 45 kHz, as in the two-dimensional assay.

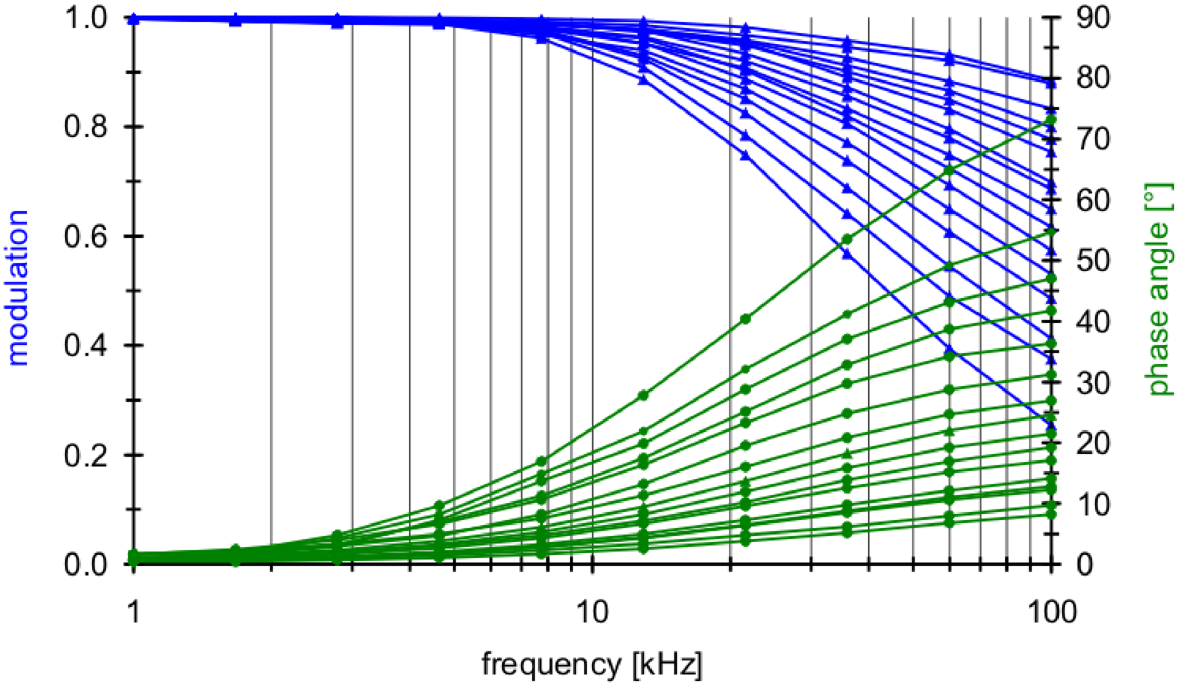

Figure 4.17. Three-dimensional assay. Frequency spectra in MES buffer [modulation (▲): **F**$_1$ – **F**$_{16}$ from bottom to top, phase angles: (●) **F**$_1$ – **F**$_{16}$ from top to bottom].

(I) F_1, F_2, F_3, F_4

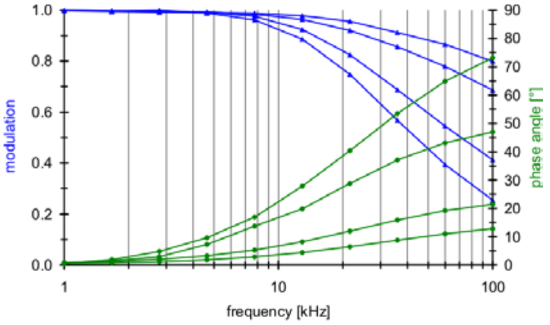

(II) F_5, F_6, F_7, F_8

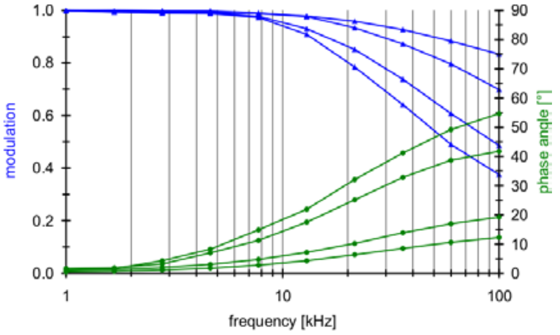

(III) F_9, F_{10}, F_{11}, F_{12}

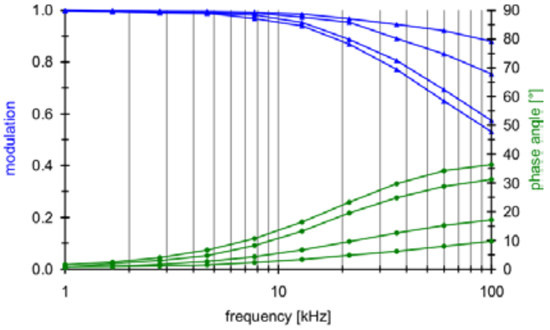

(IV) F_{13}, F_{14}, F_{15}, F_{16}

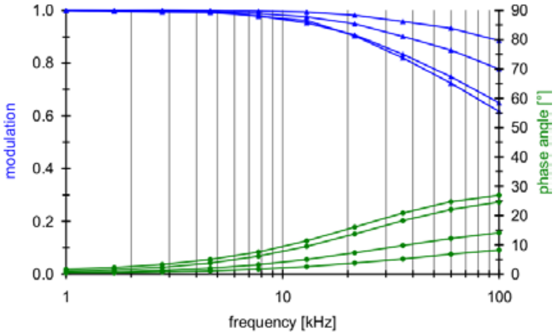

(V) F_1, F_5, F_9, F_{13}

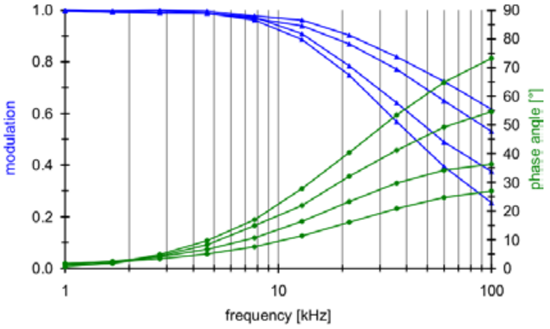

(VI) F_2, F_6, F_{10}, F_{14}

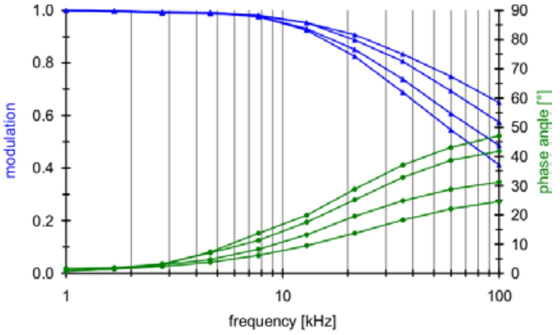

(VII) F_3, F_7, F_{11}, F_{15}

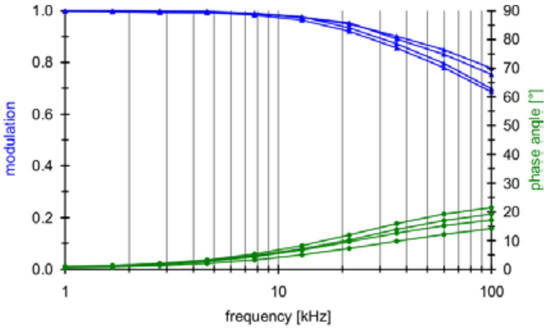

(VIII) F_4, F_8, F_{12}, F_{16}

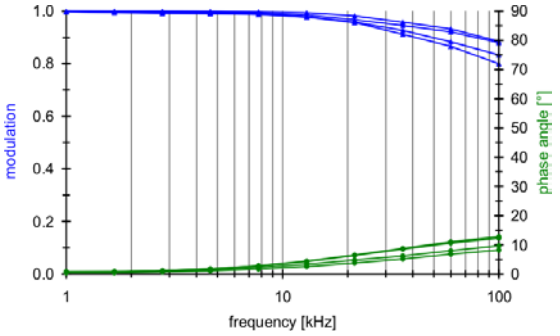

Figure 4.18. Three-dimensional assay. Frequency spectra of eight combinations (I) – (VIII) of always four different suspensions in MES buffer [for acceptor concentrations see Table 4.10.]: (I) **F_1**, **F_2**, **F_3**, **F_4**; (II) **F_5**, **F_6**, **F_7**, **F_8**; (III) **F_9**, **F_{10}**, **F_{11}**, **F_{12}**; (IV) **F_{13}**, **F_{14}**, **F_{15}**, **F_{16}**; (V) **F_1**, **F_5**, **F_9**, **F_{13}**; (VI) **F_2**, **F_6**, **F_{10}**, **F_{14}**; (VII) **F_3**, **F_7**, **F_{11}**, **F_{15}**; (VIII) **F_4**, **F_8**, **F_{12}**, **F_{16}** [always modulation (▲) from bottom to top and phase angles (●) from top to bottom].

4.3.4. Physical characterization of nanospheres

4.3.4.1. Diameter, shape and surface charge

In addition to the spectral characterization of the nanospheres, their physical properties were examined, too. Scanning electron microscopic pictures of gold/palladium (60/40)-coated nanospheres as well as transission electron microscopic pictures both showed a nearly circular shape and a diameter of roughly 50 nm. Static and dynamic light scattering along with laser Doppler velocimetry experiments revealed a polydisperse coil with a diameter of the nanospheres of 50 – 70 nm and a ζ potential confirming the negative surface charge resulting from the carboxylic groups. Suspension **C3a** (c_{CY655} 0 mmol/kg, $c_{Ru(dpp)}$ 5.00 mmol/kg), for instance, showed a hydrodynamic diameter of 65 nm (Figure 4.19.) and a ς-potential of -60 mV.

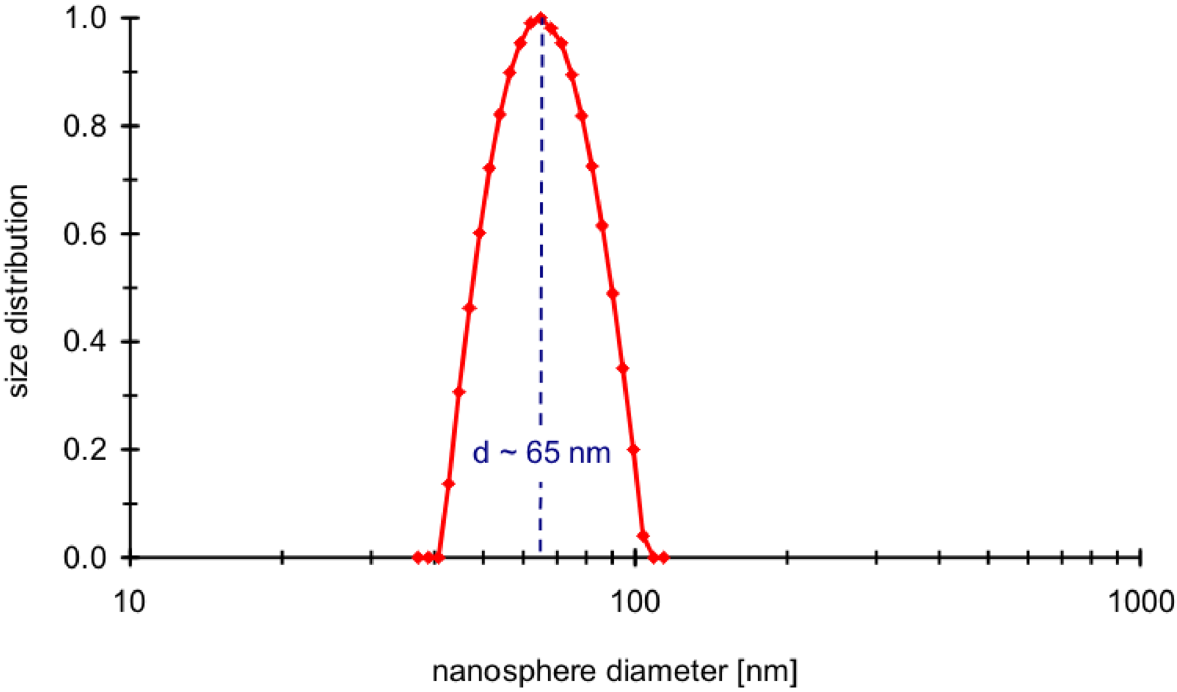

Figure 4.19. Radius of nanospheres (suspension **C3a**) as determined by dynamic light scattering at a detection angle of 90°.

4.3.4.2. Apparent decay time, quantum yield and cross-sensitivity to oxygen

TWO-DIMENSIONAL ASSAY. Table 4.9. shows a summary of the spectral characterization of the nanospheres of the four different cyanines at varying dye concentrations in phosphate buffer (pH 7.0, IS 50 mM, 0.5% (w/w) sodium azide, 0.5% (w/w) trehalose) with c being the concentration, τ the apparent decay time, Φ the quantum yield (air/N_2) and ΔΦ the oxygen cross-sensitivity (change of Φ between air and N_2).

Table 4.9. Two-dimensional assay. Figures of merit for the Ru(dpp)/cyanine nanospheres suspended in phosphate buffer.

name of suspension [a]	**c (acceptor/matrix)** [b] **[mmol/kg]**	**τ, air** [μs]	**Φ, air**	**Φ, N_2**	**ΔΦ, air/N_2** [%]
C_1a	0	6.23	0.37	0.39	3.4
C_1b	0.08	5.14	0.36	0.37	2.5
C_1c	0.14	4.58	0.34	0.35	3.3
C_1d	0.27	2.59	0.32	0.33	2.6
C_1e	1.30	1.03	0.27	0.28	1.2
C_2b	0.18	2.87	0.32	0.32	1.8
C_2c	0.40	1.77	0.25	0.25	1.8
C_2d	1.09	0.63	0.08	0.08	1.7
C_2e	1.82	0.39	0.03	0.03	1.5
C_3b	0.08	4.15	0.30	0.31	2.9
C_3c	0.32	1.78	0.27	0.28	1.4
C_3d	0.89	0.85	0.18	0.19	1.4
C_3e	2.43	0.38	0.07	0.08	2.1
C_4b	0.07	3.97	0.25	0.26	2.4
C_4c	0.18	2.56	0.20	0.21	2.4
C_4d	0.43	1.46	0.16	0.16	2.1
C_4e	0.58	1.16	0.06	0.06	1.7

[a] **C_1a = C_2a = C_3a = C_4a**

[b] acceptor = respective cyanine, donor = Ru(dpp), matrix = PAN-COOH5; $c_{donor/matrix}$ = 5.00 mmol/kg (constant)

THREE-DIMENSIONAL ASSAY. Table 4.10. shows a summary of the spectral characterization of the nanosphere suspenions **F_1** – **F_{16}** in MES buffer (pH 7.0, IS 30 mM, 0.5% (w/w) sodium azide, 0.5% (w/w) trehalose) with c being the concentration, τ the apparent decay time, Φ the quantum yield (air/N_2) and $\Delta\Phi$ the oxygen cross-sensitivity (change of Φ between air and N_2).

Table 4.10. Three-dimensional assay. Figures of merit for the Ru(dpp)/cyanines nanospheres suspended in MES buffer.

name of suspension	**c (CY655/m.)** [a] **[mmol/kg]**	**c (CY703/m.)** [a] **[mmol/kg]**	**τ, air** [μs]	**Φ, air**	**Φ, N_2**	**$\Delta\Phi$, air/N_2** [%]
F_1	0.00	0.00	5.92	0.39	0.39	0.7
F_2	0.96	0.00	2.23	0.15	0.15	0.7
F_3	3.86	0.00	0.89	0.06	0.06	0.4
F_4	11.57	0.00	0.56	0.04	0.04	0.5
F_5	0.00	8.33	3.12	0.20	0.20	1.8
F_6	0.96	8.33	1.67	0.10	0.10	0.5
F_7	3.86	8.33	0.73	0.05	0.05	3.3
F_8	11.57	8.33	0.53	0.03	0.03	3.2
F_9	0.00	41.64	1.36	0.09	0.09	2.1
F_{10}	0.96	41.64	1.17	0.08	0.09	2.1
F_{11}	3.86	41.64	0.66	0.04	0.04	0.7
F_{12}	11.57	41.64	0.43	0.03	0.03	3.0
F_{13}	0.00	83.28	1.11	0.07	0.07	2.5
F_{14}	0.96	83.28	0.93	0.06	0.06	0.9
F_{15}	3.86	83.28	0.65	0.04	0.04	1.3
F_{16}	11.57	83.28	0.34	0.02	0.02	1.3

[a] donor = Ru(dpp), matrix (m.) = PAN-COOH10; $c_{donor/matrix}$ = 8.55 mmol/kg (constant)

4.4. Conclusion

The multi-color multi-lifetime sensing scheme introduced here is based on the co-immobilization of two luminescent dyes into a polymer matrix, on the effect of resonance energy transfer between both dyes (compare Figure 4.11.) and the fact that the donor is not fluorescent but rather phosphorescent. This way, indesirable background fluorescence is eliminated. The multiplexing principle has each label identified by both the spectral signature and the characteristic luminescence lifetime.

Since the ruthenium complex has a rather broad emission band, it can be combined with a number of acceptor dyes of different absorbance spectra. As a result, spheres are obtained which have variable spectral properties. No cascades of dyes are necessary but rather a single donor-acceptor pair is adequate.

The same donor dye can be employed in all cases in order to obtain a whole series of multiplexing labels. A highly luminescent ruthenium(II)-tris(polypyridyl) complex, $Ru(dpp)_3(TMS)_2$, proved to be the best choice for a combination with the acceptor dyes used here. This way a one-dimensional series of fluorescent labels with identical absorbance behavior but clearly distinguishable emission properties is obtained.

Ways to increase sensitivity of luminescence assays and thus to eliminate background fluorescence of the sample are: (1) use of longwave (red light or NIR) emitting dyes with a large Stokes' shift allow the selective detection of luminescence signals in samples, such as body fluids, since biological matter hardly emits red light. (2) Use of phosphorescent dyes. Since the intrinsic fluorescence of most samples typically decays within a few nanoseconds, time-resolved measurement enables almost background-free detection of phosphorescence. Chelates of the rare earth metals Eu^{3+} and Tb^{3+} are among the most often applied phosphorescent dyes for labelling biomolecules. (3) Incorporation of fluorescent dyes into polymer matrices to yield micro- or nanospheres. The encapsulation of dyes into polymer matrices generally not only increases their quantum yields but at the same time also shields them against undesirable interferences, such as notorious luminescence quenchers (e.g. oxygen). In addition, by encapsulating dyes in high concentrations, a significant magnification in the intensity in a luminescence array is obtained.

The new labels display several attractive features: (1) The fluorescence of the acceptor which is induced by RET within the particle is decaying in the µs time regime and thus displays the characteristics of phosphorescence. With time-resolved methods of phosphorescence detection a background-free measurement is possible. (2) A two-dimensional field of phosphorescence labels can be created. With seven different dyes (one donor, six acceptors) and 10 individually differing decay times – which can easily be realized by a technical point of view – 60 distinguishable labels can be obtained. (3) The nanospheres were designed to facilitate multicolor detection, particularly in applications that use lasers with their inherent limited number of excitation wavelengths. An excitation of the emission of all labels is possible with the argon ion laser. Due to an efficient light absorbance of the ruthenium donor complex at a wavelength of 404 nm, a blue laser diode can be used as light source, as well. (4) The Stokes' shift of all labels is remarkably high. When employing the blue laser diode as light source, it varies between 190 and 360 nm. Even with the TransFluoSpheres this would only be feasible with an extremely long cascade of several dyes and each step of the cascade causes an additional loss of signal. These large Stokes' shifts are determined by the spectral properties of the donor. (5) The donor can be encapsulated in concentrations of up to 10% (w/w) into the polymer matrix without a significant decrease of quantum yield. The missing overlap of absorbance and emission bands of the donor molecules prevents self-quenching, resulting in an exceptionally high brightness of the luminescence signals. (6) By using a known method of embedding phosphorescent dyes into nanospheres, the preparation of those particles is very easy to accomplish[109]. The preparation is based on a co-precipitation of both donor and acceptor dyes and polyacrylonitrile (PAN) derivatives from a solution in DMF. Essential is the complete solubility of the polyacrylonitrile matrix and the donor and acceptor dyes in DMF. Those features lead to universally useful immuno-sensing systems since all lipophilic dyes can be encapsulated within the polyacrylonitrile copolymer. (7) The encapsulation of a phosphorescent donor into a polymer matrix with little pO_2 permeability prevents quenching of the phosphorescence and warrants high signal intensities. (8) By using PAN copolymers, phosphorescent nanospheres with reactive surfaces for the covalent coupling to proteins or other biomolecules can be produced. This coupling is done by conventional methods and is demonstrated in chapter 5.2.4. The loading density of the surface with functional reactive groups can be adjusted by the properties of the copolymer. (9) This method can be applied for numerous types of particles, for instance latex particles which can be colored subsequently. The dyes can be incorporated during the precipitation.

5. Homogeneous Luminescence Decay Time-Based Assay Using Energy Transfer From Nanospheres

A NEW SCHEME FOR HOMOGENEOUS ASSAYS IS PRESENTED THAT IS BASED ON RESONANCE ENERGY TRANSFER (RET) FROM PHOSPHORESCENT BIOTINYLATED NANOSPHERES TO FLUORESCENTLY-LABELLED STREPTAVIDIN (SA). THE PHOSPHORESCENT NANOSPHERES, WITH A DIAMETER OF WELL BELOW 50 NM, ARE MADE FROM CARBOXYLATED POLYACRYLONITRILE, DYED WITH RUTHENIUM(II)-TRIS-4,7-DIPHENYL-1,10-PHENANTHROLINE DICHLORIDE ($RU(DPP)_3CL_2$). DUE TO THE SMALL SIZE OF THE NANOSPHERES AND THE COMPLETE EXTRACTION OF THE RUTHENIUM DYE INTO THE NANOSPHERES DURING THE PRECIPITATION PROCESS, RET OCCURS FROM THE RU(DPP) TO THE LABEL IF LABELLED SA BINDS TO THE SURFACE OF THE NANOSPHERES. LUMINESCENCE QUENCHING BY OXYGEN OR OTHER SPECIES PRESENT IN THE SAMPLE CAN BE NEGLECTED DUE TO THE SHIELDING EFFECT OF THE POLYMER MATRIX. BASED ON THIS FINDING, A COMPETITIVE BINDING ASSAY WAS ESTABLISHED, WHERE AVIDIN AND LABELLED SA COMPETE FOR THE BINDING SITES ON THE NANOSPHERE. THE PROCESS OF BINDING TO THE SURFACE CAN BE DETECTED BY MEASUREMENT OF LUMINESCENCE INTENSITY OR DECAY TIME WHICH IS IN THE ORDER OF 2.5 TO 4.4 µS.

5.1. Introduction

Luminescence techniques are becoming more and more attractive for immunoassays[112-125]. Among the existing concepts for immunoassays are (1) radioimmunoassays (RIAs), (2) enzyme-linked immunosorbent assays (ELISAs), (3) dissociation enhanced lanthanoide fluoro-immunoassays (DELFIAs), (4) fluorescence polarization immunoassays (FPIAs), (5) time-resolved immunoassays and (6) energy-transfer immunoassays[126]. ELISAs and DELFIAs are heterogeneous and require several washing steps, while bioassays based on energy transfer, measurement of polarization or decay time can be homogeneous, making them faster and less prone to sources of error during the washing steps. In order to further improve the limit of detection (by eliminating interferences by shortwave fluorophores), longwave-emitting dyes were used and this was combined with measurements of lifetimes in the microsecond regime, thus enabling time-resolved or gated measurements.

In chapter 3.2.4., a simple encapsulation technique was presented to prepare highly phosphorescent, inert nanospheres which are viable luminescent labels[109]. This method is based on the co-precipitation of the phosphorescent ruthenium(II)-tris-4,7-diphenyl-1,10-phenanthroline dichloride, referred to as Ru(dpp) and derivatives of polyacrylonitrile (PAN) from a solution in N,N-dimethylformamide (DMF). The beads precipitate in the form of very small aggregates of spherical shape and a typical particle diameter of less than 50 nm. This process allows the encapsulation of phosphorescent and fluorescent dyes in an individual nanosphere provided that they are sufficiently lipophilic. The most important characteristic of the nanospheres is their very low cross-sensitivity to oxygen, with a quenching rate $\Delta\tau$ of only 3-5% (change of τ air/N_2), and a quantum yield of up to 0.40. The apparent decay time of free Ru(dpp) in water varies between 1.20 µs when saturated with air and 4.70 µs when saturated with nitrogen, but can be as high as 6.00 µs in apolar organic solvents. The extremely low oxygen quenching of the incorporated dye proves the excellent shielding effect of the PAN copolymers and thus shows that the matrix itself does not act as a quencher.

Such nanospheres have now been used to establish a novel scheme for a homogeneous binding assay based on long-lived luminescence[78, 127]. Resonance energy transfer (RET) becomes possible from those nanospheres to an acceptor bound to the surface because of the fractal structure of the nanospheres and a size close to the Förster distance.

5.2. Materials and methods

5.2.1. Chemicals and reagents

All chemicals and solvents used were of analytical grade and used without further purification. Doubly distilled water was used throughout. Poly-(acrylonitrile-co-acrylic acid-co-ethylene glycol) containing 8.3% (w/w) of acrylic acid and 8.3% (w/w) of ethylene glycol (PAN-COOH/OH, equivalent to polymer **7** in Table 3.1.) and poly-(acrylonitrile-co-acrylic acid) containing 5.0% (w/w) of acrylic acid (PAN-COOH5, equivalent to polymer **2** in Table 3.1.) were both obtained from Optosense. The preparation of ruthenium(II)-tris-4,7-diphenyl-1,10-phenanthroline dichloride ($Ru(dpp)_3Cl_2$) is described in chapter 3.2.3. The names, net formulas, molecular weights and suppliers of all other reagents used in the experiments are listed in Table 5.1.

Table 5.1. Chemicals and solvents used in the experiments of chapter 5.

name	**net formula**	**MW [g/mol]**	**company**
1-ethyl-(3-(3-dimethylamino-propyl)-carbodiimide = EDC	$C_8H_{17}N_3$	155.24	Fluka
2-morpholinoethansulfonic acid monohydrate = MES	$C_6H_{13}NO_4S \cdot H_2O$	213.25	Fluka
avidin/egg white	-	66,000	Molecular Probes
bromophenol blue, sodium salt	$C_{19}H_9Br_4NaO_5S$	691.97	Fluka
Superfloc C-587, 20% polymer concentration in water	-	200,000	Cytec (West Paterson/NJ, USA)
disodium hydrogen phosphate dihydrate	$Na_2HPO_4 \cdot 2H_2O$	177.99	Merck
N-(2-aminoethyl) biotinamide hydrobromide = biotin ethylenediamine	$C_{12}H_{23}BrN_4O_2S$	367.30	Molecular Probes
N,N-dimethylformamide = DMF	C_3H_7NO	73.10	Merck
ruthenium(II)-tris-4,7-diphenyl-1,10-phenanthroline dichloride = $Ru(dpp)_3Cl_2$	$RuC_{72}H_{48}N_6Cl_2$	1169.20	synthesis (chapter 3.2.3.)
sodium azide	NaN_3	65.01	Merck
sodium chloride	NaCl	58.44	Merck
sodium dihydrogenphosphate monohydrate	$NaH_2PO_4 \cdot H_2O$	137.99	Merck
sodium hydroxide pellets	NaOH	40.00	Merck
streptavidin/Alexa Fluor 633 conjugate	-	-	Molecular Probes
trehalose	$C_{12}H_{22}O_{11}$	342.30	Merck

5.2.2. Instrumentation and measurements

A detailed description of all apparatus used in this chapter is given in chapter 3.2.2. All formulas needed in connection with calculations of luminescence decay times, quantum yields and their corrections are given in chapters 2.1. – 2.3.

5.2.3. Preparation of phosphorescent donor nanospheres

The precipitation procedure to prepare the phosphorescent nanospheres is described in detail in chapter 3.3.3. In essence, a solution of PAN derivatives and Ru(dpp) is co-precipitated from a solution in DMF. The preparation of the PAN-COOH/OH nanospheres (for the avidin assay) and the PAN-COOH5 nanospheres (for the polyelectrolyte binding study) is virtually identical.

While stirring vigorously, 250 mL of a 1 mM solution of sodium hydroxide were added dropwise to a solution of 250 mg PAN-COOH/OH or PAN-COOH5 (equivalent to 0.5% (w/w) matrix/DMF) and 7.5 mg $Ru(dpp)_3Cl_2$ (equivalent to 3.0% (w/w) dye/matrix) in 52.7 mL DMF (ρ_{DMF} 0.948 kg/L). Then, 1 M hydrochloric acid was added to the flask until a pH of 4.0 was reached. This caused the precipitation of finely dispersed nanospheres. The DMF water mixture was centrifuged at 3000 rpm for 15 min and the colored precipitate was thoroughly washed with water. All washing solutions remained colorless. The precipitate was suspended in 25 mL of water, heated to 70 °C for 10 min, centrifuged and then taken up in 100 mL of 2-morpholinoethanesulfonic acid (MES) buffer (pH 7.0, IS 30 mM, 0.5% (w/w) sodium azide, 0.5% (w/w) trehalose). After sonication for 1 h, the suspension remained clear and stable for months when stored in the dark at 4 °C.

5.2.4. Coupling of biotin to carboxy-modified nanospheres

Among the various known immobilization techniques are[128]. (1) adsorption of molecules to surfaces which is the most simple method, (2) microencapsulation by trapping molecules between membranes, (3) entrapment in a gel, paste or polymer, (4) cross-linking with a bifunctional agent, such as glutardialdehyde, and (5) covalent attachment by formation of a chemical bond between the molecule and the matrix.

In this case, the last possibility was taken. In order to covalently link biomolecules to the carboxy-modified PAN-COOH/OH nanospheres for the avidin assay, a two-step reaction was preferred over the one-step coupling reaction due to limitations that may be expected when coupling larger molecules[129-139]. A few drops of 1 M hydrochloric acid were added to 50 mL of the nanosphere suspension described above until the nanospheres were precipitated. The precipitate was washed twice with water, taken up in 50 mL of MES buffer (pH 6.5, IS 30 mM, 0.5% (w/w) sodium azide, 0.5% (w/w) trehalose) and then sonicated for 1 h. While stirring, 100 mg of 1-ethyl-3-(3-dimethylaminopropyl) carbodiimide hydrochloride (EDC) were added to the completely suspended nanospheres. They were allowed to react for 20 min at 25 °C, with continuous mixing. After centrifugation, the nanospheres were washed twice with water, taken up in 25 mL of phosphate buffer (pH 8.0, IS 30 mM, 0.5% (w/w) sodium azide, 0.5% (w/w) trehalose) and then sonicated for 1 h. Then, 3.4 mg of biotin ethylenediamine were dissolved in 10 mL of phosphate buffer (pH 8.0, IS 30 mM, 0.5% (w/w) sodium azide, 0.5% (w/w) trehalose) and combined with the nanosphere suspension. After a reaction time of 2 h at 25 °C with constant mixing, a few drops of 1 M hydrochlorid acid were added and the precipitated nanospheres were centrifuged. They were thoroughly washed with water, sonicated for 1 h and resuspended in 50 mL of MES buffer (pH 7.0, IS 30 mM, 0.5% (w/w) sodium azide, 0.5% (w/w) trehalose). The suspension was stored in the dark at 4 °C.

To block remaining free carboxy groups on the surface, they were converted into hydroxylic groups to prevent aggregation and nonspecific binding[140]. The following protocol was used. 50 mg of EDC and 125 mL of 2-aminoethanol were added at once to 25 mL of the above suspension of biotin-labelled nanospheres. They were allowed to react for 2 h at 25 °C, centrifuged, washed twice with water, treated under sonication for 1 h and resuspended in 25 mL of MES buffer (pH 7.0, IS 30 mM, 0.5% (w/w) sodium azide, 0.5% (w/w) trehalose). The suspension was stored in the dark at 4 °C.

5.2.5. Preparation of polyelectrolyte acceptor solution

The cationic polyelectrolyte Superfloc C-587 solution (1.0 g) and 6.92 mg (10.0 µmol) of the sodium salt of bromophenol blue (BPB) were dissolved in 1 L of water to yield a solution with the following concentrations: $c_{polyelectrolyte}$ 1.0 µmol/L, c_{BPB} 10.0 µmol/L. This solution with a polyelectrolyte/dye ratio of 1:10 was used undiluted for the polyelectrolyte titration experiment.

5.2.6. Implementation of polyelectrolyte binding study

In the polyelectrolyte binding study, the energy transfer from the phosphorescent donor nanospheres to the polyelectrolyte acceptor solution was investigated. The six samples of the titration experiment contained each 100 µL of Ru(dpp) donor suspension (PAN-COOH5 nanospheres, $c_{nanospheres}$ 0.678 g/L) and 0, 10, 20, 40, 65, 115 µL of the polyelectrolyte solution ($c_{polyelectrolyte}$ 1.0 µmol/L, c_{BPB} 10.0 µmol/L), respectively. All samples were filled up with phosphate buffer (c_{buffer} 10 mM, pH 7.0, IS 20 mM, 0.5% (w/w) sodium azide, 0.5% (w/w) trehalose) to a total volume of 2 mL and the solution was mixed and incubated for 1 h. Then, phase angles were recorded with the set-up given in Figure 3.4.

5.2.7. Implementation of assay

In the avidin assay applying the biotinylated phosphorescent donor nanospheres described above, ten samples containing 100 µL of Ru(dpp) donor suspension (PAN-COOH/OH nanospheres labelled with biotin, $c_{nanospheres}$ 0.662 g/L) were mixed with 0, 10, 50, 100, 250, 500, 750, 1000, 1250, 1500 µL avidin (c_{avidin} 9.47 µmol/L), respectively. MES buffer (c_{buffer} 10 mM, pH 7.0, IS 30 mM, 0.5% (w/w) sodium azide, 0.5% (w/w) trehalose) was added to a total volume of 1650 µL and the samples were mixed and incubated for 1 h. Afterwards, 350 µL of the solution of the streptavidin (SA) labelled with Alexa Fluor 633 ($c_{Alexa\ Fluor\ 633} \approx 4.0$ µmol/L; $MW_{SA} >> MW_{Alexa\ Fluor\ 633}$, Alexa Fluor 633-SA-ratio 3.5) was added to each of the ten samples and the solutions were incubated for another 1 h. Then, luminescence emission spectra were recorded and phase angles were measured using the set-up illustrated in Figure 3.4.

5.3. Results and discussion

In a first experiment, Ru(dpp) donor nanospheres were titrated with a cationic polyelectrolyte solution containing BPB as the energy acceptor in the RET[141-150]. Since the nanospheres contain negatively charged carboxy groups on the surface (due to the acrylic acid copolymer), they attract and electrostatically interact with the cationic polyelectrolyte. The resulting spatial proximity enables a transfer of luminescence energy from the Ru(dpp) donor to the BPB acceptor which can be detected by a decrease in the apparent decay time[151]. This polyelectrolyte binding study proves that RET occurs from the nanospheres to the dye and also quantifies the maximum extent of quenching that is feasible with BPB. The polyelectrolyte binding study is schematically shown in Figure 5.1.

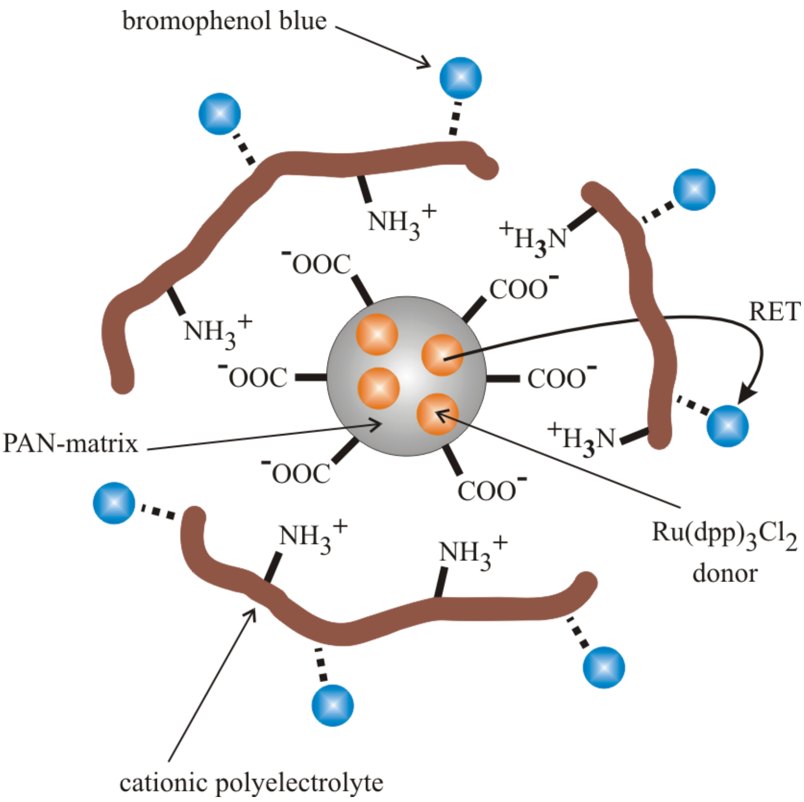

Figure 5.1. Scheme of polyelectrolyte binding study using RET from nanospheres dyed with Ru(dpp) (acting as the donor) to bromophenol blue (the acceptor).

Based on this experiment, a RET competitive binding assay for avidin was set up, with an acceptor fluorophore instead of a non-luminescent acceptor dye like BPB[152-153]. This leads to increased luminescence signals. The avidin assay presented is based on the scheme illustrated in Figure 5.2. In essence, avidin and labelled SA – which reportedly exhibits less nonspecific binding than avidin[154] – bind competitively to the biotin on the surface of the Ru(dpp) donor nanospheres[155-156]. If labelled SA binds to the nanospheres, RET occurs from Ru(dpp) (excited at 470 nm) to the label of SA, which does not measurably absorb at 470 nm. As a result, the apparent decay time of the emission of the donor decreases and the luminescence intensity of the Alexa Fluor 633 label increases.

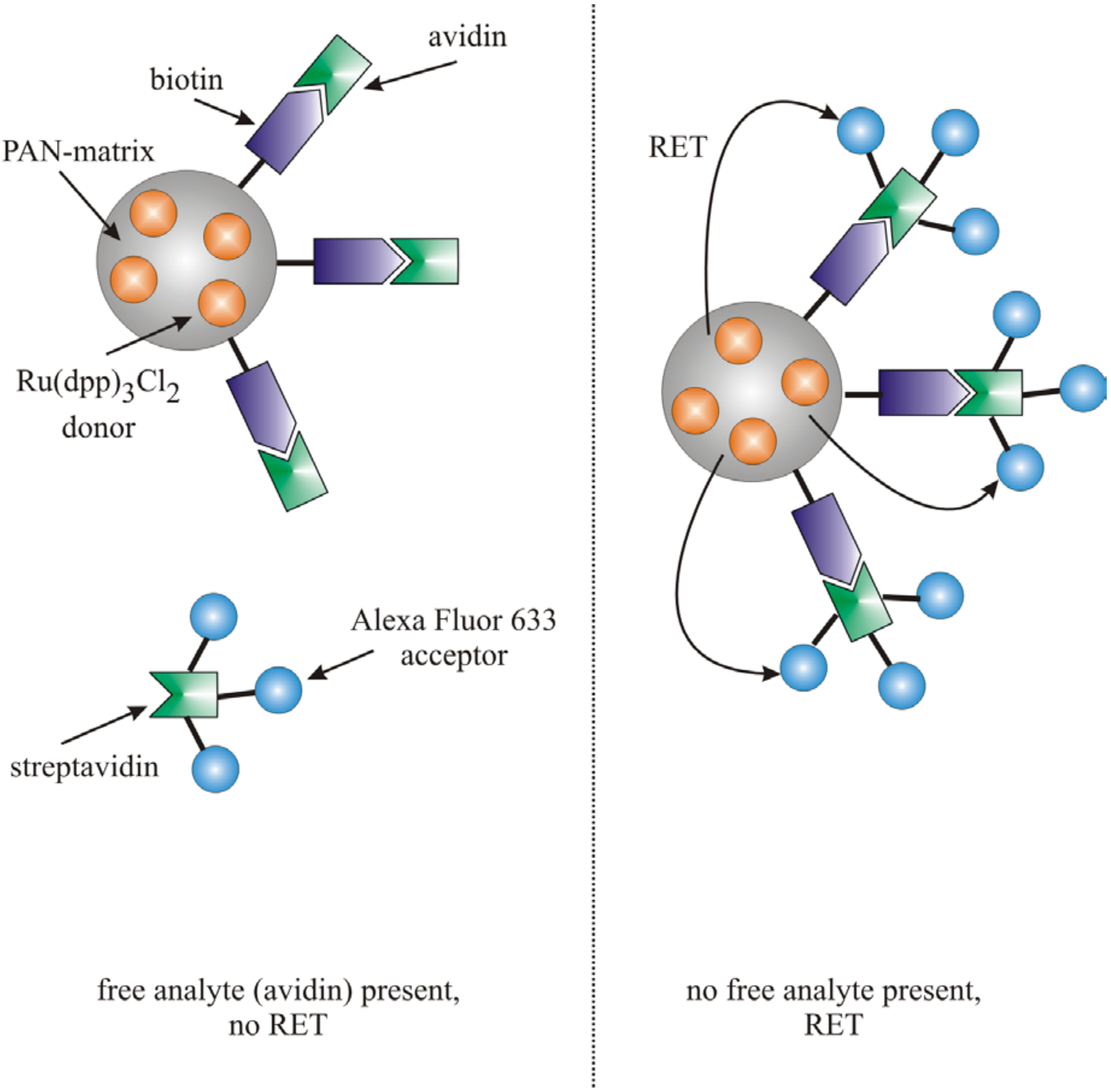
avidin
biotin
PAN-matrix
$Ru(dpp)_3Cl_2$
donor
Alexa Fluor 633
acceptor
streptavidin
free analyte (avidin) present,
no RET
RET
no free analyte present,
RET

Figure 5.2. Scheme of avidin assay with RET from the Ru(dpp)-dyed nanospheres to Alexa Fluor 633 (the acceptor). Left: situation at high levels of avidin; right: situation at low levels of avidin.

5.3.1. Choice of luminescent donor and acceptor dyes

The donor dye used in both cases is the phosphorescent ruthenium(II) complex Ru(dpp). It has a luminescence decay time in the order of 6.2 µs and was selected as a label because it is well soluble in DMF and in the polymer matrix, but not in water[109, 157]. The dye yields brightly luminescent nanospheres and its luminescence has a Stokes' shift as large as 145 nm (λ_{exc} 465 nm, λ_{em} 610 nm). Due to its positive charge, it strongly interacts with polymers containing negatively charged groups. It is extracted quantitatively into the nanospheres during the preparation process. Even in a lipophilic environment, e.g. if proteins are present in the sample, no dye leaching occurs in aqueous solutions. The quantum yield is 0.38 in PAN and the relatively large molar absorbance ($\varepsilon \approx 28{,}000$ L mol^{-1} cm^{-1}) of the ruthenium complex are of further advantage. It is assumed that the encapsulation of the dye into the polymer matrix is the reason for the high quantum yield. The ruthenium complex also is excitable with an argon ion laser at 488 nm. The use of phosphorescent nanospheres eliminates background fluorescence and this leads to higher sensitivity.

The deprotonated (blue) form of BPB as the acceptor dye in the first experiments because its maximum absorbance (592 nm) is close to the emission of the Ru(dpp) donor and there is almost no absorbance at the excitation wavelength of the donor dye at 470 nm. BPB also has a high molar absorbance (73,000 L mol^{-1} cm^{-1}). The deprotonated dye is double negatively charged and can thus easily form stained macromolecules with a cationic polyelectrolyte (such as Superfloc C-587). Due to this strong electrostatic interaction, the formed complexes are stable against dissociation up to the concentrations used. The chemical structure of the neutral form of BPB is pictured in Figure 5.3.

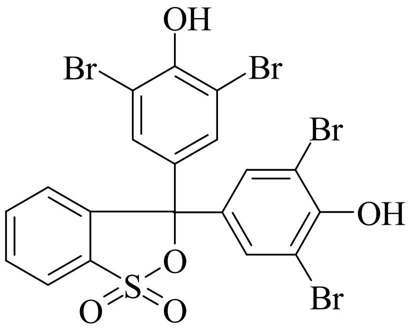

Figure 5.3. Chemical structure of the neutral form of bromophenol blue (BPB).

Alexa Fluor 633 was chosen as the acceptor for the avidin assay for several reasons. First, its absorbance spectrum strongly overlaps the Ru(dpp) emission spectrum and thus makes it attractive for RET applications. Its absorbance and emission maxima are at 633 and 650 nm, respectively. Most importantly, it has virtually no intrinsic absorbance at the excitation wavelength of the Ru(dpp) donor (470 nm). Therefore, the phosphorescent donor is selectively excited by the blue LED.

The emission of the Alexa Fluor 633 dye can be clearly distinguished from the emission of the Ru(dpp) which is at 610 nm. The Alexa Fluor 633 spectrum is well beyond the range of most samples' autofluorescence. It has a molar absorbance exceeding 115,000 L mol^{-1} cm^{-1} and a large quantum yield. Furthermore, its conjugates show bright luminescence, are photostable and pH insensitive. The Alexa Fluor 633 dye is highly water-soluble, so that protein conjugation can be performed without the use of organic solvents and the conjugates are relatively resistant to precipitation during storage. The SA-conjugate of Alexa Fluor 633 has a dye-protein-ratio of 3.5.

Table 5.2. summarizes the spectral data of the donor and both acceptor dyes. Figure 5.4. shows the absorbance and emission spectra of the Ru(dpp) donor and the absorbance spectrum of the BPB acceptor. Figure 5.5. shows the absorbance and emission spectra of both the Ru(dpp) donor and the Alexa Fluor 633 acceptor. In both figures, the hatched areas indicate the large overlap integral between the donor emission and the acceptor absorbance which is a prerequisite for efficient RET.

Table 5.2. Spectral data of donor and acceptor dyes.

dye	**λ_{max} (abs) [nm]**	**λ_{max} (em) [nm]**	**$\Delta\lambda$ [nm]**	**ε [L mol^{-1} cm^{-1}]**
Ru(dpp)	465	610	145	28,000
bromophenol blue	592	-[a]	-	73,000
Alexa Fluor 633	633	647	14	115,000

[a] no luminescence

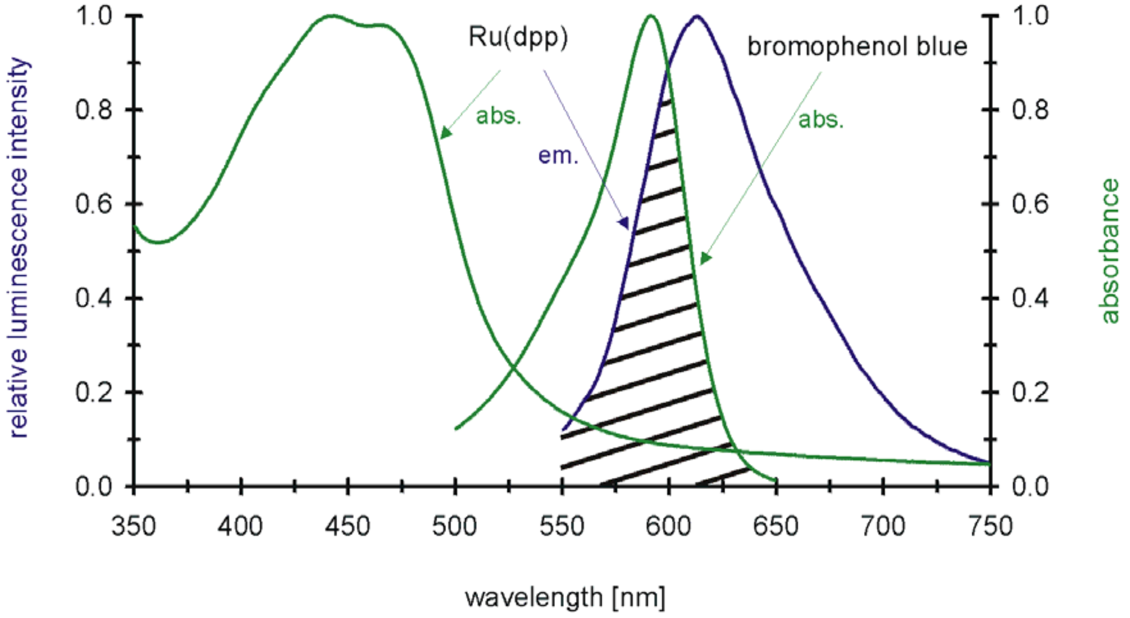

Figure 5.4. Absorbance and emission spectra of Ru(dpp) donor and absorbance spectrum of bromophenol blue acceptor. The hatched area indicates the overlap integral between the donor's emission and acceptor's absorbance.

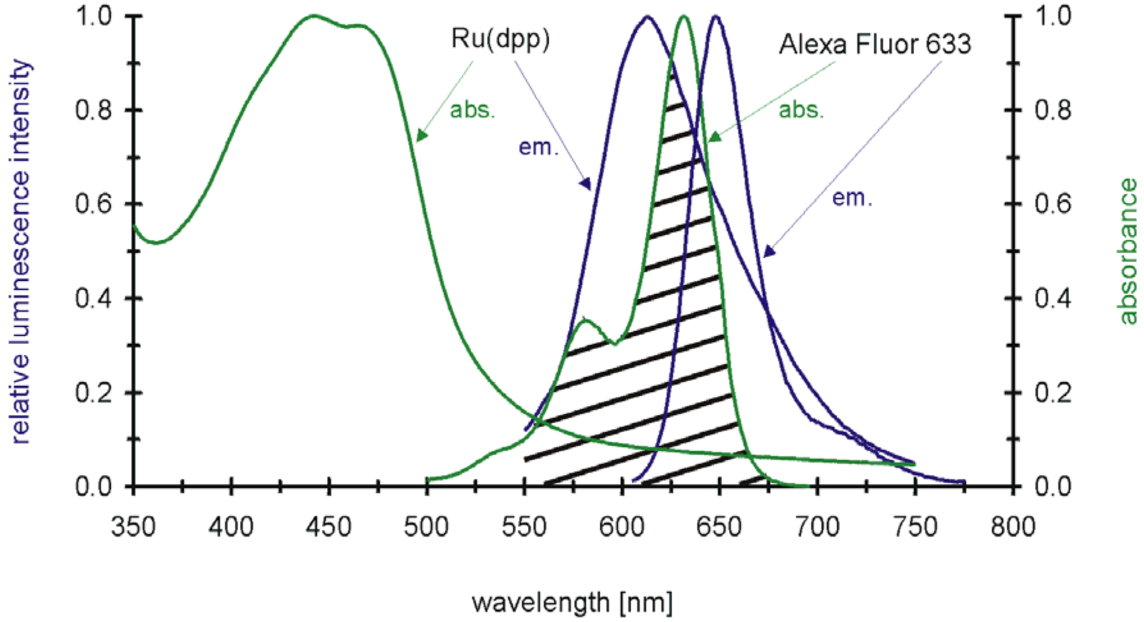

Figure 5.5. Absorbance and emission spectra of both Ru(dpp) donor and Alexa Fluor 633 acceptor. The hatched area indicates the overlap integral between the donor's emission and acceptor's absorbance.

5.3.2. RET calculations for the Ru(dpp)/bromophenol blue system

The Förster distance[158] for RET between Ru(dpp)$_3$Cl$_2$-labelled PAN-COOH5 nanospheres (donor) to a solution containing bromophenol blue (acceptor) along with the polyelectrolyte Superfloc C-587 was calculated using the following concentrations: $c_{\mathrm{dye/matrix}}$ 2.0% (w/w), $c_{\mathrm{matrix/DMF}}$ 0.5% (w/w), c_{BPB} 10^{-5} M and $c_{\mathrm{Superfloc\ C\text{-}587}}$ 10^{-6} M. The energy rate k_T from the Ru(dpp) donor to the BPB acceptor is given by equation 5.1.

$$k_T = \frac{1}{\tau_D} \cdot \left(\frac{R_0}{r} \right)^6 \qquad 5.1.$$

where τ_D is the decay time of the donor in the absence of acceptor, r the donor-to-acceptor distance and R_0 the Förster distance. The decay time τ_D was calculated from measured phase angles.

$$\tau_D = 6.20\,\mu s$$

The Förster distance R_0 (typically 20 – 60 Å), which is the distance at which RET is 50% efficient, is given by equation 5.2.

$$R_0 = \frac{0.0211 \cdot \kappa^{1/3} \cdot \Phi_D{}^{1/6} \cdot J(\lambda)^{1/6}}{n^{2/3}} \qquad 5.2.$$

where κ is a factor describing the relative orientation in space of the transition dipoles of the donor and the acceptor, Φ_D is the quantum yield of the donor in the absence of acceptor, $J(\lambda)$ is the overlap integral between the donor's emission and the acceptor's absorbance and n is the refractive index of the medium. Depending upon the relative orientation of donor and acceptor, κ can range from 0 to 2. Generally, κ^2 is assumed equal to $\frac{2}{3}$, which is the value for donors and acceptors that randomize by rotational diffusion prior to energy transfer. Φ_D was taken from experimental data. $J(\lambda)$, given by equation 5.3., is pictured in Figure 5.6. n was calculated from literature data by equation 5.4.

$$\kappa = \sqrt{\frac{2}{3}}$$

$$\Phi_D = 0.39$$

$$J(\lambda) = \frac{\int_0^\infty F_D(\lambda)\cdot\varepsilon_A(\lambda)\cdot\lambda^4\cdot d\lambda}{\int_0^\infty F_D(\lambda)\cdot d\lambda} = \frac{\int_{500\,nm}^{750\,nm} F_D(\lambda)\cdot\varepsilon_A(\lambda)\cdot\lambda^4\cdot d\lambda}{\int_{500\,nm}^{750\,nm} F_D(\lambda)\cdot d\lambda} \qquad 5.3.$$

$$n \approx \frac{n_{H_2O} + n_{PAN}}{2} = \frac{1.33 + 1.52}{2} = 1.43 \qquad 5.4.$$

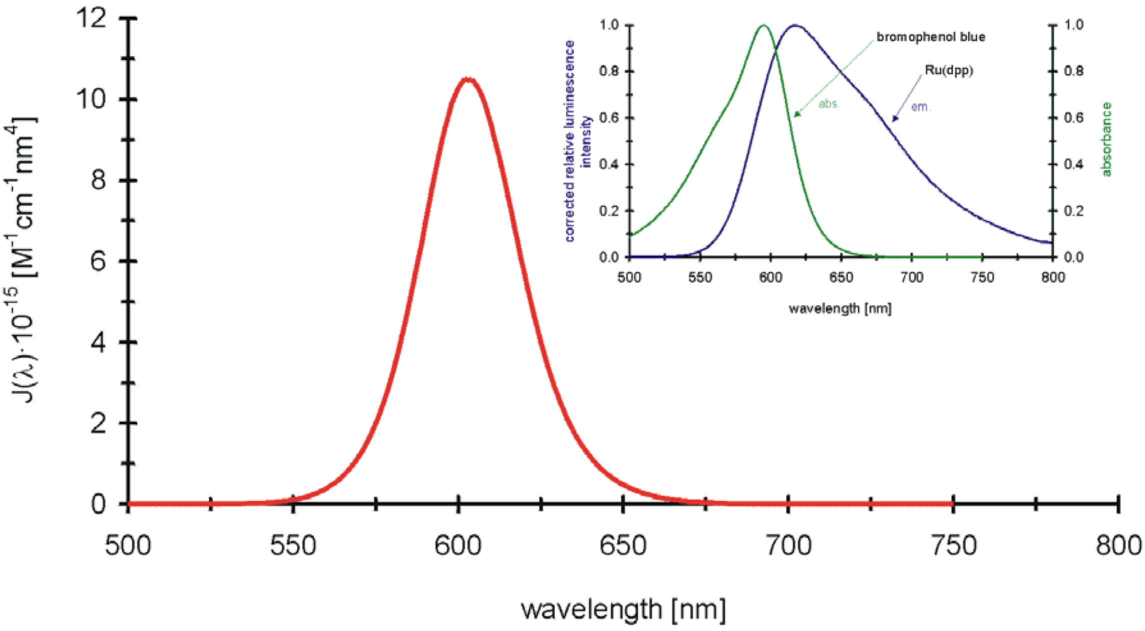

Figure 5.6. Overlap integral J between Ru(dpp) donor's emission and bromophenol blue acceptor's absorbance. Inset: Emission spectrum of Ru(dpp) and absorbance spectrum of bromophenol blue (compare also Figure 5.4.).

In equation 5.3., $F_D(\lambda)$ is the corrected fluorescence intensity of the donor in the wavelength range from λ to $\lambda + \Delta\lambda$ (500 nm to 750 nm), with the total intensity (i.e. the area under the curve) normalized to unity. With $\varepsilon_A(\lambda)$ being the molar absorbance of the acceptor at λ, $J(\lambda)$ can be calculated.

$$J(\lambda) = \frac{4.18 \cdot 10^{17}}{111.88} = 3.74 \cdot 10^{15}$$

Putting this into equation 5.2., the Förster distance R_0 can be calculated.

$$R_0 = 5.24\,nm$$

Finally, the energy rate k_T from the Ru(dpp) donor to the BPB acceptor can be calculated at different donor-to-acceptor distances r, using equation 5.1.

5.3.3. Choice of polymer matrix for donor encapsulation

Polyacrylonitrile (PAN) and its derivatives are attractive polymeric matrices for the encapsulation of phosphorescent dyes in micro- and nanospheres[90-91, 109, 111]. They display an extraordinarily poor permeability for gases and ionic as well as uncharged chemical species. Hence, they can protect luminescent dyes against potential luminescence quenchers, such as oxygen. In fact, the intensity of luminescence drops by less than 5% only on changing from nitrogen to air atmosphere. PAN with an acrylic acid content of 5% (w/w) proved to be the best choice to obtain stable suspensions due to electrostatic repulsion of the surface of the nanospheres and to provide for active groups on the surface of the nanospheres for the covalent coupling of biomolecules by conventional methods[109].

PAN derivatives are soluble in DMF, swell in DMF/water mixtures and act themselves as good solvents for many lipophilic dyes. On dropwise addition of water to a dilute solution of PAN in DMF, a stable dispersion of nanoscale PAN aggregates is formed. Surprisingly, the nanospheres do not aggregate or sediment. If the nanospheres are precipitated from DMF solutions containing Ru(dpp), the ruthenium complex is co-precipitated with the nanospheres. This is an elegant way to stain nanospheres in a defined manner.

The nanospheres have a highly porous structure with a large surface-to-bulk ratio. This opens the way to create a two-sided RET assay with donor and acceptor dyes located in two different phases: Any luminescent donor dye incorporated into the nanospheres during the preparation process is very well accessible to an acceptor dye bound to the surface of the nanospheres.

The transparency of the resulting nanosphere suspensions results from the size of the nanospheres which is far below the wavelength of visible light. Transmission electron microscopic pictures of the nanospheres before the EDC coupling with biotin showed a nearly circular shape and a diameter of roughly 10 – 50 nm. Static and dynamic light scattering along with laser Doppler anemometry experiments revealed a polydisperse coil with a diameter of the nanospheres of about 50 nm and a negative zeta potential ($\zeta \approx -50$ mV) at pH 7.0, thus confirming the negative surface charge resulting from the presence of carboxy groups[109].

The nanospheres can be made even smaller by varying the copolymer and the precipitation procedure. However, the size of the nanospheres needs to be balanced between efficent RET (better in small nanospheres) and oxygen quenching (stronger in small nanospheres).

5.3.4. Choice of polyelectrolyte matrix for acceptor encapsulation

Superfloc C-587 polyDADMAC (poly-diallyl dimethyl ammonium chloride) coagulant is a highly effective amber liquid cationic polymer of medium molecular weight (20% polymer concentration in water, MW 200,000). It is uneffected by the pH of the system, effective over a wide pH range and immediately soluble at all concentrations. This cationic polyelectrolyte Superfloc C-587 was used as a matrix to form macromolecules stained with BPB for the following reasons: there is a strong interaction with the double negatively charged dye to prevent dissociation, a macromolecule with a high molecular weight can be simulated for the subsequent competitive binding assay and the polyelectrolyte acceptor solution can be easily prepared by simply mixing both matrix and dye.

5.3.5. Concept of polyelectrolyte binding study

Based on the above precipitation technique for producing highly phosphorescent, inert nanospheres, a novel scheme for a homogeneous assay based on long-lived luminescence was created[109]. In an initial test, negatively charged (i.e. carboxylated) Ru(dpp) nanospheres, acting as donor, were titrated with cationic acceptor dyes, such as crystal violet or nile blue A[159]. RET was observed in the form of decreasing apparent decay times and increasing luminescence intensities at the emission wavelength of the acceptor upon addition of acceptor to a donor suspension.

In another experiment (Figure 5.1.), the same donor nanospheres were titrated with a solution containing a negatively charged acceptor dye (BPB in the deprotonated form) along with a cationic polyelectrolyte (Superfloc C-587) with a high molecular weight. Even though the donor-acceptor distance is smaller here than in the final avidin assay and the acceptor dye is not a fluorophore, this is a fast way to prove RET from nanospheres and to quantify it. As can be seen in Figure 5.4., the emission spectrum of Ru(dpp) and the absorbance of BPB overlap significantly. This causes a transfer of energy from the luminescent donor to the polyelectrolyte/BPB acceptor. With no polyelectrolyte acceptor present and thus at 100% luminescence intensity from the donor (sample **A1**), the apparent decay time (4.9 μs) is that of Ru(dpp) (Table 5.3. and Figure 5.7.). While increasing the polyelectrolyte concentration to 54.4 nmol/L (sample **A6**), both the relative luminescence intensity (19%) and the apparent decay time (3.1 μs) drop due to RET from Ru(dpp) to BPB. During the whole titration, the concentration of the Ru(dpp) donor nanospheres was kept constant at 33.9 mg/L ($c_{Ru(dpp)}$ 0.87 μmol/L). The excitation wavelength was 470 nm.

Table 5.3. Apparent decay time of polyelectrolyte binding study depending on polyelectrolyte concentration.

sample	**c (polyelectrolyte)** [a] **[nmol/L]**	**relative luminescence intensity [%]**	**τ, air [μs]**
A1	0.0	100 ± 3	4.9 ± 0.1
A2	5.0	75 ± 3	4.2 ± 0.1
A3	9.9	46 ± 3	3.8 ± 0.1
A4	19.6	30 ± 3	3.4 ± 0.1
A5	31.5	21 ± 2	3.3 ± 0.1
A6	54.4	19 ± 2	3.1 ± 0.1

[a] the following concentrations were kept constant:
$c_{Ru(dpp)\ nanospheres}$ = 33.9 mg/L, $c_{Ru(dpp)}$ = 0.87 μmol/L

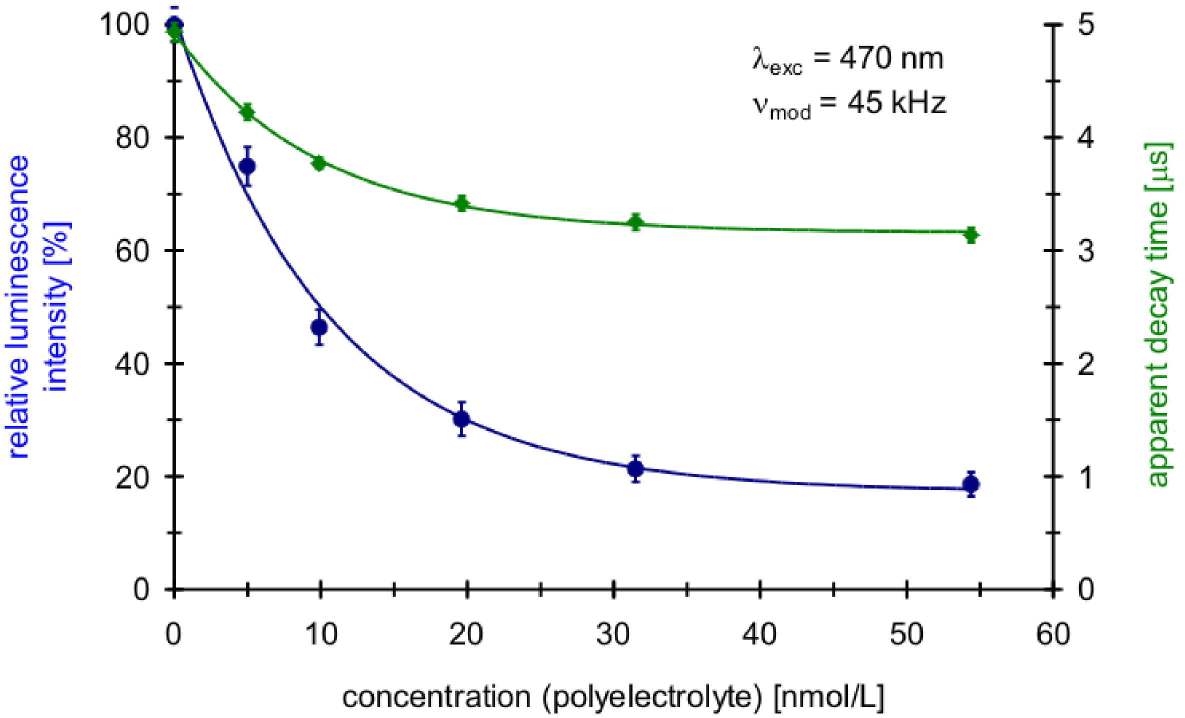

Figure 5.7. Polyelectrolyte binding study: relative luminescence intensities (•) and apparent decay times (♦) at different polyelectrolyte concentrations.

It can be seen that the percentage change in the apparent decay time is rather small compared to the drastic decrease in luminescence intensity ($\frac{\tau}{\tau_0} \neq \frac{I}{I_0}$). This can be explained by differentiating between core regions and shell regions of the nanosphere: any Ru(dpp) donor dye located in the core is much less susceptible to quenching by BTB than Ru(dpp) in the shell.

5.3.6. Concept of assay

Based on the polyelectrolyte binding study (chapter 5.3.5.) and immunoassays described in literature using phycoerythrin as energy acceptor dye, a RET avidin competitive binding assay with an acceptor fluorophore (Alexa Fluor 633) instead of the non-luminescent acceptor dye BPB was then established[152, 160-161]. This leads to increased luminescence signals and constant luminescence intensities since a new luminescence – that of the acceptor fluorophore – is stimulated in addition to the one of the donor. A high rate of RET warrants high signal intensities. Both dyes are long-lived with apparent decay times in the microsecond time region and this enables the elimination of short-lived nanosecond background fluorescence. The avidin assay is outlined in principle in Figure 5.2.

5.3.7. Prototype assay for avidin

Figure 5.5. shows the possibility to achieve RET in the avidin assay due to an overlap of the emission spectrum of the Ru(dpp) donor and the Alexa Fluor 633 acceptor absorbance spectrum. If no avidin analyte is present in the solution (sample **B1**), the apparent decay time of the assay (2.5 µs) is reduced due to RET from the Ru(dpp) donor to the Alexa Fluor 633 acceptor via a biotin-SA bridge. On the other hand, in the presence of a high avidin concentration (7.10 µmol/L, sample **B10**), the apparent decay time remains that of the donor nanospheres (4.4 µs) since the biotin binding sites on the nanosphere surface are occupied by avidin.

In this assay, the concentrations of both the Ru(dpp) donor nanospheres and the Alexa Fluor 633-labelled SA acceptor are kept constant at 33.1 mg/L ($c_{Ru(dpp)}$ 0.85 µmol/L) and 0.7 µmol/L ($c_{Alexa\ Fluor\ 633}$ 2.41 µmol/L), respectively, so that the ratio of acceptor to donor (2.8) is constant during the whole assay, as well. The relatively high donor concentration was chosen in order to obtain bright luminescence signals and to prove the feasibility of the assay. Naturally, a high donor concentration goes along with a high biotin concentration on the surface of the nanosphere and thus a poor sensitivity of the assay. However, this may be overcome by performing a time-resolved measurement. Then, much smaller concentrations become possible.

Due to those constant donor and acceptor concentrations, also the relative luminescence intensities stay nearly the same, varying only between 97% (sample **B1** and **B9**) and 100% (sample **B5**). The excitation wavelength for all measurements was 470 nm. Table 5.4. and Figure 5.8. summarize the apparent decay times and relative luminescence intensities of the overall luminescence signal, i.e. the emission of Ru(dpp) and Alexa Fluor 633. It is obvious that the overall luminescence strongly depends on the avidin concentration present. Figure 5.9. gives a plot of the ratio of the luminescence intensities at 645 and 610 nm at different avidin concentrations. Figure 5.10. pictures normalized luminescence emission spectra of that assay. Here, with decreasing avidin concentration, the luminescence emission peak of the Alexa Fluor 633 acceptor at about 650 nm increases relative to the Ru(dpp) emission.

Table 5.4. Apparent decay time of avidin assay depending on analyte concentration.

sample	**c (avidin)** [a] **[μmol/L]**	**relative luminescence intensity [%]**	**τ, air [μs]**
B1	0.00	97 ± 3	2.5 ± 0.1
B2	0.05	98 ± 3	2.6 ± 0.1
B3	0.24	99 ± 3	2.8 ± 0.1
B4	0.47	98 ± 3	3.0 ± 0.1
B5	1.18	100 ± 3	3.2 ± 0.1
B6	2.37	98 ± 3	3.6 ± 0.1
B7	3.55	98 ± 3	3.8 ± 0.1
B8	4.73	99 ± 3	4.0 ± 0.1
B9	5.92	97 ± 3	4.2 ± 0.1
B10	7.10	98 ± 3	4.4 ± 0.1

[a] the following concentrations were kept constant:
$c_{\text{Ru(dpp) nanospheres}} = 33.1$ mg/L, $c_{\text{Ru(dpp)}} = 0.85$ μmol/L,
$c_{\text{Alexa Fluor 633-labelled SA}} = 0.7$ μmol/L, $c_{\text{Alexa Fluor 633}} = 2.41$ μmol/L
$\Rightarrow c_{\text{Alexa Fluor 633}} / c_{\text{Ru(dpp)}} = 2.8$

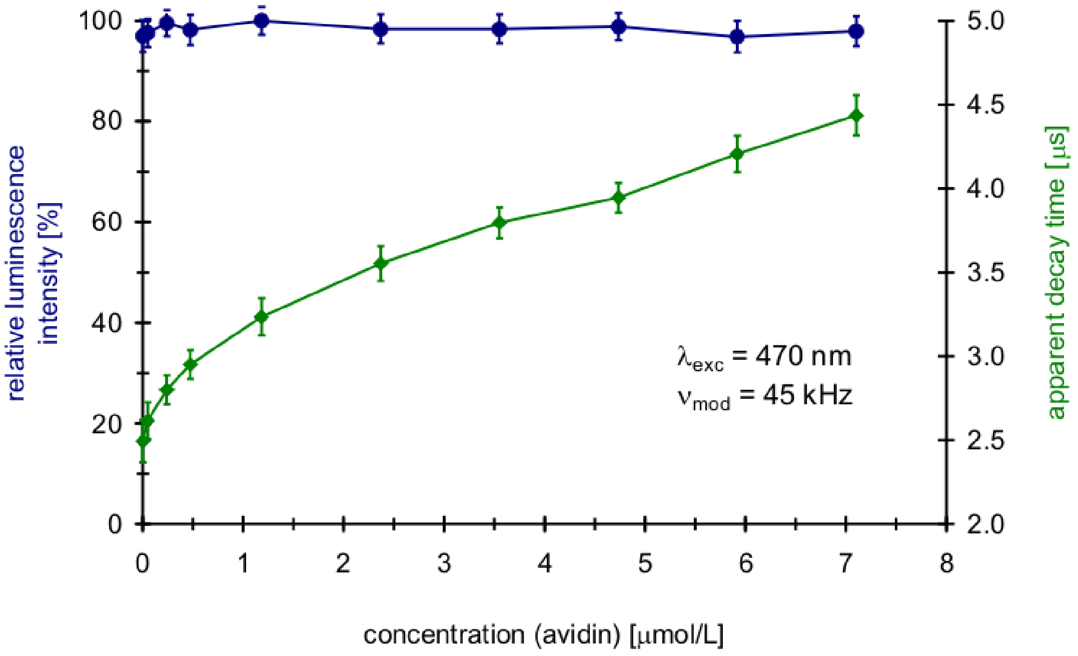

Figure 5.8. Avidin assay: constant intensities of overall luminescence signals (●) due to constant concentrations of Ru(dpp) and Alexa Fluor 633 and increase of apparent decay times (♦) with rising avidin concentrations due to decreasingly efficient RET.

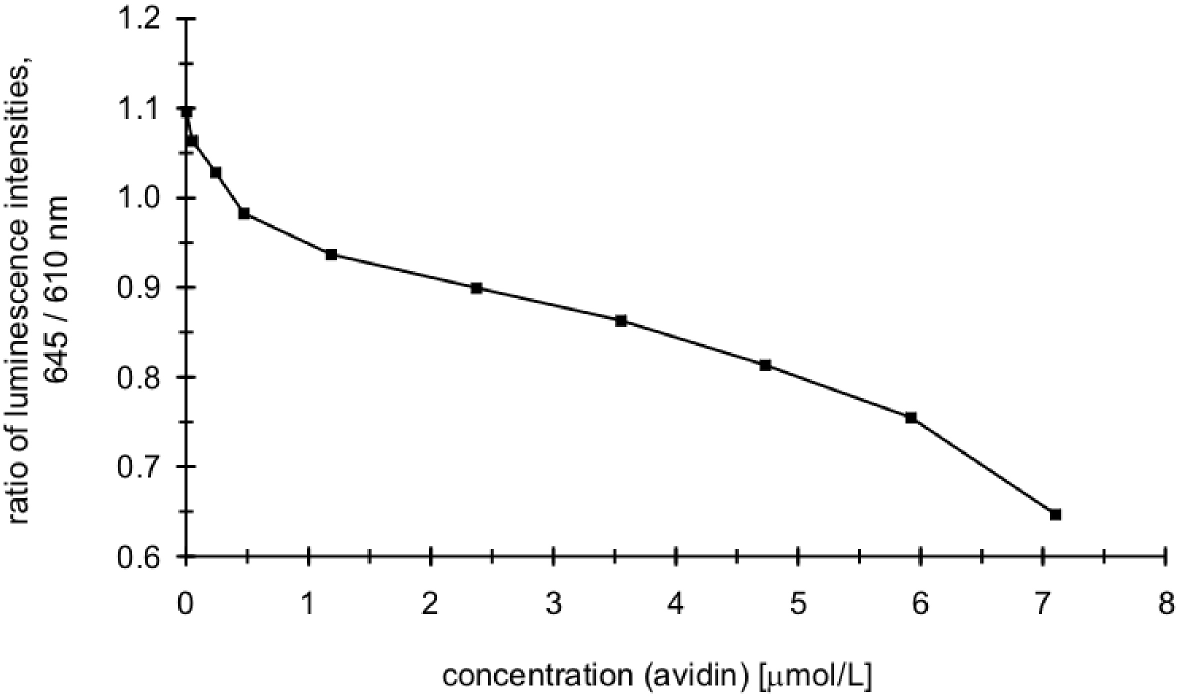

Figure 5.9. Avidin assay: ratio of luminescence intensities at 645 and 610 nm at different avidin concentrations.

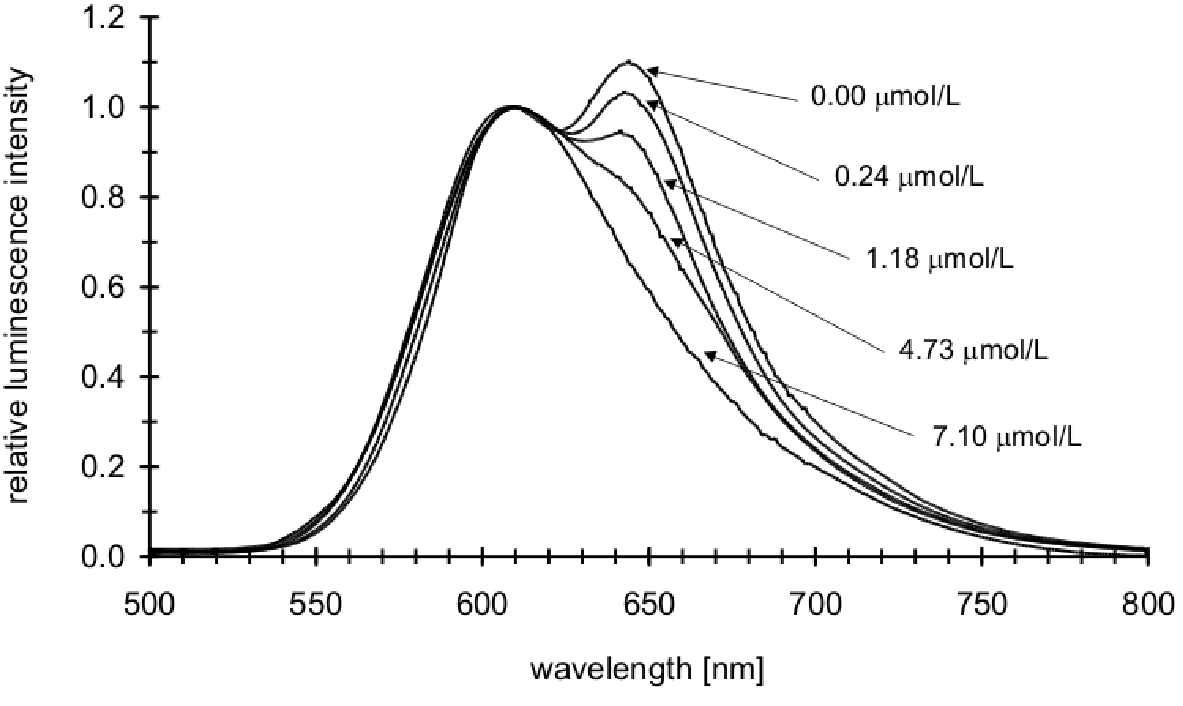

Figure 5.10. Avidin assay: emission spectra of samples at selected avidin concentrations.

To prove that there was indeed specific binding of Alexa Fluor 633-labelled SA to the biotin-labelled donor nanospheres, yet no binding of Alexa Fluor 633-labelled SA to simply carboxylated nanospheres and to show that any increase of the apparent decay time thus came from RET via the biotin-SA bridge, the following negative experiment was carried out. Apparent decay times and luminescence emission spectra were recorded of the following solutions: (1) a solution containing biotin-labelled Ru(dpp) donor nanospheres and Alexa Fluor 633-labelled SA, (2) a solution containing carboxylated Ru(dpp) donor nanospheres and Alexa Fluor 633-labelled SA, (3) a solution containing carboxylated Ru(dpp) donor nanospheres and (4) a solution containing biotin-labelled Ru(dpp) donor nanospheres (compare Figure 5.11.). In case of applying only the carboxylated donor nanospheres, no change in the emission spectra was observed and the apparent decay time stayed nearly constant at about 4.4 µs. No RET occurred since the SA acceptor molecules were prevented from accumulating on the nanosphere surface by the negatively charged carboxy groups. Only when using the biotin-labelled donor nanospheres, the Alexa Fluor 633 peak could clearly be observed in the emission spectra at about 650 nm and the decay time decreased from 4.4 µs to about 2.5 µs upon addition of acceptor.

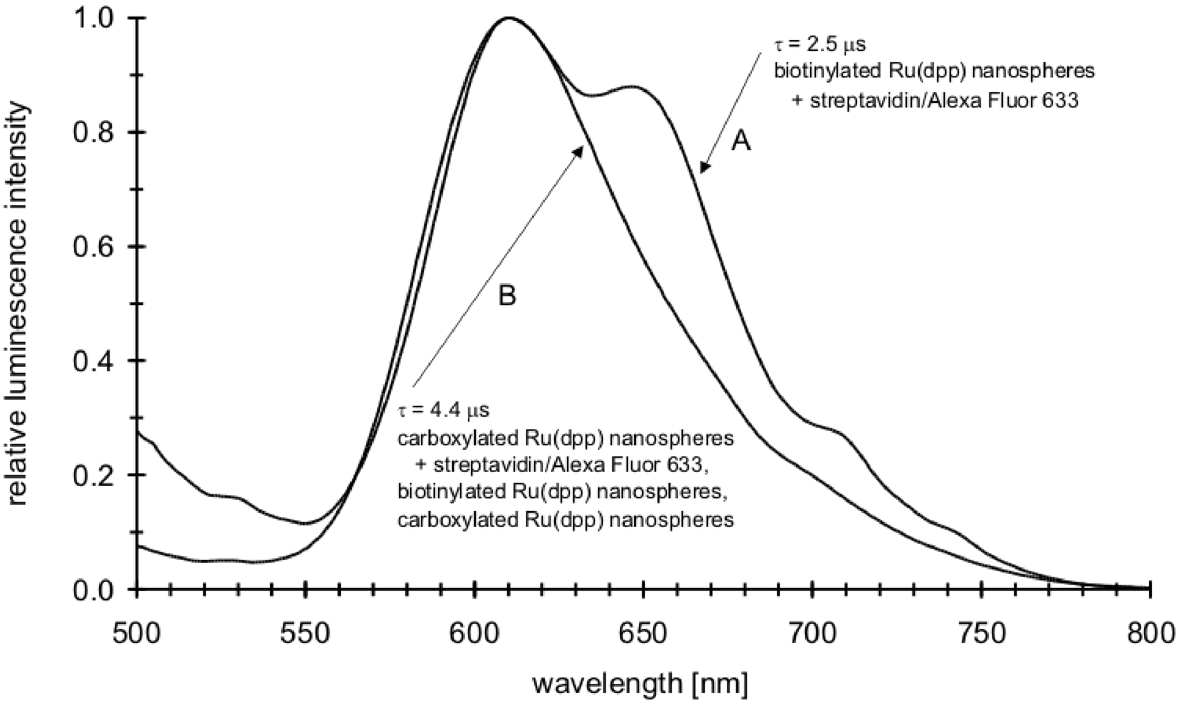

Figure 5.11. (A) Emission spectra of biotin-labelled Ru(dpp) nanospheres after interaction with Alexa Fluor 633-labelled SA. (B) carboxylated Ru(dpp) nanospheres (not biotinylated) after interaction with Alexa-labelled SA. Biotin-labelled Ru(dpp) nanospheres and carboxylated Ru(dpp) nanospheres gave spectra that are virtually identical to (B).

5.4. Conclusion

When trying to realize an assay based on RET between donor-labelled nanospheres and an acceptor dye bound to the surface of the nanospheres via an antibody-antigen bridge, two fundamental arrangements are feasible (Figure 5.12.). On the one hand, the acceptor can be attached to an antigen, for instance a hapten, such as biotin, which is then connected to the donor nanosphere via an antibody which is covalently linked to the nanosphere. Here, a large distance (d >> 10 nm) between donor and acceptor dye is prevalent due to the high molecular weight and thus diameter of the antibody. Only small rates of RET can be achieved if at all (Figure 5.12., left). On the other hand, a small antigen can be bound to the surface of the donor nanospheres. If an antibody labelled with an acceptor dye attaches to the nanosphere via the antigen, the donor-acceptor distance (d < 10 nm) is now smaller than the Förster distance and RET becomes possible (Figure 5.12., right). This arrangement was chosen for our biotin-avidin binding assay.

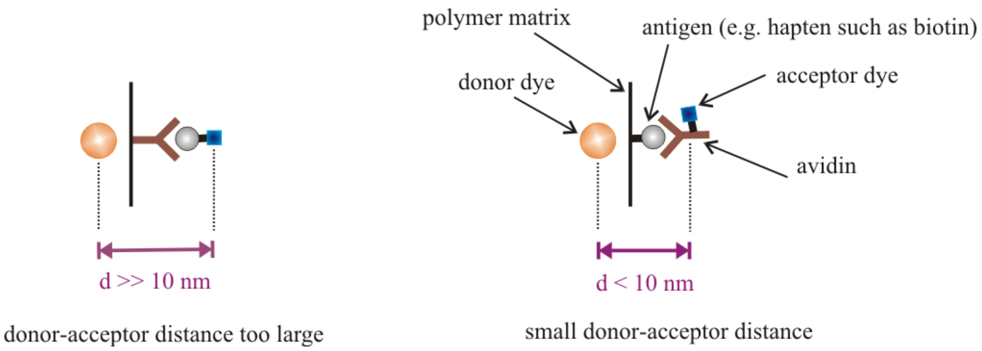
polymer matrix
antigen (e.g. hapten such as biotin)
donor dye
acceptor dye
avidin
d >> 10 nm
d < 10 nm
donor-acceptor distance too large
small donor-acceptor distance

Figure 5.12. Concept of assay: surface of nanospheres, with small donor-acceptor distance (right) for efficient RET.

The results presented here demonstrate the feasibilty of an assay for avidin (or, conceivably, any other biomolecule that binds to a countermolecule on the nanosphere). The assay is based on RET from phosphorescent nanospheres to fluorescently-labelled SA. The avidin concentration is determined by measurement of changes in the decay time due to RET from the phosphorescent donor dye Ru(dpp), incorporated into biotin-labelled nanospheres, to an acceptor dye (here Alexa Fluor 633) labelled to SA. While the luminescence intensity remains nearly constant, the apparent decay time increases with increasing concentration of avidin. The assay uses simple instrumentation and a low modulation frequency (45 kHz) for the measurements of lifetimes which are in the microsecond regime. The assay works well for small molecules, such as avidin.

6. Abbreviations, Acronyms and Symbols

A	absorbance
Å	Angström (10^{-10} m)
AP	alkaline phosphatase
ArH	aromatic protons
bipy	bipyridyl
BPB	bromophenol blue
c	molar concentration
CTAB	cetyltrimethylammonium bromide
CY582	3,3’-diethyloxadicarbocyanine iodide
CY604	1,1’-diethyl-2,2’-carbocyanine chloride
CY655	3,3’-diethylthiadicarbocyanine iodide
CY703	1,1’-diethyl-4,4’-carbocyanine iodide
δ	chemical shift
d	layer thickness
DLS	dynamic light scattering
DMF	N,N-dimethylformamide
DMSO	dimethyl sulfoxide
dpp	4,7-diphenyl-1,10-phenanthroline
ε	molar absorbance
E	energy
EDC	1-ethyl-(3-(3-dimethylaminopropyl)-carbodiimide
ELISA	enzyme-linked immunosorbent assay
ESI	electrospray ionization
F	fluorescence
FRET	fluorescence resonance energy transfer
FT-IR	Fourier transformation infrared
h	Planck’s constant ($6.626 \cdot 10^{-34}$ J s)
h	hour(s)
I_S	intensity of scattered light
IC	internal conversion
IR	infrared

IS	ionic strength
ISC	intersystem crossing
IUPAC	International Union of Pure and Applied Chemistry
J	coupling constant
KSV	Stern-Volmer constant
λ	wavelength
λ_{abs}	wavelength of absorption maximum
λ_{em}	wavelength of emission maximum
λ_{exc}	wavelength of excitation maximum
LDA	laser Doppler anemometer
LDV	laser Doppler velocimetry
LED	light emitting diode
m	mass
min	minute(s)
MLC	metal ligand complex
mM	10^{-3} mol/L
MW	molar weight
ν	frequency
ν_{mod}	light modulation frequency
n	refractive index
n	amount of substance
NIR	near-infrared
NMR	nuclear magnetic resonance
θ	phase shift or phase angle of the modulated light
P	phosphorescence
PAN	polyacrylonitrile
PAN-COOH	poly-(acrylonitrile-co-acrylic acid)
PCS	photon correlation spectroscopy
PEBBLE	probe encapsulated by biologically localized embedding
phen	phenanthroline
PMT	photomultiplier
polyDADMAC	polydiallyl dimethyl ammonium chloride
Φ	quantum yield of fluorescence
QELS	quasi-elastic light scattering

R	electric resistance
RET	resonance energy transfer
rpm	rotations per minute
Ru(bipy)	ruthenium(II)-tris-2,2-bipyridyl
Ru(dpp)	ruthenium(II)-tris-4,7-diphenyl-1,10-phenanthroline
ΔS	relative signal change
S_0	ground electronic state
S_1	excited electronic state
SC	semiconductor
SDS	sodium dodecyl sulfate
SEM	scanning electron microscopy
SPR	surface plasmon resonance
τ	fluorescence lifetime (decay time)
TEM	transmission electron microscopy
TMS	trimethylsilylpropanesulfonate
UV	ultraviolet
V	volume
VIS	visible

7. References

[1] Hall E. A. H. (**1990**) Biosensors in context. In *Biosensors*, Open University Press, Buckingham, 3-29.

[2] Karol P. J. (**2001**) Label. In *Glossary of Terms for Radiochemistry and Nuclear Techniques* (http://www.iupac.org/V7_karol/Main.html).

[3] Karol P. J. (**2001**) Tracer. In *Glossary of Terms for Radiochemistry and Nuclear Techniques* (http://www.iupac.org/V7_karol/Main.html).

[4] Haugland R. P. (**2001**) Ultrasensitive detection technology. In *Handbook of Fluorescent Probes and Research Chemicals*, 8th edition (http://www.probes.com/handbook/sections/0600.html), Molecular Probes, Eugene.

[5] Wolfbeis O. S., Böhmer M., Dürkop A., Enderlein J., Gruber M., Klimant I., Krause C., Kürner J. M., Liebsch G., Lin Z., Oswald B., Wu M. (**2002**) Advanced luminescent labels, probes, and beads, and their application to luminescence bioassay and imaging. In *Fluorescence Spectroscopy, Imaging and Probes* (Kraayenhof R., Visser A. J. W. G., Gerritsen H. C., Ed.), Springer-Verlag, Berlin, in press.

[6] Assay Design (**2000**) Competitive immunoassay. In *Immunoassay Basics* (http://www.assaydesigns.com/products/immuno.htm).

[7] Assay Design (**2000**) Immunometric assays. In *Immunoassay Basics* (http://www.assaydesigns.com/products/immuno.htm).

[8] Assay Design (**2000**) Immunosorbant assays. In *Immunoassay Basics* (http://www.assaydesigns.com/products/immuno.htm).

[9] Soukka T., Paukkunen J., Härmä H., Lönnberg S., Lindroos H., Lövgren T. (**2001**) Supersensitive time-resolved immunofluorometric assay of free prostate-specific antigen with nanoparticle label technology. *Clinical Chem.* 47, 1269-1278.

[10] Bangs L. B. (**2000**) Recent uses of microspheres in diagnostic tests and assays. In *Novel Approaches in Biosensors and Rapid Diagnostic Assays* (Liron Z., Bromberg A., Fisher M., Ed.), Kluwer Academic/Plenum Publishers, New York, 245-263.

[11] Chan W. C. W., Nie S. (**1998**) Quantum dot bioconjugates for ultrasensitive nonisotopic detection. *Science* 281, 2016-2018.

[12] Taylor J. R., Fang M. M., Nie S. (**2000**) Probing specific sequences on single DNA molecules with bioconjugated fluorescent nanoparticles. *Anal. Chem.* 72, 1979-1986.

[13] Soukka T., Härmä H., Paukkunen J., Lövgren T. (**2001**) Utilization of kinetically enhanced monovalent binding affinity by immunoassays based on multivalent nanoparticle-antibody bioconjugates. *Anal. Chem.* 73, 2254-2260.

[14] Lakowicz J. R., Piszczek G., Kang J. S. (**2001**) On the possibility of long-wavelength long-lifetime high-quantum-yield luminophores. *Anal. Biochem.* 288, 62-75.

[15] Oswald B., Patsenker L., Duschl J., Szmacinski H., Wolfbeis O. S., Terpetschnig E. (**1999**) Synthesis, spectral properties, and detection limits of reactive squaraine dyes, a new class of diode laser compatible fluorescent protein labels. *Bioconj. Chem.* 10, 925-931.

[16] Oswald B., Lehmann F., Simon L., Terpetschnig E., Wolfbeis O. S. (**2000**) Red laser-induced fluorescence energy transfer in an immunosystem. *Anal. Biochem.* 280, 272-277.

[17] Hemmilä I. (**1993**) Progress in delayed fluorescence immunoassay. In *Fluorescence Spectroscopy – New Methods and Applications* (Wolfbeis O. S., Ed.) Springer-Verlag, Berlin, 259-266.

[18] Härmä H., Soukka T., Lönnberg S., Paukkunen J., Tarkkinen P., Lövgren T. (**2000**) Zeptomole detection sensitivity of prostate-specific antigen in a rapid microtitre plate assay using time-resolved fluorescence. *Luminescence* 15, 351-355.

[19] Hall E. A. H. (**1990**) Photometric assay techniques. In *Biosensors*, Open University Press, Buckingham, 141-219.

[20] Lakowicz J. R. (**1999**) Introduction to fluorescence. In *Principles of Fluorescence Spectroscopy*, 2nd edition, Kluwer Academic/Plenum Publishers, New York, 1-23.

[21] Lakowicz J. R. (**1999**) Time-domain lifetime measurements. In *Principles of Fluorescence Spectroscopy*, 2nd edition, Kluwer Academic/Plenum Publishers, New York, 95-140.

[22] Lakowicz J. R. (**1999**) Frequency-domain lifetime measurements. In *Principles of Fluorescence Spectroscopy*, 2nd edition, Kluwer Academic/Plenum Publishers, New York, 141-184.

[23] Demas J. N., Crosby G. A. (**1971**) The measurement of photoluminescence quantum yields. A review. *J. Phys. Chem.* 75, 991-1024.

[24] Wehry E. L., Rogers L. B. (**1966**) Fluorescence quenching and energy transfer in organic compounds. In *Fluorescence and Phosphorescence Analysis* (Hercules D. M., Ed.), Interscience Publishers, New York, 100-113.

[25] Lakowicz J. R. (**1999**) Quenching of fluorescence. In *Principles of Fluorescence Spectroscopy*, 2nd edition, Kluwer Academic/Plenum Publishers, New York, 237-265.

[26] Udenfriend S. (**1962**) Interference due to light absorption by the sample. In *Fluorescence Assay in Biology and Medicine* I (Horecker B., Kaplan N. O., Marmur J., Scheraga H. A., Ed.), Academic Press, New York, 108-109.

[27] Udenfriend S. (**1969**) Problems of light absorption. In *Fluorescence Assay in Biology and Medicine* II (Horecker B., Kaplan N. O., Marmur J., Scheraga H. A., Ed.), Academic Press, New York, 182-185.

[28] Schulman S. G. (**1977**) Concentration effects. In *Fluorescence and Phosphorescence Spectroscopy: Physiochemical Principles and Practice* 59 (Belcher R., Freiser H., Ed.), Pergamon Press, Oxford, 107-116.

[29] Bashford C. L. (**1987**) Quantitation of fluorescence. In *Spectrophotometry and Spectrofluorimetry: A Practical Approach* (Harris D. A., Bashford C. L., Ed.), IRL Press, Oxford, 15-18.

[30] Ellis D. W. (**1966**) Luminescence instrumentation and experimental details. In *Fluorescence and Phosphorescence Analysis* (Hercules D. M., Ed.), Interscience Publishers, New York, 41-79.

[31] Lakowicz J. R. (**1999**) Energy transfer. In *Principles of Fluorescence Spectroscopy*, 2nd edition, Kluwer Academic/Plenum Publishers, New York, 367-394.

[32] Völker M., Siegmund H.-U. (**1997**) Förster energy transfer in ultrathin polymer layers as a basis for biosensors. In *Frontiers in Biosensorics I* (Scheller F. W., Schubert F., Fedrowitz J., Ed.), Birkhäuser Verlag, Basel, 175-191.

[33] Powell R. C., Blasse G. (**1980**) Energy transfer in concentrated systems. *Structure and Bonding* 42, 43-93.

[34] Ullman E. F., Schwarzberg M., Rubenstein K. E. (**1976**) Fluorescent excitation transfer immunoassay. A general method for determinatin of antigens. *J. Biol. Chem.* 251, 4172-4178.

[35] Förster T. (**1948**) Zwischenmolekulare Energiewanderung und Fluoreszenz. *Ann. Phys.* 2, 55-75.

[36] Dexter D. L. (**1953**) A theory of sensitized luminescence in solids. *J. Chem. Physics* 21, 836-850.

[37] Gilbert R. G. (**1995**) Particle size distributions. In *Emulsion Polymerization*, Academic Press, London, 208-243.

[38] Schneider M. (**1994**) Morphologie der Mikropartikel. In *Synthese und Charakterisierung polyfunktioneller Mikropartikel*, PhD Thesis, University of Freiburg, 94-105.

[39] Nitzsche R. (**1998**) Ladungscharakterisierung an Fest/flüssig-Grenzflächen. *CLB Chemie in Labor und Biotechnik* 49, 171-179.

[40] Nitzsche R. (**1997**) Partikelgrößenmessung im Submikron-Bereich. *CLB Chemie in Labor und Biotechnik* 48, 422-427.

[41] Steib J. (**1988**) Partikelgrößenbestimmung mit der Photonen-Korrelations-Spektroskopie. *Chem.-Ing.-Techn.* 60, 138-139.

[42] Winkler K., Lerche K.-H. (**2000**) Zertifizierte NIST- bzw. BCR-konforme monodisperse Partikel für die Standardisierung von Partikelgrößenbestimmungen. *GIT Labor-Fachzeitschrift* 5, 605-608.

[43] Lerche K.-H., Bohrisch J. (**1996**) Charakterisierung neuer monodisperser Mikropartikel. *LaborPraxis* 3, 66-68.

[44] Basten R. (**1994**) Statische und dynamische Lichtstreuung. In *Proteinfunktionalisierte, biologisch aktive Nanopartikel – Eine Anwendung der Mikroemulsionspolymerisation mit natürlichen Tensiden*, PhD Thesis, University of Marburg, 96-103.

[45] Nestl T. (**1994**) Theoretischer Teil. In *Synthese und Charakterisierung von Mikrolatices mit spezieller Form und Funktion*, Phd Thesis, University of Frankfurt, 4-21.

[46] Schnablegger H., Glatter O. (**1993**) Simultaneous determination of size distribution and refractive index of colloidal particles from static light-scattering experiments. *J. Colloid Interface Sci.* 158, 228-242.

[47] Wallis K. (**1992**) Messung der Partikelradien mit Photonen-Korrelations-Spektroskopie. In *Herstellung, Modifikation und Charakterisierung Polymerer Nanopartikel*, PhD Thesis, University of Kiel, 35-36.

[48] Wallis K. (**1992**) Bestimmung des ζ-Potentials mit Laser-Doppler-Anemometrie (LDA). In *Herstellung, Modifikation und Charakterisierung Polymerer Nanopartikel*, PhD Thesis, University of Kiel, 36-40.

[49] Göbel G., Wriedt T., Bauckhage K. (**1998**) Micron and sub-micron aerosol sizing with a standard phase-Doppler anemometer. *J. Aerosol Sci.* 29, 1063-1073.

[50] Reimer L. (**1993**) Types of electron microscope. In *Transmission Electron Microscopy*, 3rd edition, Springer-Verlag, Heidelberg, 1-18.

[51] Watt I. M. (**1997**) The electron microscope family. In *The principles and practice of electron microscopy* (Watt I. M., Ed.), 2nd edition, Cambridge University Press, New York, 59-135.

[52] Pratt P. L. (**1988**) Physical methods for the identification of microstructures. *Materials and Structures* 21, 106-117.

[53] Amelinckx S., Van Dyck D. (**1997**) Transmission electron microscopy. In *Electron Microscopy – Principles and Fundamentals* (Amelinckx S., Van Dyck D., Van Landuyt J., Van Tendeloo G., Ed.), VCH-Wiley, Weinheim, 3-162.

[54] Cowley J. M. (**1997**) Reflection electron microscopy. In *Electron Microscopy – Principles and Fundamentals* (Amelinckx S., Van Dyck D., Van Landuyt J., Van Tendeloo G., Ed.), VCH-Wiley, Weinheim, 163-180.

[55] Walt D. R. (**2000**) Bead-based fiber-optic arrays. *Science* 287, 451-452.

[56] McNamara K. P., Nguyen T., Dumitrascu G., Ji J., Rosenzweig N., Rosenzweig Z. (**2001**) Synthesis, characterization, and application of fluorescence sensing lipobeads for intracellular pH measurements. *Anal. Chem.* 73, 3240-3246.

[57] Clark H. A., Hoyer M., Philbert M. A., Kopelman R. (**1999**) Optical nanosensors for chemical analysis inside single living cells. 1. Fabrication, characterization, and methods for intracellular delivery of PEBBLE sensors. *Anal. Chem.* 71, 4831-4836.

[58] Clark H. A., Baker S. L. R., Brasuel M., Miller M. T., Monson E., Parus S., Shi Z.-Y., Song A., Thorsrud B., Kopelman R., Ade A., Meixner W., Athey B., Hoyer M., Hill D., Lightle R., Philbert M. A. (**1998**) Subcellular optochemical nanobiosensors: probes encapsulated by biologically localised embedding (PEBBLEs). *Sensors and Actuators B* 51, 12-16.

[59] Clark H. A., Hoyer M., Parus S., Philbert M. A., Kopelman R. (**1999**) Optochemical nanosensors and subcellular applications in living cells. *Mikrochim. Acta* 131, 121-128.

[60] Clark H. A., Kopelman R., Tjalkens R., Philbert M. A. (**1999**) Optical nanosensors for chemical analysis inside single living cells. 1. Sensors for pH and calcium and the intracellular application of PEBBLE sensors. *Anal. Chem.* 71, 4837-4843.

[61] Klink S. I., Keizer H., Van Veggel F. C. J. M. (**2000**) Transition metal complexes as photosensitizers for near-infrared lanthanide luminescence. *Angew. Chem. Int. Ed.* 39, 4319-4321.

[62] Meyer J., Karst U. (**1999**) Zeitverzögerte Fluoreszenzspektroskopie mit Lanthanoidkomplexen – Prinzipien und Anwendungen. *Nachr. Chem. Tech. Lab.* 47, 1116-1119.

[63] Diamanidis E. P., Christopoulos T. K. (**1990**) Europium chelate labels in time-resolved fluorescence immunoassays and DNA hybridization assays. *Anal. Chem.* 62, 1149A-1157A.

[64] Sinha S. P. (**1982**) Fluorescence spectra and lifetimes of the lanthanide aquo ions and their complexes. In *Systematics and the Properties of the Lanthanides*, Kluwer Academic Publishers, Dordrecht, 451-500.

[65] Carnall W. T. (**1979**) The absorption and fluorescence spectra of rare earth ions in solution. In *Handbook on the Physics and Chemistry of Rare Earths* 3 (Gschneidner K. A. Jr., Eyring L. R., Ed.), North-Holland Publishing Company, Amsterdam, 171-207.

[66] Rakicioglu Y., Perrin J. H., Schulman S. G. (**1999**) Increased luminescence of the tetracycline-europium (III) system following oxidation by hydrogen peroxide. *J. Pharmaceutical and Biomedical Analysis* 20, 397-399.

[67] Kessler M. A. (**1999**) Probing the dissociation state of acid-base indicators by time-resolved lanthanide luminescence: a convenient transduction scheme for optical chemical sensors. *Anal. Chem.* 71, 1540-1543.

[68] Chan A., Diamandis E. P., Krajden M. (**1993**) Quantification of polymerase chain reaction products in agarose gels with a fluorescent europium chelate as label and time-resolved fluorescence spectroscopy. *Anal. Chem.* 65, 158-163.

[69] Yam V. W.-W., Lo K. K.-W. (**1999**) Recent advances in utilization of transition metal complexes and lanthanides as diagnostic tools. *Coord. Chem. Rev.* 184, 157-240.

[70] Yan B., Zhang H., Wang S., Ni J. (**1998**) Spectroscopic study of luminescence and energy transfer of binary and ternary complexes of rare earth with aromatic carboxylic acids and 1,10-phenanthroline. *Spectroscopy Letters* 31, 603-613.

[71] Parker D., Senanayake P. K., Williams J. A. G. (**1998**) Luminescent sensors for pH, pO_2, halide and hydroxide ions using phenanthridine as a photosensitiser in macrocyclic europium and terbium complexes. *J. Chem. Soc. Perkin Trans.* 2, 2129-2139.

[72] Demas J. N., DeGraff B. A. (**1997**) Applications of luminescent transition metal complexes to sensor technology and molecular probes. *J. Chem. Education* 74, 690-695.

[73] Juris A., Balzani V., Barigelletti F., Campagna S., Belser P., Zelewsky A. v. (**1988**) Ru(II) polypyridine complexes: photophysics, photochemistry, electrochemistry, and chemiluminescence. *Coord. Chem. Rev.* 84, 85-277.

[74] Szmacinski H., Terpetschnig E., Lakowicz J. R. (**1996**) Synthesis and evaluation of Ru-complexes as anisotropy probes for protein hydrodynamics and immunoassays of high-molecular-weight antigens. *Biophys. Chem.* 62, 109-120.

[75] Guo X.-Q., Castellano F. N., Li L., Lakowicz J. R. (**1998**) Use of a long-lifetime Re(I) complex in fluorescence polarization immunoassays of high-molecular-weight analytes. *Anal. Chem.* 70, 632-637.

[76] Guo X.-Q., Castellano F. N., Li L., Szmacinski H., Lakowicz J. R., Sipior J. (**1997**) A long-lived, highly luminescent Re(I) metal-ligand complex as a biomolecular probe. *Anal. Biochem.* 254, 179-186.

[77] Blackburn G. F., Shah H. P., Kenten J. H., Leland J., Kamin R. A., Link J., Peterman J., Powell M. J., Shah A., Talley D. B., Tyagi S. K., Wilkins E., Wu T.-G., Massey R. J. (**1991**) Electrochemiluminescence detection for development of immunoassays and DANN probe assays for clinical diagnostics. *Clin. Chem.* 37, 1534-1539.

[78] Hemmila I. A., Hurskainen J. P., Blomberg K. R., Mukkala V.-M., Takalo H. J., Satu S. A., Webb S. A. (**1998**) Improved homogeneous luminescence energy transfer assays using lanthanide chelate labels as energy donors and optimized energy acceptors. Patent WO9815830.

[79] Liebsch G., Klimant I., Wolfbeis O. S. (**1999**) Luminescence lifetime temperature sensing based on sol-gels and poly(acrylonitrile)s dyed with ruthenium metal-ligand complexes. *Adv. Mater.* 11, 1296-1299.

[80] Klimant I. (**2001**) Production and use of luminescent microparticles and nanoparticles. Patent WO0106227.

[81] Beynon R. J., Easterby J. S. (**1996**) Theory of buffer action. In *Buffer Solutions: The Basics*, Oxford University Press, Oxford, 18-34.

[82] Galster H. (**1990**) pH-Skalen. In *pH-Messung - Grundlagen, Methoden, Anwendungen, Geräte*, VCH, Weinheim, 1-61.

[83] Harris D. C. (**1998**) Aktivität. In *Lehrbuch der Quantitativen Analyse*, Vieweg Verlag, Braunschweig, 227-244.

[84] Falbe J., Regitz M. (**1990**) Ionenstärke. In *Römpp Chemie Lexikon*, 9th edition, Georg Thieme Verlag, Stuttgart, 2034.

[85] Kosch U., Klimant I., Wolfbeis O. S. (**1999**) Long-lifetime based pH micro-optodes without oxygen interference, *Fresenius J. Anal. Chem.* 364, 48-53.

[86] de Chasteigner S., Cavé G., Fessi H., Devissaguet J.-P., Puisieux F. (**1996**) Freeze-drying of itraconazole-loaded nanosphere suspensions: a feasibility study. *Drug Development Research* 38, 116-124.

[87] Klimant I., Wolfbeis O. S. (**1995**) Oxygen-sensitive luminescent materials based on silicone-soluble ruthenium diimine complexes. *Anal. Chem.* 67, 3160-3166.

[88] Bacon J. R., Demas J. N. (**1987**) Determination of oxygen concentrations by luminescence quenching of a polymer-immobilized transition-metal complex. *Anal. Chem.* 59, 2780-2785.

[89] Carraway E. R., Demas J. N., DeGraff B. A., Bacon J. R. (**1991**) Photophysics and photochemistry of oxygen sensors based on luminescent transition-metal complexes. *Anal. Chem.* 63, 337-342.

[90] Bucheńska J. (**1997**) Modified polyacrylonitrile (PAN) fibers. *J. Appl. Polym. Sci.* 65, 1955-1966.

[91] Korte S. (**1999**) Physical constants of poly(acrylonitrile). In *Polymer Handbook* (Brandrup J., Immergut E. H., Grulke E. A., Ed.), John Wiley & Sons, New York, V/59-V/66.

[92] Usmani A. M. (**1994**) Diagnostic polymers and coatings. In *Diagnostic Biosensor Polymers* (Usmani A. M., Akmal N., Ed.), Library of Congress, Washington, 2-20.

[93] Wallis K. (**1992**) Herstellung von Nanopartikeln mit der 'solvent evaporation technique'. In *Herstellung, Modifikation und Charakterisierung Polymerer Nanopartikel*, PhD Thesis, University of Kiel, 27-29.

[94] Fadini A., Schnepel F.-M. (**1985**) Auswertung der Schwingungsspektren. In *Schwingungsspektroskopie: Methoden, Anwendungen*, Thieme Verlag, Stuttgart, 60-64.

[95] Wang H. Y., Kobayashi T., Fukaya T., Fujii N. (**1997**) Molecular imprint membranes prepared by the phase inversion precipitation technique. 2. Influence of coagulation temperature in the phase inversion process on the encoding in polymeric membranes. *Langmuir* 13, 5396-5400.

[96] Wang P., Zhu G.-Y (**1999**) Synthesis, fluorescence and electrochemistry of three new ruthenium (II) complexes. *Chemical Research in Chinese Universities* 15, 79-82.

[97] Ausborn M., Schreier H., Brezesinski G., Fabian H., Meyer H. W., Nuhn P. (**1994**) The protective effect of free and membrane-bound cryoprotectants during freezing and freeze-drying of liposomes. *J. Controlled Release* 30, 105-116.

[98] Orr C. (**1976**) Der derzeitige Stand der Methoden zur Bestimmung von Pulver-Oberflächen. *Chem.-Ing.-Tech.* 48, 680-689.

[99] Sing K. S. W., Everett D. H., Haul R. A. W., Moscou L., Pierotti R. A., Rouquérol J., Siemieniewska T. (**1985**) Reporting physisorption data for gas/solid systems with special reference to the determination of surface area and porosity. *Pure & Appl. Chem.* 57, 603-619.

[100] Haugland R. P. (**2001**) Fluorophores and their amine-reactive derivatives. In *Handbook of Fluorescent Probes and Research Chemicals*, 8th edition (http://www.probes.com/handbook/sections/0100.html), Molecular Probes, Eugene.

[101] Ferguson J. A., Boles T. C., Adams C. P., Walt D. R. (**1996**) A fiber-optic DNA biosensor microarray for the analysis of gene expression. *Nature Biotechnology* 14, 1681-1684.

[102] Szurdoki F., Michael K. L., Agrawal D., Taylor L. C., Schultz S. L., Walt D. R. (**1999**) Immunofluorescence detection methods using microspheres. *Proceedings – SPIE The International Society For Opctical Engineering* 3544, 52-62.

[103] Méallet-Renault R., Denjean P., Pansu R. B. (**1999**) Polymer beads as nano-sensors. *Sensors and Actuators B* 59, 108-112.

[104] Fortin M., Hugo P. (**1999**) Surface antigen detection with non-fluorescent, antibody-coated microbeads: an alternative method compatible with conventional fluorochrome-based labelling. *Cytometry* 36, 27-35.

[105] Sukhorukov G. B., Donath E., Moya S., Susha A. S., Voigt A., Hartmann J., Möhwald H. (**2000**) Microencapsulation by means of step-wise adsorption of polyelectrolytes. *J. Microencapsulation* 17, 177-185.

[106] Fulton R. J., McDade R. L., Smith P. L., Kienker L. J., Kettman J. R. (**1997**) Advanced multiplexed analysis with the FlowMetrix System. *Clinical Chem.* 43, 1749-1756.

[107] Pelssers E. G. M., Lerche K.-H. (**1989**) A new red fluorescent melamine-formaldehyde latex particle for single particle optical sizing (SPOS) and flow cytometry. *Colloids and Surfaces* 34, 241-245.

[108] Huang M.-C., Afromowitz M., Van den Engh G., Weigl B. H., Yager P. (**1998**) Development of a flow cytometry based miniature chemical fluid analysis system using fluorescent microbeads. *Proceedings – SPIE The International Society For Optical Engineering* 3256, 178-185.

[109] Kürner J. M., Klimant I., Krause C., Preu H., Kunz W., Wolfbeis O. S. (**2001**) Inert phosphorescent nanospheres as markers for optical assays. *Bioconjug. Chem.* 12, 883-889.

[110] Brooker L. G. S., Sprague R. H., Smyth C. P., Lewis G. L.(**1940**) Color and constitution. I. Halochromism of anhydronim bases related to the cyanine dyes. *J. Am. Chem. Soc.* 62, 1116-1125.

[111] Kosch U., Klimant I., Werner T., Wolfbeis O. S. (**1998**) Strategies to design pH optodes with luminescence decay times in the microsecond time regime. *Anal. Chem.* 70, 3892-3897.

[112] Diamandis E. P., Christopoulos T. K. (**1996**) Fluorescence Immunoassays. In *Immunoassay*, Academic Press, San Diego, 309-335.

[113] Elings V. B., Nicoli D. F., Briggs J. (**1983**) Fluorescence fluctuation immunoassay. In *Methods in Enzymology – Immunochemical Techniques* 92 (Langone J. J., Vunakis H. V., Ed.), Academic Press, New York, 458-472.

[114] Weeks I. (**1992**) Immunoassay. In *Comprehensive Analytical Chemistry – Chemiluminescence immunoassay* XXIX (Svehla G., Ed.), Elsevier Science Publishers, Amsterdam, 53-119.

[115] Pal S. B. (**1978**) Reagents antisera and developments. In *Enzyme Labelled Immunoassays of Hormones and Drugs* (Pal S. B., Ed.), de Gruyter, Berlin, 1-136.

[116] Stryer L. (**1995**) Exploring proteins. In *Biochemistry*, 4th edition, W. H. Freeman and Company, New York, 45-74.

[117] Wood W. G. (**1985**) Luminescence immunoassays in theory and practice – the state of the art. In *Immunoassay Technology* 1 (Pal S. B., Ed.), de Gruyter, Berlin, 105-125.

[118] Smith C. J. (**1990**) Evolution of the immunoassay. In *Development and Application of Immunoassay for Food Analysis* (Rittenburg J. H., Ed.), Elsevier Applied Science, London, 3-27.

[119] Rittenburg J. H. (**1990**) Fundamentals of immunoassay. In *Development and Application of Immunoassay for Food Analysis*, Elsevier Applied Science, London, 29-57.

[120] Jansen E. H. J. M. (**1993**) Chemiluminescence detection in immunochemical techniques. Applications to environmental monitoring. In *Fluorescence Spectroscopy – New Methods and Applications* (Wolfbeis O. S., Ed.), Springer-Verlag, Berlin, 267-278.

[121] Borque L., Maside C., Rus A., del Cura J. (**1994**) Latex immunoassay of β_2-mircoglobulin in serum and urine. *J. Clinical Immunoassay* 17, 160-165.

[122] Lee M., Walt D. R., Nugent P. (**1999**) Fluorescent excitation transfer immunoassay for the determination of spinosyn in water, *J. Agric. Food Chem.* 47, 2766-2770.

[123] Lövgren T., Pettersson K. (**1990**) Time-resolved fluoroimmunoassay, advantages and limitations. In *Luminescence Immunoassay and Molecular Applications* (Van Dyke K., Van Dyke R., Ed.), CRC Press, Boca Raton, 233-253.

[124] Gosling J. P., Wilchek M. (**1996**) Enzyme immunoassay. In *Immunoassay* (Diamandis E. P., Christopoulos T. K., Ed.), Academic Press, San Diego, 287-308.

[125] Christopoulos T. K., Diamandis E. P. (**1996**) Fluorescence immunoassays. In *Immunoassay* (Diamandis E. P., Christopoulos T. K., Ed.), Academic Press, San Diego, 237-267.

[126] Lakowicz J. R. (**1999**) Fluorescence sensing. In *Principles of Fluorescence Spectroscopy*, 2nd edition, Kluwer Academic/Plenum Publishers, New York, 531-572.

[127] Kürner J. M., Wolfbeis O. S., Klimant I. (**2002**) Homogeneous luminescence decay time-based assay using energy transfer from nanospheres. *Anal. Chem.*, submitted.

[128] Koller E., Wolfbeis O. S. (**1991**) Sensor chemistry. In *Fiber Optic Chemical Sensors and Biosensors* I (Wolfbeis O. S., Ed.), CRC Press, Boca Raton, 303-358.

[129] Bangs Laboratories, Fishers (**1999**) Covalent Coupling. In *TechNote 205* (http://www.bangslabs.com/support/index.php).

[130] Bangs L. B. (**1996**) New developments in particle-based immunoassays: introduction. *Pure & Appl. Chem.* 68, 1873-1879.

[131] Nathan C. F., Cohn Z. A. (**1981**) Antitumor effects of hydrogen peroxide in vivo. *J. Exp. Med.* 154, 1539-1553.

[132] Hager H. J. (**1974**) Latex polymer reagents for diagnostic tests. US patent 3,857,9331.

[133] Quash G., Roch A. M., Niveleau A., Grange J., Keolouangkhot T., Huppert J. (**1978**) The preparation of latex particles with covalently bound polyamines, IgG and measles agglutinins and their use in visual agglutination tests. *J. Immun. Meth.* 22, 165-174.

[134] Hermanson G. T. (**1996**) Zero-length cross-linkers. In *Bioconjugate Techniques*, Academic Press, San Diego, 169-186.

[135] Hermanson G. T. (**1996**) Tags and probes. In *Bioconjugate Techniques*, Academic Press, San Diego, 297-416.

[136] Hermanson G. T. (**1996**) Antibody modification and conjugation. In *Bioconjugate Techniques*, Academic Press, San Diego, 456-493.

[137] Hermanson G. T., Mallia A. K., Smith P. K. (**1992**) Immobilized ligands. In *Immobilized Affinity Ligand Techniques*, Academic Press, London, 80-85.

[138] Staros J. V., Wright R. W., Swingle D. M. (**1986**) Enhancement by N-hydroxysulfosuccinimide of water-soluble carbodiimide-mediated coupling reactions. *Anal. Biochem.* 156, 220-222.

[139] Quash Q., Roch A.-M., Niveleau A., Grange J., Keolouangkhot T., Huppert J. (**1978**) The preparation of latex particles with covalently bound polyamines, IgG and measles agglutinins and their use in visual agglutination tests. *J. Immunological Methods* 22, 165-174.

[140] Thomas R. N., Guo C.-Y. (**2001**) Nanosphere-antibody conjugates with releasable fluorescent probes. *Fresenius J. Anal. Chem.* 369, 477-482.

[141] Sukhorukov G. B., Donath E., Davis S., Lichtenfeld H., Caruso F., Popov V. I., Möhwald H. (**1998**) Stepwise polyelectrolyte assembly on particle surfaces: a novel approach to colloid design. *Polym. Adv. Technol.* 9, 759-767.

[142] Sukhorukov G. B., Donath E., Lichtenfeld H., Knippel E., Knippel M., Budde A., Möhwald H. (**1998**) Layer-by-layer self assembly of polyelectrolytes on colloidal particles. *Colloids Surfaces A: Physiochem. Eng. Aspects* 137, 253-266.

[143] Donath E., Sukhorukov G. B., Caruso F., Davis S. A., Möhwald H. (**1998**) Neuartige Polymerhohlkörper durch Selbstorganisation von Polyelectrolyten auf kolloidalen Templaten. *Angew. Chem.* 110, 2324-2327.

[144] Caruso F. (**2000**) Hollow capsule processing through colloidal templating and self-assembly, *Chem. Eur. J.* 6, 413-419.

[145] Susha A. S., Caruso F., Rogach A. L., Sukhorukov G. B., Kornowski A., Möhwald H., Giersig M., Eychmüller A., Weller H. (**2000**) Formation of luminescent spherical core-shell particles by the consecutive adsorption of polyelectrolyte and CdTe(S) nanocrystals on latex colloids. *Colloids Surfaces A: Physiochem. Eng. Aspects* 163, 39-44.

[146] Sukhorukov G. B., Brumen M., Donath E., Möhwald H. (**1999**) Hollow polyelectrolyte shells: exclusion of polymers and donnan equilibrium. *J. Phys. Chem. B* 103, 6434-6440.

[147] Bergbreiter D. E. (**1999**) Selbstorganisierte, semipermeable Kapseln mit Durchmessern im Sub-Mikrometerbereich. *Angew. Chem.* 111, 3044-3046.

[148] Donath E., Sukhorukov G. B., Möhwald H. (**1999**) Polyelektrolytkapseln im Submikrometer- und Mikrometerbereich. *Nachr. Chem. Tech. Lab.* 47, 400-404.

[149] Caruso F., Caruso R. A., Möhwald H. (**1998**) Nanoengineering of inorganic and hybrid hollow spheres by colloidal templating. *Science* 282, 1111-1114.

[150] Caruso F., Lichtenfeld H., Giersig M., Möhwald H. (**1998**) Electrostatic self-assembly of silica nanoparticle-polyelectrolyte multilayers on polystyrene latex particles. *J. Am. Chem. Soc.* 120, 8523-8524.

[151] Caruso F., Donath E., Möhwald H. (**1998**) Influence of polyelectrolyte multilayer coatings on Förster resonance energy transfer between 6-carboxyfluorescein and rhodamine B-labelled particles in aqueous solution. *J. Phys. Chem. B* 102, 2011-2016.

[152] Schröder H. R., Vogelhut P. O., Carrico R. J., Boguslaski R. C., Buckler R. T. (**1976**) Competitive protein binding assay for biotin monitored by chemiluminescence. *Anal. Chem.* 48, 1933-1937.

[153] Blake R. C., Pavlov A. R., Blake D. A. (**1999**) Automated kinetic exlusion assays to quantify protein binding interactions in homogeneous solution. *Anal. Chem.* 272, 123-134.

[154] Bayer E. A., Wilchek M. (**1996**) The avidin-biotin system. In *Immunoassay* (Diamandis E. P., Christopoulos T. K., Ed.), Academic Press, San Diego, 237-267.

[155] Hermanson G. T. (**1996**) Avidin-biotin systems. In *Bioconjugate Techniques*, Academic Press, San Diego, 570-592.

[156] Wilchek M., Bayer E. A. (**1990**) Introduction to avidin-biotin technology. In *Methods in Enzymology – Avidin-Biotin Technology* 184, Academic Press, San Diego, 5-13.

[157] Kürner J. M., Klimant I., Krause C., Pringsheim E., Wolfbeis O. S. (**2001**) A new type of phosphorescent nanospheres for use in advanced time-resolved multiplexed bioassays. *Anal. Biochem.* 297, 32-41.

[158] Deniz A. A., Dahan M., Grunwell J. R., Ha T., Faulhaber A. E., Chemla D. S., Weiss S., Schultz P. G. (**1999**) Single-pair fluorescence resonance energy transfer on freely diffusing molecules: Observation of Förster distance dependence and subpopulations. *Proc. Natl. Acad. Sci. USA* 96, 3670-3675.

[159] Kürner J. M. (**2002**) Inert phosphorescent nanospheres as markers for optical assays. In *PhD Thesis*, University of Regensburg.

[160] Mathis G. (**1993**) Rare earth cryptates and homogeneous fluoroimmunoassays with human sera. *Clin. Chem.* 39, 1953-1959.

[161] Morrison L. E. (**1988**) Time-resolved detection of energy transfer: theory and application to immunoassays. *Anal. Biochem.* 174, 101-120.

8. Summary

8.1. Summary

This work describes both the preparation and various applications of a new class of nanometer-sized, inert, brightly luminescent particles that are of potential use as ultrasensitive labels for bioassays. The nanospheres are fabricated by a simple and time-saving precipitation technique using N,N-dimethylformamide (DMF) as solvent.

The most important prerequisites for the polymer matrix of the nanospheres is its poor permeability for quenchers. Among the different polyacrylonitrile (PAN) copolymers tested, polyacrylonitrile with an acrylic acid content of between 5 – 10% (w/w) was the most attractive matrix for the encapsulation of organic phosphorescent dyes since is has a superb shielding effect against luminescence quenching caused by molecular oxygen. The ideal matrix concentration for the precipitation proved to be 0.5% (w/w matrix/DMF). Due to the acrylic acid copolymer the nanospheres have an activated surface for the coupling of biomolecules or chemically responsive indicators.

The phosphorescent complexes ruthenium(II)-tris-4,7-diphenyl-1,10-phenanthroline bis-trimethylsilylpropanesulfonate [$Ru(dpp)_3(TMS)_2$] and ruthenium(II)-tris-4,7-diphenyl-1,10-phenanthroline dichloride [$Ru(dpp)_3Cl_2$] were selected as dyes. The apparent decay time of both free ruthenium complexes in water varies from 1.20 μs in air to 4.70 μs in nitrogen, but can be as high as 6.20 μs in apolar organic solvents. Both dyes, when incorporated into PAN, have a very low quenching rate ($\Delta\tau_{air/nitrogen}$ 3 – 5%), a high quantum yield ($\Phi > 40\%$) and a large molar absorbance ($\varepsilon \approx 30{,}000$ L mol^{-1} cm^{-1}). They yield extremely bright nanospheres that display a large Stokes' shift of about 150 nm (λ_{exc} 465 nm, λ_{em} 610 nm) and are highly resistant against photo-bleaching. They are excitable with an argon ion laser at 488 nm or blue light emitting diodes (LEDs) at 450 nm or 470 nm. The ideal fraction of ruthenium complex within the nanospheres varies between 1 – 2% (w/w dye/matrix) depending on the matrix used.

Scanning and transmission electron microscopic studies of the nanospheres showed an average diameter of about 5 – 50 nm and a spherical shape. Static and dynamic light scattering experiments confirmed a polydisperse coil with a negative zeta potential ($\zeta \approx -50$ mV) resulting from the carboxy groups of the copolymer. The nanospheres have a very high surface-to-bulk ratio which is an evidence for a highly branched, porous structure.

Suspensions of such phosphorescent nanospheres show no tendency to sedimentation in an aqueous buffered environment (pH 7.0, ionic strength 20 – 100 mM, 0.5% (w/w) sodium azide, 0.5% (w/w) trehalose). No dye leaching was observed in aqueous solutions.

In chapter 4, a new concept to design phosphorescent nanospheres is presented in order to create well over 100 different labels. The multi-color multi-lifetime sensing scheme introduced is based on the co-immobilization of two or three luminescent dyes into a polymer matrix. The nanospheres, with an average diameter of approximately 50 - 70 nm, are composed of the phosphorescent metal ligand complex (MLC) Ru(dpp) (λ_{exc} 465 nm, λ_{em} 610 nm) which is dissolved, along with one (for a two-dimensional assay) or two (for a three-dimensional assay) strongly fluorescent cyanine dyes ($\lambda_{exc/em}$ 587/608, 612/633, 659/678, 713/731 nm; $\varepsilon >> 200{,}000$ L mol^{-1} cm^{-1}), in nanospheres made of poly-(acrylonitrile-co-acrylic acid). Due to the long lifetime of the donor ($\tau \approx 6$ µs), indesired short-lived background fluorescence is eliminated.

Since the emission spectrum of the ruthenium MLC strongly overlaps the absorbance spectra of all four cyanines and both the MLC (donor) and the cyanines (acceptor) are in close spatial proximity, efficient resonance energy transfer (RET) does occur. Consequently, the nanospheres emit dual luminescence. One originates from the donor (at 610 nm) which is present in constant concentration, the other one from the acceptor which varies in terms of both spectral properties and concentration. Variation of the concentrations of the cyanine acceptors results in a varying efficiency of RET, making the nanospheres distinguishable. Thus, the labels obtained can be differentiated in terms of both their individual decay time (reflecting the acceptor concentration) and the distribution of their emission maximum (reflecting the kind of acceptor dye). In the two-dimensional assay with only one cyanine acceptor present, the apparent decay time τ in air consecutively decreases from 6.23 µs (no acceptor) to 0.38 – 1.16 µs (maximal acceptor concentration) depending on the applied cyanine and its concentration. Along with it, the quantum yield Φ in air also decreases from 0.38 to 0.03 – 0.27, once again depending on the acceptor characteristics. In the three-dimensional assay with two types of acceptors in the nanospheres, the lifetime decreases from 5.92 µs (no acceptor) to 0.34 µs (maximal acceptor concentrations). The quantum yield Φ in air also decreases from 0.39 to 0.02.

All nanospheres can be excited with the same light source at the absorbance wavelength of the Ru(dpp) donor (at 465 nm). The levels of oxygen quenching are always below 3.5% ($\Delta\Phi_{air/nitrogen}$) for both the two- and three-dimensional assay.

In chapter 5, a new scheme for homogeneous assays is presented that is based on RET from phosphorescent biotinylated nanospheres to fluorescently-labelled streptavidin (SA). The results presented demonstrate the feasibilty of an assay for avidin or any other biomolecule that binds to a countermolecule on the nanosphere surface. The nanospheres, about 10 – 50 nm in diameter, are made from poly-(acrylonitrile-co-acrylic acid), dyed with $Ru(dpp)_3Cl_2$.

In a first study, the Ru(dpp) donor nanospheres (λ_{exc} 465 nm, λ_{em} 610 nm) were titrated with a cationic polyelectrolyte solution containing bromophenol blue (BPB, λ_{max} 592 nm, ε 73,000 L mol^{-1} cm^{-1}) as the energy acceptor. This was to prove that RET occurs from the nanospheres to the dye and to quantify the maximum extent of quenching that is feasible. Since the nanospheres contain negatively charged carboxy groups on the surface due to the acrylic acid copolymer, they attract and electrostatically interact with the cationic polyelectrolyte. The resulting spatial proximity of donor and acceptor (Förster distance R_0 5.24 nm) enables a transfer of luminescence energy from the Ru(dpp) donor to the BPB acceptor which can be detected by a decrease in the apparent decay time from 4.9 µs (no polyelectrolyte) to 3.1 µs (54.4 nmol/L polyelectrolyte).

Based on this experiment, a competitive binding assay for avidin based on RET was established, with an acceptor fluorophore – Alexa Fluor 633 (λ_{exc} 633 nm, λ_{em} 647 nm, ε 115,000 L mol^{-1} cm^{-1}) – instead of a non-luminescent acceptor like BPB. In essence, avidin and Alexa Fluor 633-labelled SA bind competitively to biotin covalently bound to the surface of the Ru(dpp) donor nanospheres. If labelled SA binds to the nanospheres, RET occurs from Ru(dpp) to the label of SA (Alexa Fluor 633), which does not measurably absorb itself at the excitation wavelength of the donor (470 nm). As a result, the apparent decay time τ of the emission decreases from 4.4 µs (7.10 µmol/L avidin) to 2.5 µs (no avidin) while the overall luminescence intensity remains nearly constant since the ratio of the concentrations of Alexa Fluor 633 to Ru(dpp) was kept constant at 2.8.

8.2. Zusammenfassung

Diese Arbeit beschreibt sowohl die Herstellung als auch verschiedene Anwendungen einer neuen Klasse von inerten, stark lumineszierenden Partikeln im Nanometer-Größenbereich, die als hochsensitive Marker für Bioassays Anwendung finden. Die Nanopartikel werden durch eine einfache, zeitsparende Fällungstechnik mit N,N-Dimethylformamid (DMF) als Lösungsmittel hergestellt.

Die wichtigste Anforderung an die Polymermatrix der Nanopartikel ist eine geringe Permeabilität für Lumineszenzlöscher. Von den verschiedenen getesteten Polyacrylnitril (PAN) Copolymeren war Polyacrylnitril mit einem Acrylsäureanteil von 5 – 10% (w/w) die geeignetste Matrix für den Einbau von organischen phosphoreszierenden Farbstoffen, da es hervorragende Abschirmeigenschaften gegen Lumineszenzlöschung, verursacht durch molekularen Sauerstoff, besitzt. Es hat sich herausgestellt, daß die ideale Matrixkonzentration für die Fällung 0.5% (w/w Matrix/DMF) ist. Wegen des Acrylsäurecopolymers besitzen die Nanopartikel eine aktivierte Oberfläche für die Kopplung von Biomolekülen oder chemischen Indikatoren.

Die phosphoreszierenden Komplexe Ruthenium(II)-tris-4,7-diphenyl-1,10-phenanthrolin Bis-trimethylsilylpropansulfonat [$Ru(dpp)_3(TMS)_2$] und Ruthenium(II)-tris-4,7-diphenyl-1,10-phenanthrolin Dichlorid [$Ru(dpp)_3Cl_2$] wurden als Farbstoffe ausgesucht. Die Abklingzeit beider freier Rutheniumkomplexe in Wasser variiert von 1.20 µs in Luft bis 4.70 µs in Stickstoff, kann aber bis zu 6.20 µs in apolaren organischen Lösungsmitteln betragen. Beide Farbstoffe haben, wenn sie in PAN eingebaut sind, eine sehr niedrige Löschungsrate ($\Delta\tau_{\mathrm{Luft/Stickstoff}}$ 3 – 5%), eine hohe Quantenausbeute ($\Phi > 40\%$) und einen großen Extinktionskoeffizienten ($\varepsilon \approx 30{,}000\ \mathrm{L\ mol^{-1}\ cm^{-1}}$). Sie ergeben extrem leuchtende Nanopartikel mit einer großen Stokes' Verschiebung von etwa 150 nm (λ_{exc} 465 nm, λ_{em} 610 nm) und sind in hohem Maße resistent gegen Ausbleichen. Sie sind mit einem blauen Argon-Ionenlaser bei 488 nm oder blauen Leuchtdioden (LEDs) bei 450 nm oder 470 nm anregbar. Der ideale Gehalt an Rutheniumkomplex in den Nanopartikeln liegt, abhängig von der verwendeten Matrix, zwischen 1 – 2% (w/w Farbstoff/Matrix).

Raster- und transmissionselektronenmikroskopische Studien ergaben einen durchschnittlichen Durchmesser der Nanopartikel von etwa 5 – 50 nm und eine Kugelform. Statische und dynamische Lichtstreuungsexperimente bestätigten ein polydispersed Knäuel mit einem negativen Zetapotential ($\zeta \approx$ -50 mV), das von den

Carboxylgruppen des Copolymers stammt. Das Verhältnis von Oberfläche zu Volumen der Nanopartikel ist groß, was ein Hinweis auf eine hoch verzweigte, poröse Struktur ist.

Suspensionen solcher phosphoreszierender Nanopartikel zeigen keine Tendenz zur Sedimentation in wässriger gepufferter Umgebung (pH 7.0, Ionenstärke 20 – 100 mM, 0.5% (w/w) Natriumazid, 0.5% (w/w) Trehalose). Ein Auswaschen des Farbstoffes in wässrigen Lösungen wurde nicht beobachtet.

In Kapitel 4 wird ein neues Konzept vorgestellt, phosphoreszierende Nanopartikel herzustellen, um weit über 100 verschiedene Marker zu erhalten. Das eingeführte Multi-Color Multi-Lifetime Meßprinzip basiert auf der gleichzeitigen Immobilisierung von zwei oder drei lumineszierenden Farbstoffen in eine polymere Matrix. Die Nanopartikel haben einen durchschnittlichen Durchmesser von etwa 50 – 70 nm und bestehen aus dem phosphoreszierenden Metall-Ligand-Komplex (MLC) Ru(dpp) (λ_{exc} 465 nm, λ_{em} 610 nm), der zusammen mit einem (für einen zweidimensionalen Assay) oder zwei (für einen dreidimensionalen Assay) stark fluoreszierenden Cyanin-Farbstoffen ($\lambda_{exc/em}$ 587/608, 612/633, 659/678, 713/731 nm; $\varepsilon >> 200{,}000$ L mol^{-1} cm^{-1}) in Nanopartikeln aus Poly-(acrylnitril-co-acrylsäure) gelöst ist. Wegen der langen Lebenszeit des Donors ($\tau \approx 6$ µs) wird unerwünschte kurzlebige Hintergrundfluoreszenz eliminiert.

Da sich das Emissionsspektrum des Ruthenium MLC stark mit den Absorptionsspektren aller vier Cyanine überlappt und sowohl der MLC (Donor) und die Cyanine (Akzeptor) in enger räumlicher Nähe befinden, findet effizienter Resonanz-Energietransfer (RET) statt. Demzufolge emittieren die Nanopartikel Doppellumineszenz. Eine stammt vom Donor (bei 610 nm), der in konstanter Konzentration anwesend ist, die andere vom Akzeptor, der sich sowohl in Bezug auf seine spektralen Eigenschaften als auch auf seine Konzentration unterscheidet. Verändert man die Konzentrationen der Cyaninakzeptoren, ergibt sich eine variierende Effizienz RET, was die Nanopartikel unterscheidbar macht. Somit können die erhaltenen Marker sowohl in Bezug auf ihre individuelle Abklingzeit (die Akzeptorkonzentration widerspiegelnd) als auch auf die Verteilung ihrer Emissionsmaxima (den Akzeptortyp widerspiegelnd) unterschieden werden. In dem zweidimensionalen Assay mit nur einem anwesenden Cyaninakzeptor nimmt die Abklingzeit τ in Luft in Abhängigkeit von dem verwendeten Cyanin und dessen Konzentration fortlaufend von 6.23 µs (kein Akzeptor) bis 0.38 – 1.16 µs (maximale Akzeptorkonzentration) ab. Gleichzeitig verringert sich auch die Quantenausbeute Φ in Luft von 0.38 bis 0.03 – 0.27, wieder abhängig von den Akzeptoreigenschaften. In dem dreidimensionalen Assay mit zwei Akzeptortypen in den Nanopartikeln nimmt die

Lebenszeit von 5.92 µs (kein Akzeptor) bis 0.34 µs (maximale Akzeptorkonzentrationen) ab. Die Quantenausbeute Φ in Luft verringert sich ebenfalls von 0.39 bis 0.02.

Alle Nanopartikel können mit der gleichen Lichtquelle bei der Absorptionswellenlänge des Ru(dpp) Donors (bei 465 nm) angeregt werden. Der Grad der Sauerstofflöschung liegt immer unterhalb von 3.5% ($\Delta\Phi_{\mathrm{Luft/Stickstoff}}$), sowohl für den zwei- als auch für den dreidimensionalen Assay.

In Kapitel 5 wird ein neues Prinzip für homogene Assays präsentiert, das auf RET von phosphoreszierenden biotinylierten Nanopartikeln zu fluoreszenz-markiertem Streptavidin (SA) basiert. Die vorgestellten Ergebnisse demonstrieren die Durchführbarkeit eines Assays für Avidin oder irgendein anderes Biomolekül, das an ein Gegenmolekül auf der Nanopartikeloberfläche bindet. Die Nanopartikel mit einem Durchmesser von etwa 10 - 50 nm bestehen aus mit $Ru(dpp)_3Cl_2$ gefärbter Poly-(acrylnitril-co-acrylsäure).

In einer ersten Studie wurden die Ru(dpp) Donor-Nanopartikel (λ_{exc} 465 nm, λ_{em} 610 nm) mit einer Lösung eines kationischen Polyelektrolyten, der Bromphenolblau (BPB, λ_{max} 592 nm, ε 73,000 L mol^{-1} cm^{-1}) als Energieakzeptor enthält, titriert. Dies sollte beweisen, daß RET von den Nanopartikeln zum Farbstoff auftritt und das maximal mögliche Ausmaß an Löschung quantifizieren. Da die Nanopartikel aufgrund des Acrylsäurecopolymers negativ geladene Carboxylgruppen auf der Oberfläche enthalten, ziehen sie den kationischen Polyelektrolyten an und wechselwirken elektrostatisch. Die resultierende räumliche Nähe von Donor und Akzeptor (Förster Radius R_0 5.24 nm) ermöglicht einen Transfer von Lumineszenzenergie vom Ru(dpp) Donor zum BPB Akzeptor, was durch die Abnahme der Abklingzeit von 4.9 µs (kein Polyelektrolyt) nach 3.1 µs (54.4 nmol/L Polyelektrolyt) festgestellt werden kann.

Ausgehend von diesem Experiment wurde ein auf RET basierender kompetitiver Bindungsassay für Avidin aufgestellt, mit einem Akzeptorfluorophor – Alexa Fluor 633 (λ_{exc} 633 nm, λ_{em} 647 nm, ε 115,000 L mol^{-1} cm^{-1}) – anstatt eines nicht-lumineszierendem Akzeptors wie BPB. Im wesentlichen binden Avidin und Alexa Fluor 633-markiertes SA kompetitiv an Biotin, das kovalent an die Oberfläche von Ru(dpp) Donornanopartikeln gebunden ist. Falls markiertes SA an die Nanopartikel bindet, findet RET von Ru(dpp) zum Marker von SA (Alexa Fluor 633) statt, der selbst nicht meßbar bei der Anregungswellenlänge des Donors (470 nm) absorbiert. Folglich nimmt die Abklingzeit τ der Emission von 4.4 µs (7.10 µmol/L Avidin) nach 2.5 µs (kein Avidin) ab, während die

Gesamtlumineszenzintensität annähernd konstant bleibt, da das Verhältnis der Konzentrationen von Alexa Fluor 633 zu Ru(dpp) konstant bei 2.8 gehalten wurde.

9. Curriculum Vitae

PERSONAL DATA

Surname	Kürner
First name	Jens Martin
Date of birth	16.04.1972
Place of birth	Hanau (Main-Kinzig-Kreis/Hessen)
Nationality	German

EDUCATION

08/1978 – 07/1982	Primary School, Neuberg/Hessen
09/1982 – 07/1988	Gymnasium, Rosenheim
08/1988 – 07/1989	High School scholarship, Arlington/Ohio (USA)
07/1989	Degree: High School Diploma
09/1989 – 07/1992	Gymnasium, Rosenheim
07/1992	Degree: Abitur

MILITARY SERVICE

10/1992 – 12/1992	Basic training at the *Sanitätslehrbataillon 851*, Munich
01/1993 – 09/1993	*Zentrales Institut des Sanitätsdienstes der Bundeswehr* Munich, Department of Environmental Chemistry

STUDIES

11/1993 – 03/1998	Chemistry (Diploma) at the University of Regensburg
03/1998	Exam: Diplom
05/1998 – 02/1999	Diploma Work at the Institute of Analytical Chemistry, Chemo- and Biosensors (Prof. Wolfbeis) at the University of Regensburg (Title: Synthesis and characterization of a diode laser compatible calixarene-chromoionophore for calcium detection)
02/1999	Degree: Diplomchemiker
04/1999 – 02/2002	PhD Work at the Institute of Analytical Chemistry, Chemo- and Biosensors (Prof. Wolfbeis) at the University of Regensburg

EXTRACURRICULAR ACTIVITIES

08 – 09/1996	Research stay at the *Institut für Spektrochemie und Angewandte Spektroskopie*, Berlin
03 – 04/1997	Laboratory course at Hoechst/Courtaulds European Fibres, Kelheim
10/1998	Participation at the *8th Vienna Opt(r)ode Workshop*, Prague
03 – 04/2000	Visiting scientist at the Salford University (Prof. C. Morgan), Manchester
10/2000 – 03/2002	Participation at the DFG Graduate College *Sensory Photoreceptors in Natural and Artificial Systems*
04 – 06/2001	Visiting scientist at the Université Louis Pasteur (Prof. J.-M. Lehn), Strasbourg

LECTURES

04/1999	*European School - Sensors for Food Applications*, Marciana Marina/Elba
09/1999	*Advanced Study Course on Optical Chemical Sensors* (ASCOS), Neusiedl/Wien
05/2001	College de France (Prof. J.-M. Lehn), Strasbourg
07/2001	Summer Meeting of the DFG Graduate College, Nové Hrady/South Bohemia

POSTER PRESENTATIONS

04/2000	*Europt(r)ode V*, Lyon
07/2001	Summer Meeting of the DFG Graduate College, Nové Hrady/South Bohemia
09/2001	*7th Conference on Methods and Applications of Fluorescence: Spectroscopy, Imaging and Probes*, Amsterdam

10. Publications and Patents

Diploma Thesis

Synthesis and characterization of a diode laser compatible calixarene-chromoionophore for calcium detection. Institute of Analytical Chemistry, Chemo- and Biosensors, University of Regensburg (**1999**).

Publications

1. Hoffmann E., Lüdke C., Kürner J. M., Scholze H., Ullrich E., Stephanowitz H. (**1999**) Studies on the use of XeF_2 as digestion reagent. *Fresenius J. Anal. Chem.* 365, 592-596.
2. Werner T., Kürner J. M., Krause C., Wolfbeis O. S. (**2000**) New longwave absorbing chromogenic calix[4]arene for calcium determination in aqueous environment. *Analytica Chimica Acta* 421, 199-205.
3. Kürner J. M., Werner T. (**2000**) A calix[4]arene-based calcium-selective optode membrane: measuring the absorbance maximum wavelength shift. *Fresenius J. Anal. Chem.* 368, 759-762.
4. Kürner J. M., Klimant I., Krause C., Pringsheim E., Wolfbeis O. S. (**2001**) A new type of phosphorescent nanospheres for use in advanced time-resolved multiplexed bioassays. *Anal. Biochem.* 297, 32-41.
5. Kürner J. M., Klimant I., Krause C., Preu H., Kunz W., Wolfbeis O. S. (**2001**) Inert phosphorescent nanospheres as markers for optical assays. *Bioconjug. Chem.* 12, 883-889.
6. Kürner J. M., Wolfbeis O. S., Klimant I. (**2002**) Homogeneous luminescence decay time-based assay using energy transfer from nanospheres. *Anal. Chem.*, submitted.
7. Wolfbeis O. S., Böhmer M., Dürkop A., Enderlein J., Gruber M., Klimant I., Krause C., Kürner J. M., Liebsch G., Lin Z., Oswald B., Wu M. (**2002**) Advanced luminescent labels, probes, and beads, and their application to luminescence bioassay and imaging. In *Fluorescence Spectroscopy, Imaging and Probes* (Kraayenhof R., Visser A. J. W. G., Gerritsen H. C., Ed.), Springer-Verlag, Berlin, in press.

Patents

1. Stangelmayer A., Klimant I., Kürner J. M. (**2001**) Anordnung und Verfahren zur Mehrfach-Fluoreszenzmessung. German patent application no. 101375301.